



OPTICAL AND ELECTRICAL TRANSPORT PROPERTIES OF SOME QUATERNARY  
THALLIUM DICHALCOGENIDES

A THESIS SUBMITTED TO  
THE GRADUATE SCHOOL OF NATURAL AND APPLIED SCIENCES  
OF  
MIDDLE EAST TECHNICAL UNIVERSITY

BY

İPEK GÜLER

IN PARTIAL FULFILLMENT OF THE REQUIREMENTS  
FOR  
THE DEGREE OF DOCTOR OF PHILOSOPHY  
IN  
PHYSICS

JUNE 2011

Approval of the thesis:

**OPTICAL AND ELECTRICAL TRANSPORT PROPERTIES OF SOME QUATERNARY  
THALLIUM DICHALCOGENIDES**

submitted by **İPEK GÜLER** in partial fulfillment of the requirements for the degree of  
**Doctor of Philosophy in Physics Department, Middle East Technical University** by,

Prof. Dr. Canan Özgen  
Dean, Graduate School of **Natural and Applied Sciences**

\_\_\_\_\_

Prof. Dr. Sinan Bilikmen  
Head of Department, **Physics**

\_\_\_\_\_

Prof. Dr. Nizami Hasanli  
Supervisor, **Physics Department, METU**

\_\_\_\_\_

**Examining Committee Members:**

Prof. Dr. Yakup Cevdet Akgöz  
Engineering Sciences Dept., METU

\_\_\_\_\_

Prof. Dr. Nizami Hasanli  
Physics Dept., METU

\_\_\_\_\_

Prof. Dr. Mehmet Parlak  
Physics Dept., METU

\_\_\_\_\_

Prof. Dr. Tofig Mammadov  
Physics Dept., Gazi University

\_\_\_\_\_

Assoc. Prof. Dr. Enver Bulur  
Physics Dept., METU

\_\_\_\_\_

**Date:**

\_\_\_\_\_

**I hereby declare that all information in this document has been obtained and presented in accordance with academic rules and ethical conduct. I also declare that, as required by these rules and conduct, I have fully cited and referenced all material and results that are not original to this work.**

Name, Last Name: İPEK GÜLER

Signature :



# ABSTRACT

## OPTICAL AND ELECTRICAL TRANSPORT PROPERTIES OF SOME QUATERNARY THALLIUM DICHALCOGENIDES

Güler, İpek

PH.D., Department of Physics

Supervisor : Prof. Dr. Nizami Hasanli

June 2011, 112 pages

In this thesis, in order to study the structural, optical and electrical transport properties of  $\text{Tl}_2\text{In}_2\text{S}_3\text{Se}$ ,  $\text{TlInSeS}$  and  $\text{Tl}_2\text{In}_2\text{SSe}_3$  crystals, X-ray diffraction (XRD), energy dispersive spectroscopic analysis (EDSA), transmission, reflection, photoluminescence (PL), thermally stimulated current (TSC) and photoconductivity decay (PC) measurements were carried out.

Lattice parameters and atomic composition of these crystals were determined from XRD and EDSA experiments, respectively. By the help of transmission and reflection experiments, the room temperature absorption data were analyzed and it was revealed the coexistence of indirect and direct band gap energies of the studied crystals. Moreover, the refractive index dispersion parameters - oscillator energies, dispersion energies, oscillator strengths, oscillator wavelengths and zero-frequency refractive indexes were determined. Temperature-dependent transmission measurements made it possible to find the rate of change of indirect band gaps with temperature, absolute zero values of the band gap energies and Debye temperatures of these crystals. From the analysis of the transmission and reflection measurements, it was established that, there is a decrease in the values of indirect and direct band gaps energies and

an increase in zero-frequency refractive indexes with increasing of selenium content.

PL measurements were carried out to obtain the detailed information about recombination levels in crystals studied. The behavior of PL spectra were investigated as a function of laser excitation intensity and temperature. The variation of the spectra with laser excitation intensity and temperature suggested that the observed emission bands in these crystals were due to the donor-acceptor pair recombination.

TSC measurements were carried out with various heating rates at different illumination temperatures to obtain information about trap levels in these crystals. The mean activation energies, attempt-to-escape frequencies, concentrations and capture cross sections of the traps were determined as a result of TSC spectra analysis. The analysis of experimental TSC curves registered at different light illumination temperatures revealed the exponential trap distribution in the studied crystals. From the analysis of PC measurements, carrier lifetimes were obtained.

**Keywords:** Layered crystals, Optical properties, Photoluminescence, Thermally stimulated current, Defect states.

# ÖZ

## BAZI DÖRTLÜ TALYUM İKİLİ-KALKOJENLERİN OPTİK VE ELEKTRİKSEL TAŞIMA ÖZELLİKLERİ

Güler, İpek

DOKTORA, Fizik bölümü

Tez Yöneticisi : Prof. Dr. Nizami Hasanlı

Haziran 2011, 112 sayfa

Bu tezde,  $Tl_2In_2S_3Se$ ,  $TlInSeS$  ve  $Tl_2In_2SSe_3$  kristallerinin yapısal, optik ve elektriksel taşıma özelliklerini incelemek için, X ışını kırınım, enerji dağılımlı spektrum analizi, geçirgenlik, yansıma, fotoişma, ısıt uyarılmış akım ve fotoiletkenlik bozulma ölçümleri yapıldı.

Bu kristallerin, örgü parametreleri ve atomik bileşimleri sırasıyla X ışını kırınım ve enerji dağılımlı spektrum analizi deneyleriyle belirlendi. Geçirgenlik ve yansıma deneyleri yardımıyla oda sıcaklığı soğurma datası incelendi ve bu inceleme, üzerinde çalışılan kristallerin direkt ve indirekt bant genişliği enerjilerinin bir arada bulunduğunu gösterdi. Diğer taraftan, kırılma indeksi parametreleri- salınım enerjileri, dağılım enerjileri, salınım güçleri, salınım dalga boyları ve sıfır-frekans kırılma indeksleri belirlendi. Sıcaklık bağımlı geçirgenlik ölçümleri, indirekt bant aralığının sıcaklıkla değişim oranını, mutlak sıcaklıktaki bant genişliği enerji değerlerini ve Debye sıcaklıklarını bulmaya olanak sağladı. Selenyum atomlarının içeriğinin artması ile indirekt ve direkt bant genişliği enerjilerinde azalma ve sıfır frekanslı yansıma indekslerinde artma olduğu, geçirgenlik ve yansıma deneylerinin analizlerinden tespit edildi.

Fotoişma deneyleri, çalışılan kristallerin tekrar birleşme seviyeleri hakkında detaylı bilgi

elde etmek için yapıldı. Fotoışma spektrumlarının davranışı lazer uyarma şiddetinin ve sıcaklığın fonksiyonu olarak incelendi. Fotoışma spektrumun, lazer uyarma yoğunluğu ve sıcaklık ile değişimi bu kristallerde gözlemlenen emisyon bantlarının verici-alıcı çiftlerinin tekrar birleşmelerinden kaynaklandığını önerdi.

Bu kristallerdeki tuzaklanma seviyeleri hakkında bilgi elde etmek için, ısıtılmış akım ölçümleri farklı aydınlatma sıcaklıklarındaki çeşitli ısıtma hızları ile yapıldı. Ortalama aktivasyon enerjileri, kaçış frekansları, tuzakların yoğunlukları ve yakalama tesir kesitleri ısıtılmış spektrum analizi sonucunda belirlendi. Farklı ışıklarla aydınlatma sıcaklıklarındaki deneysel ısıtılmış akım eğrilerinin analizi, incelenen kristallerdeki tuzakların üstel dağılımını gösterdi. Fotoiletkenlik bozulma ölçümlerinin analizinden, taşıyıcıların ömrü belirlendi.

Anahtar Kelimeler: Tabakalı kristaller, Optik özellikler, Fotoışma, Isıtılmış akım, Kusur durumları.

*To my family*

## ACKNOWLEDGMENTS

I would like to express my deepest feelings to my supervisor Prof. Dr. Nizami Hasanli. I am very grateful to him. This work would be impossible without his valuable guidance, knowledge, experience, encouragements and support. I learned a lot not only about solid state physics but also about life thanks to him. The most important one I learned is that spending my time on major works without losing life.

I would like to thank Prof Dr. Hüsni Özkan for the opportunities to work in optic laboratory. I am also thankful to Prof. Dr. Raşit Turan for his collaboration in photoluminescence laboratory.

I want to express my sincere thanks to Asiss. Prof. Dr. Kadir Gökşen. He was there when I was confused, curious, hopeless and any time I needed him. He had too much labor on this work especially on photoluminescence measurements.

I am grateful to my father Sefa Koçer, my mother Kafiye Koçer and my brother Kemal Koçer for their endless love, support and patience throughout my education.

My special thank is to my husband Ali Murat Güler. I know I owe a lot to METU physics department but especially I owe a lot for the cause to meet him. He always remind me how a lucky woman I am but during this PhD period even he did not efface it. I also want to thank to our little princess İzgi Nisa. If she did not kick my stomach during my pregnancy, I could not wake up and finish to write my thesis on time. It was so excited for me that I would get my baby and my thesis at the same time.

I want to thank my roommate Özge Amutgan Aygar for her patience and support. I also want to thank Mehmet Işık, Deniz Tekin, Olcay Üzengi Aktürk, Esin Kenar and Arife İmer for their friendships.

Last but not least, my friends more than my sisters; Ayşe Bekmezcioglu, Firdes Yenilmez, Aslı Özdilek, Ferhunde Ayşin, thanks a lot. Without giving me moral support in our dinner meetings, it would be very difficult to finish PhD.

## TABLE OF CONTENTS

ABSTRACT . . . . .	iv
ÖZ . . . . .	vi
ACKNOWLEDGMENTS . . . . .	ix
TABLE OF CONTENTS . . . . .	x
LIST OF TABLES . . . . .	xiii
LIST OF FIGURES . . . . .	xiv
CHAPTERS	
1 INTRODUCTION . . . . .	1
2 THEORETICAL APPROACH . . . . .	5
2.1 Theoretical Approach to Semiconductor Physics . . . . .	5
2.1.1 Band Structure in Semiconductors . . . . .	5
2.1.2 Direct and Indirect Band Gap Materials . . . . .	10
2.1.3 Intrinsic and Extrinsic Semiconductors . . . . .	12
2.1.4 Structural Defects in Semiconductors . . . . .	15
2.2 Theoretical Approach to Experiments . . . . .	16
2.2.1 X-Ray Diffraction Experiment . . . . .	16
2.2.2 Energy Dispersive Spectral Analysis (EDSA) Experiments	18
2.2.3 Optical Absorption, Transmission and Reflection Spectroscopy	19
2.2.3.1 Absorption . . . . .	19
2.2.3.2 Reflection . . . . .	20
2.2.3.3 Transmission . . . . .	20
2.2.4 Photoluminescence Experiments . . . . .	22
2.2.4.1 Recombination Mechanisms . . . . .	23

	2.2.4.2	Laser Excitation Power Dependence of Photoluminescence of Semiconductors . . . . .	26
	2.2.4.3	Temperature Dependence of Photoluminescence of Semiconductors . . . . .	29
	2.2.5	Thermally Stimulated Current Measurements . . . . .	30
	2.2.5.1	Traps and Recombination Centers . . . . .	31
	2.2.5.2	First and Second Order Kinetics . . . . .	33
	2.2.5.3	Isothermal Decay Method . . . . .	38
	2.2.5.4	Initial Rise Method . . . . .	38
	2.2.5.5	The Various Heating Rates Method . . . . .	39
	2.2.5.6	Curve Fitting Method . . . . .	39
	2.2.5.7	Traps Distribution Method . . . . .	41
	2.2.5.8	Trap Concentration Determination . . . . .	42
3		EXPERIMENTAL DETAILS . . . . .	43
	3.1	XRD Experiments . . . . .	43
	3.2	EDSA Experiments . . . . .	44
	3.3	Transmission and Reflection Experiments . . . . .	44
	3.4	PL Experiments . . . . .	45
	3.5	TSC Experiments . . . . .	46
	3.6	Photoconductivity Decay Experiments . . . . .	48
	3.7	Bridgman Method . . . . .	48
4		RESULTS AND DISCUSSION . . . . .	49
	4.1	Introduction . . . . .	49
	4.2	Structural, Optical and Electrical Transport Properties of $\text{Tl}_2\text{In}_2\text{S}_3\text{Se}$ Layered Crystals . . . . .	51
	4.2.1	Results of X-ray Experiments and Energy Dispersive Spectral Analysis . . . . .	51
	4.2.2	Results of Transmission and Reflection Experiments . . . . .	52
	4.2.3	Results of Photoluminescence Experiments . . . . .	57
	4.2.4	Results of Thermally Stimulated Current Experiments . . . . .	63
	4.3	Structural, Optical and Electrical Transport Properties of $\text{TlInSeS}$ Layered Crystals . . . . .	70



4.3.1	Results of X-ray Experiments and Energy Dispersive Spectral Analysis . . . . .	70
4.3.2	Results of Transmission and Reflection Experiments . . .	71
4.3.3	Results of Photoluminescence Experiments . . . . .	75
4.3.4	Results of Thermally Stimulated Current Experiments . .	76
4.4	Structural, Optical and Electrical Transport Properties of $\text{Tl}_2\text{In}_2\text{SSe}_3$ Layered Crystals . . . . .	83
4.4.1	Results of X-ray Experiments and Energy Dispersive Spectral Analysis . . . . .	83
4.4.2	Results of Transmission and Reflection Experiments . . .	84
4.4.3	Results of Photoluminescence Experiments . . . . .	88
4.4.4	Results of Thermally Stimulated Current Experiments . .	92
5	CONCLUSION . . . . .	100
	REFERENCES . . . . .	105
	CURRICULUM VITAE . . . . .	110

## LIST OF TABLES

### TABLES

Table 2.1 Seven types of crystal cells and corresponding formulas for interplanar spacings [37]. . . . .	18
Table 4.1 X-ray powder diffraction data for $\text{Tl}_2\text{In}_2\text{S}_3\text{Se}$ crystals. . . . .	52
Table 4.2 The illumination temperatures of two successive experimental TSC curves ( $T_{0i}-T_{0i+1}$ ); maximum temperature ( $T_{mi}$ ) and area ( $Q_i$ ) of calculated TSC curves ; mean activation energy ( $E_{ti}$ ), capture cross section ( $S_{ti}$ ), attempt-to-escape frequency ( $\nu_i$ ) and concentration ( $N_{ti}$ ) of traps in $\text{Tl}_2\text{In}_2\text{S}_3\text{Se}$ crystal. . . . .	69
Table 4.3 X-ray powder diffraction data for $\text{TlInSSe}$ crystals. . . . .	71
Table 4.4 The illumination temperatures of two successive experimental TSC curves ( $T_{0i}-T_{0i+1}$ ); maximum temperature ( $T_{mi}$ ) and area ( $Q_i$ ) of calculated TSC curves ; mean activation energy ( $E_{ti}$ ), capture cross section ( $S_{ti}$ ), attempt-to-escape frequency ( $\nu_i$ ) and concentration ( $N_{ti}$ ) of traps in $\text{TlInSeS}$ crystal. . . . .	81
Table 4.5 X-ray powder diffraction data for $\text{Tl}_2\text{In}_2\text{SSe}_3$ crystals. . . . .	83
Table 4.6 The illumination temperatures of two successive experimental TSC curves ( $T_{0i}-T_{0i+1}$ ); maximum temperature ( $T_{mi}$ ) and area ( $Q_i$ ) of calculated TSC curves ; mean activation energy ( $E_{ti}$ ), capture cross section ( $S_{ti}$ ), attempt-to-escape frequency ( $\nu_i$ ) and concentration ( $N_{ti}$ ) of traps in $\text{Tl}_2\text{In}_2\text{SSe}_3$ crystal. . . . .	98

## LIST OF FIGURES

### FIGURES

Figure 2.1	An energy band diagram for semiconductors. . . . .	7
Figure 2.2	Schematic electron occupancy of allowed energy bands for an insulator, semiconductor and conductor. . . . .	7
Figure 2.3	Energy levels in a diamond as a function of atomic distance. . . . .	8
Figure 2.4	Energy bands of diamond crystal. Energy band separated into two groups, valence band and conduction band and each of bands contain $4N$ states. . . . .	9
Figure 2.5	Parabolic dependence of energy vs. momentum. . . . .	10
Figure 2.6	Energy vs. momentum in a direct-gap two-band system, where $E_{gd}$ is the energy of direct band gap. . . . .	10
Figure 2.7	Energy vs. momentum diagram for a semiconductor with valleys at $k = < 000 >$ and $k = < 111 >$ directions. . . . .	11
Figure 2.8	a) In a direct band gap material the conduction band minimum and valence band maximum occur at the same $k$ values b) In an indirect band gap material the conduction band minimum and valence band maximum occur at different $k$ values [33]. . . . .	11
Figure 2.9	Intrinsic conductivity occurs in a semiconductor as a result of thermal excitation of electrons from the valence band to conduction band. . . . .	13
Figure 2.10	Substitution of antimony atom into silicon. Antimony atoms act as donor impurity. . . . .	14
Figure 2.11	Energy levels of Si created by substitution of antimony atoms. . . . .	14
Figure 2.12	Substitution of gallium atom into silicon. Gallium atoms act as acceptor impurity. . . . .	15
Figure 2.13	Energy levels of Si created by substitution of gallium atoms. . . . .	15

Figure 2.14 Representation of X-ray diffraction by a crystal lattice. . . . .	17
Figure 2.15 Excitation and recombination process in a PL experiment. . . . .	23
Figure 2.16 Direct band to band transition. . . . .	24
Figure 2.17 Indirect band to band transition. . . . .	25
Figure 2.18 Donor to acceptor transition. . . . .	26
Figure 2.19 Effect of coulomb interaction on emission energy ( $r$ is the donor-acceptor separation). . . . .	26
Figure 2.20 Electronic transitions in semiconductors. Solid circles are electrons and open circles are holes. . . . .	31
Figure 2.21 Energy levels in an insulator in equilibrium at absolute zero. The below $E_f$ are full of electrons whereas those above are empty [32]. . . . .	32
Figure 2.22 Energy levels in a solid. $n$ , $m$ and $n_c$ are the concentrations of trapped electrons, holes in the centres and free electrons in the conduction band, respectively. $N$ is total concentration of traps even filled and empty [78]. . . . .	35
Figure 3.1 The simple schematic representation of XRD experiment. . . . .	43
Figure 3.2 Schematic representation of room temperature transmission experiment set-up. . . . .	44
Figure 3.3 Schematic representation of reflection experiment set-up. . . . .	45
Figure 3.4 Schematic representation of temperature-dependent transmission experiment set-up. . . . .	45
Figure 3.5 Schematic representation of PL experiment set-up. . . . .	46
Figure 3.6 The representation of sample attached to sample holder in sandwich geometry. . . . .	47
Figure 3.7 Schematic representation of TSC experiment set-up. . . . .	47
Figure 3.8 Schematic representation of PC experiment set-up. . . . .	48
Figure 4.1 Projection of the crystal structure of thallium and indium chalcogenides on the $ac$ - plane. . . . .	50
Figure 4.2 Projection of the crystal structure of thallium and indium chalcogenides on the $ab$ - plane. . . . .	50
Figure 4.3 X-ray diffraction pattern of $Tl_2In_2S_3Se$ powder sample. . . . .	51

Figure 4.4	Energy dispersive spectroscopic analysis of $\text{Ti}_2\text{In}_2\text{S}_3\text{Se}$ crystal. . . . .	52
Figure 4.5	The spectral dependence of transmittance and reflectivity for $\text{Ti}_2\text{In}_2\text{S}_3\text{Se}$ crystal at room temperature. . . . .	53
Figure 4.6	The variation of absorption coefficient as a function of photon energy for $\text{Ti}_2\text{In}_2\text{S}_3\text{Se}$ crystal at $T = 300$ K. Circles represent the experimental data that were fitted to a linear equation (the solid lines) to find the band gaps. Insets 1 and 2 represent the dependencies of $(\alpha h\nu)^{1/2}$ and $(\alpha h\nu)^2$ on photon energy, respectively. . . . .	54
Figure 4.7	The spectral dependence of transmittance for $\text{Ti}_2\text{In}_2\text{S}_3\text{Se}$ crystal in the temperature range of 10-300 K. Inset: The indirect band gap energy as a function of temperature. The solid line represents the fit using equation 4.4. . . . .	56
Figure 4.8	The dependence of refractive index on the wavelength for $\text{Ti}_2\text{In}_2\text{S}_3\text{Se}$ crystal. Inset: Plot of $(n^2 - 1)^{-1}$ versus $(h\nu)^2$ . The solid line represents the fit using equation 4.5. . . . .	57
Figure 4.9	Temperature dependence of PL spectra from $\text{Ti}_2\text{In}_2\text{S}_3\text{Se}$ crystal at excitation laser intensity $L = 78 \text{ mW cm}^{-2}$ . Note that for curves 16-18, intensities have been multiplied by a factor of four. . . . .	58
Figure 4.10	Decomposition of the PL spectrum from $\text{Ti}_2\text{In}_2\text{S}_3\text{Se}$ crystal into two Gaussian lineshapes ( $T = 22 \text{ K}$ , $L = 516 \text{ mW cm}^{-2}$ ). . . . .	59
Figure 4.11	Temperature dependences of PL bands intensities for $\text{Ti}_2\text{In}_2\text{S}_3\text{Se}$ crystal. Circles are the experimental data. Solid curves show the theoretical fits using equation 4.8. The inset: temperature dependences of emission A- and B-bands peak energies. . . . .	60
Figure 4.12	PL spectra of $\text{Ti}_2\text{In}_2\text{S}_3\text{Se}$ crystal as a function of excitation laser intensity at $T = 22 \text{ K}$ . . . . .	61
Figure 4.13	Excitation laser intensity versus emission peak energy for $\text{Ti}_2\text{In}_2\text{S}_3\text{Se}$ crystal for B-band at $T = 22 \text{ K}$ . The solid curve represents the theoretical fit using equation 4.9. Inset: Dependence of PL intensities at the emission maximums versus excitation laser intensity for A- and B-bands at $T = 22 \text{ K}$ . The solid lines show the theoretical fits using equation 4.10. . . . .	62

Figure 4.14 Principles of the TSC experiment for $\text{Ti}_2\text{In}_2\text{S}_3\text{Se}$ crystals; (1) time period of applied illumination; (2) variation of bias voltage; (3) temperature variation with time for four different light illumination temperatures; (4) TSC spectra for four different light illumination temperatures: 20 (1), 30 (2), 37 (3) and 40 K (4).	64
Figure 4.15 Typical experimental TSC curve of $\text{Ti}_2\text{In}_2\text{S}_3\text{Se}$ crystals under bias voltage. Circles and stars show the experimental data obtained when the polarity of illuminated surface was negative and positive, respectively. . . . .	64
Figure 4.16 TSC spectra of the $\text{Ti}_2\text{In}_2\text{S}_3\text{Se}$ crystals for various illumination times at a constant heating rate of $\beta = 1.0 \text{ Ks}^{-1}$ . Inset: maximum thermally stimulated currents as a function of illumination time. The dash-dotted line is only guide for the eye. . . . .	65
Figure 4.17 The experimental TSC spectra of $\text{Ti}_2\text{In}_2\text{S}_3\text{Se}$ crystals at different heating rates. . . . .	66
Figure 4.18 The TSC spectra of $\text{Ti}_2\text{In}_2\text{S}_3\text{Se}$ crystals at different illumination temperatures $T_0$ . . . . .	67
Figure 4.19 Thermally stimulated currents versus $1000 / T$ for the TSC spectra of $\text{Ti}_2\text{In}_2\text{S}_3\text{Se}$ crystals, calculated from the difference of two successive experimental TSC spectra for the selective pairs of temperatures 20-30 K, 30-37 K and 37-40 K (curves from 1 to 3). Solid lines present the theoretical fits according to the initial rise method. Inset: The logarithmic plot of released charge as a function of activation energy. Squares show the experimental data for the peak. Solid line is theoretical fit according to equation 4.12. . . . .	68
Figure 4.20 The photoconductivity decay curve for the $\text{Ti}_2\text{In}_2\text{S}_3\text{Se}$ crystals. . . . .	70
Figure 4.21 X-ray diffraction pattern of $\text{TiInSeS}$ powder sample. . . . .	71
Figure 4.22 Energy dispersive spectroscopic analysis of $\text{TiInSeS}$ crystal. . . . .	72
Figure 4.23 The spectral dependence of transmittance and reflectivity for $\text{TiInSeS}$ crystal at room temperature. . . . .	72
Figure 4.24 The variation of absorption coefficient as a function of photon energy for $\text{TiInSeS}$ crystal at $T = 300 \text{ K}$ . Circles represent the experimental data that were fitted to a linear equation (the solid lines) to find the band gaps. Insets 1 and 2 represent the dependencies of $(\alpha h\nu)^{1/2}$ and $(\alpha h\nu)^2$ on photon energy, respectively.	73

Figure 4.25 The spectral dependence of transmittance for TlInSeS crystal in the temperature range of 10-300 K. Inset: The indirect band gap energy as a function of temperature. The solid line represents the fit using equation 4.4. . . . .	74
Figure 4.26 The dependence of refractive index on the wavelength for TlInSeS crystal. Inset: Plot of $(n^2 - 1)^{-1}$ versus $(h\nu)^2$ . The solid line represents the fit using equation 4.5. . . . .	75
Figure 4.27 Principles of the TSC experiment for TlInSeS crystals; (1) time period of applied illumination; (2) variation of bias voltage; (3) temperature variation with time for four different light illumination temperatures; (4) TSC spectra for four different light illumination temperatures: 30 (1), 45 (2), 52 (3) and 57 K (4). . . .	77
Figure 4.28 Typical experimental TSC curve of TlInSeS crystals under bias voltage. Circles and stars show the experimental data obtained when the polarity of illuminated surface was negative and positive, respectively. . . . .	78
Figure 4.29 TSC spectra of the TlInSeS crystals for various illumination times at a constant heating rate of $\beta = 0.8 \text{ K s}^{-1}$ . Inset: maximum thermally stimulated currents as a function of illumination time. The dash-dotted line is only guide for the eye. . . . .	78
Figure 4.30 Experimental TSC spectra of TlInSeS crystals at different temperatures $T_p = 50, 55, 60, 65, 70, 75$ and $80 \text{ K}$ . Inset: $\gamma = \nu \exp(-E_t/kT_p)$ plot as a function of $1000/T_p$ . $\nu$ is the attempt-to-escape frequency of a trapped carrier. . . . .	79
Figure 4.31 The experimental TSC spectra of TlInSeS crystals at different heating rates.	80
Figure 4.32 The TSC spectra of TlInSeS crystals at different illumination temperatures $T_0$ . . . . .	80
Figure 4.33 Thermally stimulated currents versus $1000 / T$ for the TSC spectra of TlInSeS crystals, calculated from the difference of two successive experimental TSC spectra for the selective pairs of temperatures 30-45 K, 45-52 K and 52-57 K (curves from 1 to 3). Solid lines present the theoretical fits according to the initial rise method. Inset: The logarithmic plot of released charge as a function of activation energy. Squares show the experimental data for the peak. Solid line is theoretical fit according to equation 4.12. . . . .	81
Figure 4.34 The photoconductivity decay curve for the TlInSeS crystals. . . . .	82

Figure 4.35 X-ray diffraction pattern of $\text{Tl}_2\text{In}_2\text{SSe}_3$ powder sample. . . . .	83
Figure 4.36 Energy dispersive spectroscopic analysis of $\text{Tl}_2\text{In}_2\text{SSe}_3$ crystal. . . . .	84
Figure 4.37 The spectral dependence of transmittance and reflectivity for a $\text{Tl}_2\text{In}_2\text{SSe}_3$ crystal at room temperature. . . . .	84
Figure 4.38 The variation of absorption coefficient as a function of photon energy for $\text{Tl}_2\text{In}_2\text{SSe}_3$ crystal at $T = 300$ K. Circles represent the experimental data that were fitted to a linear equation (the solid lines) to find the band gaps. Insets 1 and 2 represent the dependencies of $(\alpha h\nu)^{1/2}$ and $(\alpha h\nu)^2$ on photon energy, respectively. . . . .	86
Figure 4.39 The spectral dependence of transmittance for $\text{Tl}_2\text{In}_2\text{SSe}_3$ crystal in the temperature range of 10-300 K. Inset: The indirect band gap energy as a function of temperature. The solid line represents the fit using equation 4.4. . . . .	87
Figure 4.40 The dependence of refractive index on the wavelength for $\text{Tl}_2\text{In}_2\text{SSe}_3$ crystal. Inset: Plot of $(n^2 - 1)^{-1}$ versus $(h\nu)^2$ . The solid line represents the fit using equation 4.5. . . . .	88
Figure 4.41 Temperature dependence of PL spectra from $\text{Tl}_2\text{In}_2\text{SSe}_3$ crystal at excitation laser intensity $L = 111.4 \text{ mW cm}^{-2}$ . Note that for curves 10-14, intensities have been multiplied by a factor of three. . . . .	89
Figure 4.42 Temperature dependences of PL bands intensities for $\text{Tl}_2\text{In}_2\text{Se}_3\text{S}$ crystal. Circles are the experimental data. Solid curves show the theoretical fits using equation 4.8. The inset: temperature dependences of emission band peak energies . . . . .	90
Figure 4.43 PL spectra of $\text{Tl}_2\text{In}_2\text{SSe}_3$ crystal as a function of excitation laser intensity at $T = 25$ K. . . . .	91
Figure 4.44 Excitation laser intensity versus emission peak energy for $\text{Tl}_2\text{In}_2\text{SSe}_3$ crystal for B-band at $T = 22$ K. The solid curve represents the theoretical fit using equation 4.9. Inset: Dependence of PL intensities at the emission maximums versus excitation laser intensity for A- and B-bands at $T = 22$ K. The solid lines show the theoretical fits using equation 4.10. . . . .	92



Figure 4.45 Principles of the TSC experiment for $\text{Tl}_2\text{In}_2\text{Se}_3\text{S}$ crystals; (1) time period of applied illumination; (2) variation of bias voltage; (3) temperature variation with time for four different light illumination temperatures; (4) TSC spectra for four different light illumination temperatures: 10 (1), 20 (2), 30 (3), 40 (4), 50 (5) and 60 K (6). . . . .	93
Figure 4.46 Typical experimental TSC curve of $\text{Tl}_2\text{In}_2\text{SSe}_3$ crystals under bias voltage. Circles and stars show the experimental data obtained when the polarity of illuminated surface was negative and positive, respectively. . . . .	94
Figure 4.47 TSC spectra of the $\text{Tl}_2\text{In}_2\text{SSe}_3$ crystals for various illumination times at a constant heating rate of $\beta = 0.8 \text{ K s}^{-1}$ . Inset: Maximum thermally stimulated currents of A and B peaks as a function of illumination time. The dash-dotted line is only guide for the eye. . . . .	94
Figure 4.48 The experimental TSC spectra of $\text{Tl}_2\text{In}_2\text{Se}_3\text{S}$ crystals at different heating rates. . . . .	95
Figure 4.49 The TSC spectra of $\text{Tl}_2\text{In}_2\text{SSe}_3$ crystals at different illumination temperatures $T_0$ . . . . .	96
Figure 4.50 Experimental TSC spectrum of $\text{Tl}_2\text{In}_2\text{SSe}_3$ crystals obtained at illumination temperature $T_{0i} = 40 \text{ K}$ with a heating rate $\beta = 0.8 \text{ K s}^{-1}$ . Open circles are experimental data. Dash-dotted curves represent the decomposed peaks A and B. Solid curve shows total fit to experimental data. . . . .	97
Figure 4.51 Thermally stimulated currents versus $1000 / T$ for the TSC spectra of $\text{Tl}_2\text{In}_2\text{SSe}_3$ crystals, calculated from the difference of two successive experimental TSC spectra for the selective pairs of temperatures 10-20 K, 20-30 K, 30-40 K for peak A (curves from 1 to 3) and 30-40 K, 40-50 K, 50-60 K for peak B (curves from 4 to 6). Circles and squares show the experimental data for peaks A and B, respectively. Solid lines present the theoretical fits according to the initial rise method. Inset: The logarithmic plots of released charge as a function of activation energy. Circles and squares show the experimental data for peaks A and B, respectively. Solid lines are theoretical fit according to equation 4.12. . . . .	98
Figure 4.52 The photoconductivity decay curve for the $\text{Tl}_2\text{In}_2\text{SSe}_3$ crystals. . . . .	99

# **CHAPTER 1**

## **INTRODUCTION**

Semiconductors are used in a wide range of electronic devices, such as transistors, switching devices, voltage regulators, photocells and photodetectors. Industry of crystal growth made it possible to produce pure and perfect crystals. As a result of industry development in crystal growth, the list of semiconductor materials has exceeded.

Defects are important on the performance of optoelectronic devices. In some optoelectronic devices, as a result of defects, scattering centers lower carrier mobility, in other words hinder high-frequency operation.

Photoluminescence (PL) is an important technique for measuring the purity and crystalline quality of semiconductors. It forms the basis of solid state lasers. It is used for display panels in electronic equipment, lighting and paints. It is also sensitive, nondestructive technique for material characterization [1] . In this technique, it creates light from a material by photoexcitation. Radiative transitions occur not only between conduction and valence bands but also between localized defect levels. As a result of this, PL spectroscopy can be used to determine specific defect centres in crystals.

Another technique to study energy levels in crystals is thermally stimulated current (TSC) technique. In TSC process, energy levels of crystals are filled by optical excitation at low temperatures. Electrons or holes are emitted by heating to a higher temperature so that information about energy levels in the crystal can be obtained.

The chalcogens are chemical elements belong to group VIA of the periodic table. This group consists of the elements oxygen (O), sulphur (S), selenium (Se), tellurium (Te), the radioactive element polonium (Po), and the synthetic element ununhexium (Uuh). The term, chalcogen,

is commonly used for sulfides, selenides, and tellurides, rather than oxides. The compounds of the heavier chalcogens (particularly the sulfides, selenides, and tellurides) are known as chalcogenides.

Ternary and quaternary layered-structured semiconductors show many peculiar properties. There are large number of applications as memory switching elements, emission modulators and nonlinear optical transducers in nonlinear optics and photoelectronics [2, 3]. Ternary thallium dichalcogenides  $\text{TlInS}_2$  and  $\text{TlInSe}_2$ , which are useful for optoelectronic applications were studied in references [4]-[8]. They have high photosensitivity in the visible range of spectra and high birefringence in conjunction with a wide transparency range of 0.5-14.0  $\mu\text{m}$  [9].

$\text{TlInS}_2$  layered crystal belongs to the group of monoclinic system. The space group is  $C2/c$  and ratio of  $\text{InS}:\text{TlS}$  is 1:1. The lattice of  $\text{TlInS}_2$  crystals consists of two dimensional layers arranged parallel to (001) plane. Each layer rotated by a right angle with respect to the previous one [10]. Very much attention has been given to the study of the structural [10]-[14], electrical [6, 15, 16] and optical [6], [17]-[21] properties in the visible range.

Optical properties of  $\text{TlInS}_2$  crystals were studied by both absorption and reflection spectroscopy [6, 21, 22]. It was observed that  $\text{TlInS}_2$  crystals have two energy band gaps, 2.23 eV for a direct and 2.28 eV for an indirect band gaps at 300 K, respectively. Absorption and reflection measurements were also performed with various temperatures. The direct band gap energy of 2.58 eV at  $T=10$  K were obtained [17, 18]. In reference [23], optical energy gap of  $\text{TlInS}_2$  crystal has been studied in the temperature range of 77-300 K. The energy gap was found to be 2.24 eV at 300 K. As a result of the temperature-dependent optical measurements,  $dE_g/dT$  was found to be  $-1.87 \times 10^{-4} \text{ eV/K}$  in the temperature range of 77-300 K.

PL spectra of  $\text{TlInS}_2$  crystal were studied in reference [24]. The temperature and excitation intensity dependence PL spectra were analyzed in the 500-860 nm wavelength region. Two PL emission bands were observed at  $T=11.5$  K and excitation intensity of  $7.24 \text{ W/cm}^2$ . A band was centered at 515 nm (2.41 eV) and B band was centered at 816 nm (1.52 eV). From the analysis of the data, it was obtained that emission A-band was due to radiative transitions from shallow donor level located at 20 meV below the bottom of the conduction band to the deep acceptor level located at 250 meV above the top of the valence band [24].

TSC technique was used to determine the trapping parameters in  $\text{TlInS}_2$  single crystals. A series of trap levels with energy depths ranging from 150 to 220 meV were obtained from the analysis of TSC spectra in the range of 90-300 K [25]. The TSC measurements in  $\text{TlInS}_2$  crystals in the temperature range of 10-90 K presented that there was a trap level in the energy gap with activation energy of 12 meV [26]. In another study, experimental evidence was found for the presence of two shallow electron trapping centers with activation energies of 12 and 14 meV in the temperature range of 10-110 K [27]. In the high temperature range of 100-300 K, three deep trapping centers with activation energies 400, 570 and 650 meV were found [28].

When we look at the structures of the other crystal  $\text{TlInSe}_2$ , it is analog of thallium selenide  $[\text{Tl}^{1+} \text{Ti}^{3+} \text{Se}_2]$  in which trivalent  $\text{Ti}^{3+}$  ions are replaced with  $\text{In}^{3+}$  ions [29]. Optical properties of  $\text{TlInSe}_2$  crystals were studied and it was revealed that they have two energy band gaps,  $E_{gi} = 1.07\text{-}1.23$  eV and  $E_{gd} = 1.27\text{-}1.44$  eV, respectively [6]-[8]. These crystals have negative differential resistance with S-type current-voltage characteristics [6] and high thermoelectric power [21].

$\text{TlInS}_2$  belongs the group of semiconductors with layered structure whereas  $\text{TlInSe}_2$  has a chain structure. Changing the chemical composition parameter  $x$  in the formula  $\text{TlInS}_x\text{Se}_{2-x}$  from 0 to 2 causes the physical properties variation in these crystals. The crystals  $\text{TlInS}_2$  [ $x = 0$ ],  $\text{Tl}_2\text{In}_2\text{SSe}_3$  [ $x = 0.5$ ],  $\text{TlInSSe}$  [ $x = 1.0$ ],  $\text{Tl}_2\text{In}_2\text{S}_3\text{Se}$  [ $x = 1.5$ ] and  $\text{TlInS}_2$  [ $x = 2.0$ ] are obtained by changing the  $x$  from 0 to 2 in order of 0.5.

$\text{Tl}_2\text{In}_2\text{S}_3\text{Se}$ ,  $\text{TlInSSe}$  and  $\text{Tl}_2\text{In}_2\text{SSe}_3$  compounds belong to the group of semiconductors with layered structure. They are the structural analogs of  $\text{TlInS}_2$ , in which one quarter, half and three quarters of sulfur atoms replaced by selenium atoms, respectively [30]. Crystals lattice consists of alternating two dimensional layers arranged parallel to the (001) plane. There is  $90^\circ$  angle between the layers. There is interlayer bonding between Tl and S(Se) atoms. Whereas the bonding between In and S(Se) atoms is an intralayer type. The fundamental structural unit of a layer is the  $\text{In}_4\text{S}_6(\text{Se}_6)$  adamantane-like units linked together by bridging S(Se) atoms. The Tl atoms are in trigonal prismatic voids resulting from the combination of the  $\text{In}_4\text{S}_6(\text{Se}_6)$  polyhedra into a layer. The Tl atoms form nearly planar chains along the  $[110]$  and  $[1\bar{1}0]$  directions.

The purpose of the present thesis is to report detailed information mainly about recombination and trap levels in  $\text{Tl}_2\text{In}_2\text{S}_3\text{Se}$ ,  $\text{TlInSSe}$  and  $\text{Tl}_2\text{In}_2\text{SSe}_3$  undoped layered single crystals by PL

and TSC techniques since impurity and defect centers in the crystal are important to fabricate high-quality optoelectronic devices. In addition to these measurements, transmission and reflection measurements were performed to make crystal characterization. Besides, energy dispersive spectroscopic analysis and X-ray diffraction analysis were used to determine the atomic composition ratio and lattice parameters of crystals studied, respectively.

## CHAPTER 2

### THEORETICAL APPROACH

A semiconductor is a material that has an electrical resistivity between that of a conductor and an insulator in the range of  $10^{-2}$  to  $10^9$  ohm-cm at room temperature. Conductivity in semiconductors is strongly depend on temperature. If we define an insulator as having a resistivity above  $10^{14}$  ohm-cm, a pure semiconductor can be act as an insulator at absolute zero temperature. In addition to heat, under the effect of light and voltage, semiconductors can act as conductors. In semiconductors, current flow by either electrons or positively charged particles "holes" whereas in metallic conductors current flow by only electrons. The conductivity of a semiconductor material can changed by adding other elements, called "impurities". Some electronic devices such as transistors, switches, diodes, photovoltaic cells, detectors and thermistors produced by semiconductors are very important in electronic device technology. They may be used as single circuit elements or as components of integrated circuits. Therefore it is very important to investigate and understand fundamentals of semiconductor materials [31].

The aim of this chapter is to give basic information about semiconductors and theoretical information for the experiments used for to understand basic properties of semiconductors.

#### 2.1 Theoretical Approach to Semiconductor Physics

##### 2.1.1 Band Structure in Semiconductors

In a single isolated atom, electrons occupy atomic orbital. The electrons in the atomic orbital form a discrete set of energy levels. In a molecule that is formed by several atoms, atomic orbitals split as in a coupled oscillation. This causes a number of molecular orbitals which are

directly proportional to the number of atoms in the molecule. When a number of molecules brought together to form a solid the number of orbitals becomes very small. These energy levels in orbitals may be considered to form continuous bands of energy. In an energy band, energy levels can be considered as continuous rather than discrete energy levels since the separation between energy levels is comparable with the energy that electrons constantly exchange with phonons ( atomic vibrations ). It is also comparable with the energy uncertainty due to the Heisenberg principle. It means that, the energy bands correspond to a large number of discrete quantum states of electrons. Most of these states with low energy are full up to a particular band called the valance band. If there is enough energy to move electrons from valence band to the uppermost, almost unoccupied band called the conduction band, current can flow. Electrons gain enough energy to jump to the conduction band by absorbing either a phonon (heat) or a photon ( light). The energy difference between the top of the valence band and the bottom of the conduction band is called energy gap or band gap (figure 2.1).

In crystalline materials, the occupancy of each band is described by the density of states function [32]

$$N(E) = Z(E)f(E), \quad (2.1)$$

where  $N(E)$  is the density of occupied energy levels,  $Z(E)$  is the density of available energy states and  $f(E)$  is the Fermi-Dirac distribution function given by

$$f(E) = \frac{1}{\exp[\frac{(E-E_f)}{kT}] + 1}, \quad (2.2)$$

where  $E_f$  is the Fermi level or chemical potential,  $k$  is the Boltzmann's constant and  $T$  is temperature . At absolute zero, the energy levels lying below the Fermi energy level are completely full. For semiconductors and insulators Fermi energy is above the uppermost valence energy so it is impossible to obtain a net transport of charge in the valence band in the direction of the applied electric field. As a result of this, these materials are non-conductors at absolute zero.

To understand the difference between conductors, insulators and semiconductors, band gap of these materials are shown in figure 2.2. In insulators the electrons in the valence band are separated by a large gap from the conduction band and the allowed energy bands are either filled or empty. In conductors the valence band overlaps the conduction band and one or more

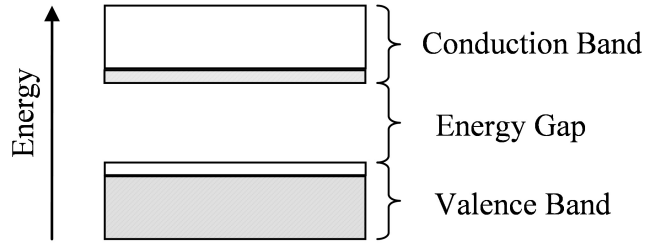


Figure 2.1: An energy band diagram for semiconductors.

bands are partly filled between 10 and 90 percent. The electron concentration is of the order of  $10^{23} \text{ cm}^{-3}$ . In semiconductors there is small enough energy gap smaller than 3 eV between the valence and conduction band and one or two bands slightly filled or slightly empty. The density of electrons in the upper band is usually less than  $10^{20} \text{ cm}^{-3}$ .

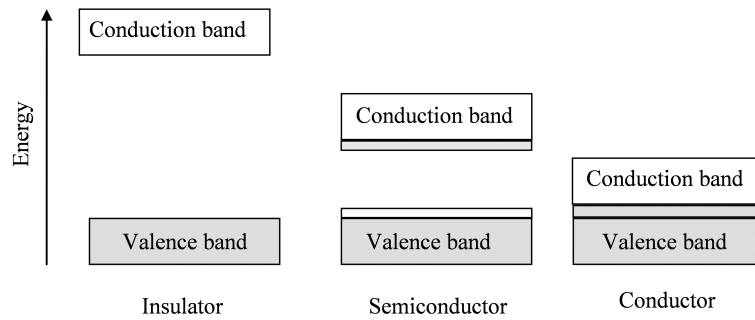


Figure 2.2: Schematic electron occupancy of allowed energy bands for an insulator, semiconductor and conductor.

To understand the band structure of crystals, carbon atoms in the diamond crystals can be investigated as an example. Energy bands of carbon in the diamond structure are shown in figure 2.3 and figure 2.4. In the s level ( $l = 0$ ), there are two atomic states coming from two different spin orientations. In the p level ( $l = 1$ ), there are six atomic states. Three different values for  $m$  ( $m = -1, 0, 1$ ) and two different spin orientations for each  $m$ . If we assume that there are  $N$  carbon atoms in a diamond crystal, the number of quantum states for 2s and 2p states are  $2N$  and  $6N$ , respectively. At large interatomic distances, the four valence electrons ( $1s^2 2s^2 2p^2$ ) are divided such as 2s band completely filled and 2p band one-third filled as diamond has 6 electrons, 4 of them are valence electrons. At smaller distances,  $8N$



quantum states split equally between the lower band called the valence band and upper band called the conduction band.

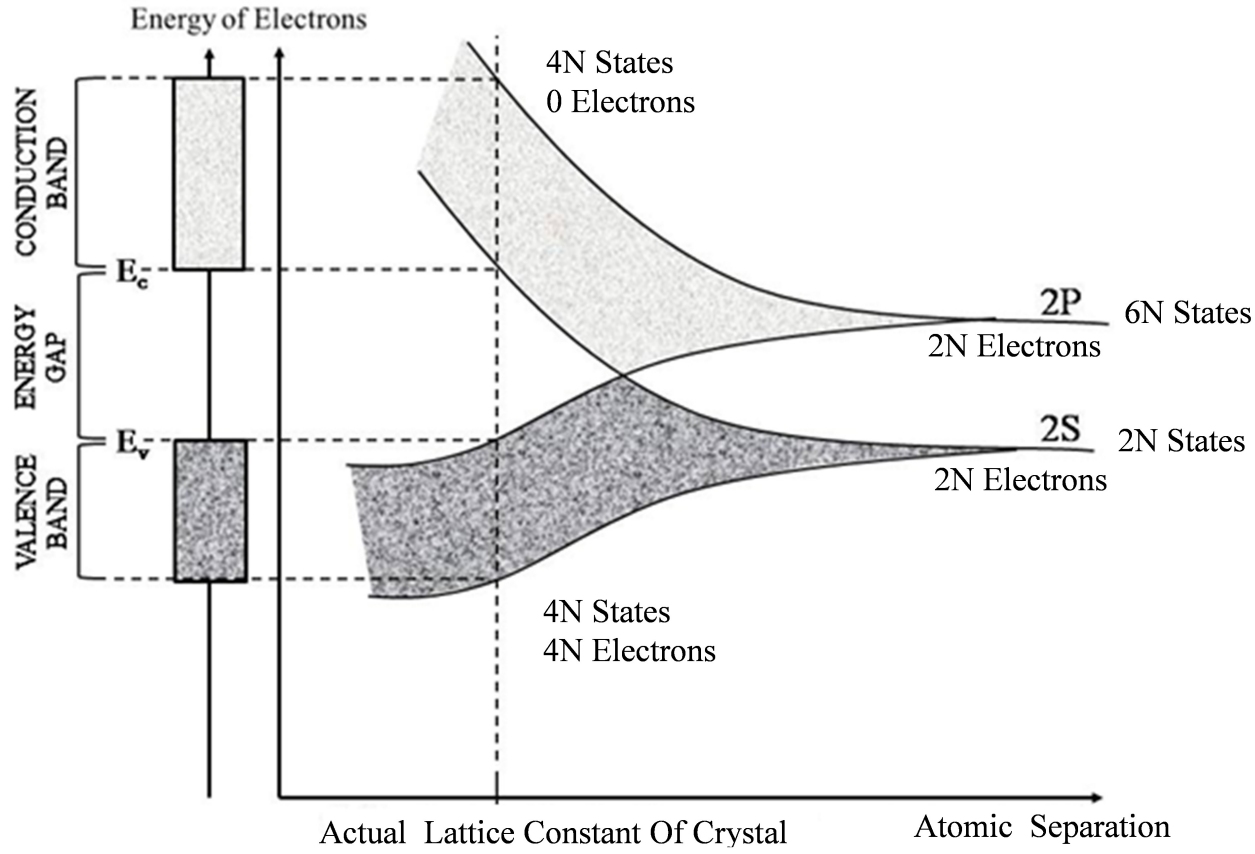


Figure 2.3: Energy levels in a diamond as a function of atomic distance.

Band gap energy has been defined in real space, now some information how the allowed states are distributed in momentum space can be given. Momentum space consideration is very important for optical transitions (direct and indirect transitions) which will be investigated in other chapters.

The kinetic energy of an electron is

$$E = \frac{p^2}{2m^*}, \quad (2.3)$$

where  $p$  is the momentum of electron,  $m^*$  is the effective mass of electron. From quantum

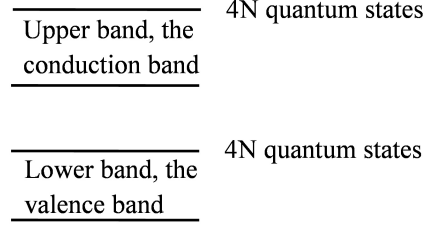


Figure 2.4: Energy bands of diamond crystal. Energy band separated into two groups, valence band and conduction band and each of bands contain  $4N$  states.

mechanics we have the following equation:

$$p = k\hbar, \quad (2.4)$$

where  $\hbar$  is Dirac's constant and  $\hbar = \frac{h}{2\pi}$ ,  $h$  is Planck's constant;  $k$  is the wave vector. If the crystal is considered as in a square well potential with an infinite barrier with a bottom width  $L$ , it can have the discrete values

$$k = \frac{n\pi}{L}, \quad (2.5)$$

where  $n$  is any integer different from zero. The kinetic energy of the electron can be written as

$$E = \frac{k^2 \hbar^2}{2m^*}. \quad (2.6)$$

If the crystal is a cube with length  $L$ , the allowed energies are

$$E = \frac{\hbar^2 \pi^2}{2m^* L^2} (n_x^2 + n_y^2 + n_z^2). \quad (2.7)$$

$E$  can be considered as discrete because of the quantum numbers  $n$  are integers. But  $E$  appears as a quasi-continuum as the energy steps are so small. It is  $10^{-18}$  eV for a  $1 \text{ cm}^3$  crystal.

Now, let us consider variation of energy with momentum along one direction of momentum space. Figure 2.5 shows the parabolic dependence of  $E$  and  $k$ . It is called a parabolic valley because of its distribution.

To define the energy gap, the top of the valence bands can be taken as the reference level. Then, the bottom of the conduction band can be thought as localized at a higher potential. The potential corresponds to energy gap. The valence band and conduction band in momentum space is shown in figure 2.6.

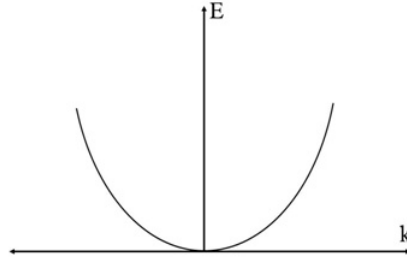


Figure 2.5: Parabolic dependence of energy vs. momentum.

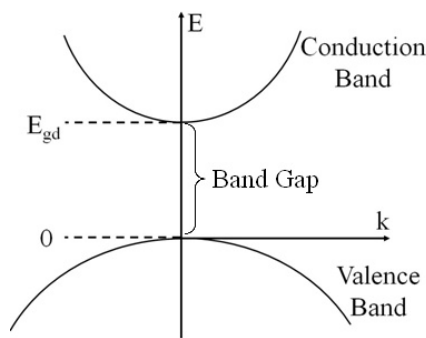


Figure 2.6: Energy vs. momentum in a direct-gap two-band system, where  $E_{gd}$  is the energy of direct band gap.

The shape of a constant-energy surface must deviate from that of a perfect sphere since nearest atoms varies in different directions. As a result of this the interactions between nearest neighbors, the minimum of the valley may occur not at  $k_x = k_y = k_z = 0$  but at some point such as [111] crystallographic direction (figure 2.7).

### 2.1.2 Direct and Indirect Band Gap Materials

There is a big difference between direct and indirect band gap materials. In a direct gap material, both the conduction band minimum and the valence band maximum occur at the zone center where  $k = 0$  where as in an indirect gap material, the conduction band minimum does not occur at  $k = 0$ . If there is enough energy exceeding the band gap energy  $E_g$  of the material, electrons are excited from valence band to the conduction band (see figure 2.8).

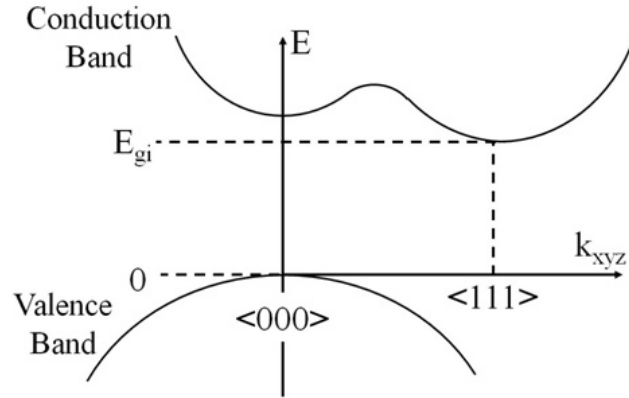


Figure 2.7: Energy vs. momentum diagram for a semiconductor with valleys at  $k = <000>$  and  $k = <111>$  directions.

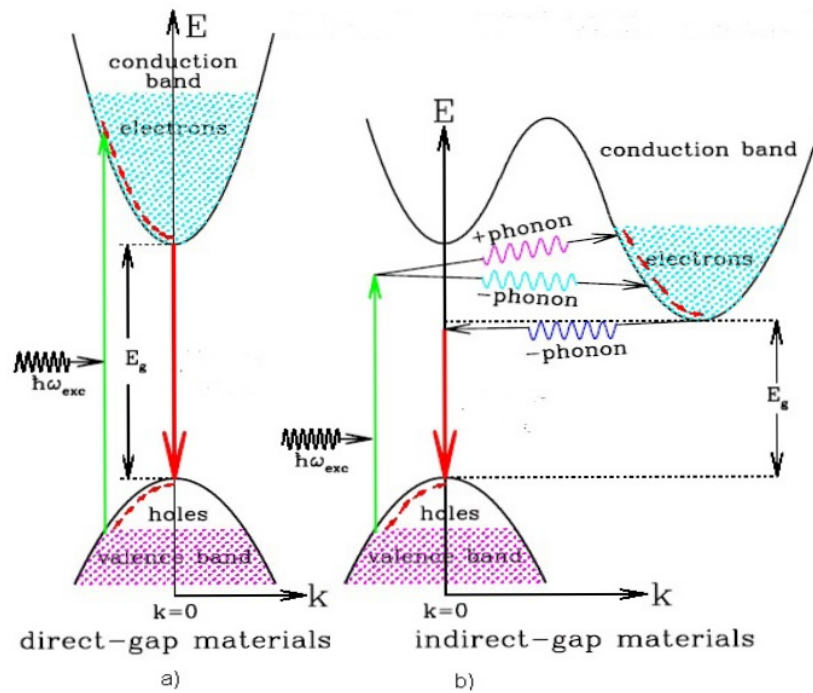


Figure 2.8: a) In a direct band gap material the conduction band minimum and valence band maximum occur at the same  $k$  values b) In an indirect band gap material the conduction band minimum and valence band maximum occur at different  $k$  values [33].

Energy and momentum must be conserved in a photon absorption process for indirect band gap materials. In a direct band gap material there is momentum conservation. Photoexcitation of electron occurs if it only involves a UV or visible photon. The wavevector of the absorbed

photon is negligible compared to wavevector of electron. This means that the electron wave vector does not change during a photon absorption in direct band gap materials.

In an indirect band gap materials, momentum conservation occur if only there is a phonon absorption or emission. Since the electron absorption can not provide the required momentum change which is  $|\vec{k}_{phot}| \ll |\vec{k}_i - \vec{k}_f|$ , where  $k_{phot}$  is the wave vector of photon,  $k_i$  and  $k_f$  are initial and final wavevectors of electrons to jump from the valence band to the conduction band, the electron wave vector must change.

### 2.1.3 Intrinsic and Extrinsic Semiconductors

In electronic conduction in semiconductors the two bands, conduction band and valence band, play very important role. Electronic conduction is possible if both electrons and vacant states are available in the same band. At absolute zero there are only electrons in the valence band and there are only vacant states in the conduction band. As a result of this situation, there is no electron conduction.

At a finite temperature, electrons are excited from valence band into conduction band. It creates electrons in the conduction band and vacant states in valence band. This process is indicated in figure 2.9. Now, electronic conduction is possible since there are electrons in an almost empty conduction band and holes in an almost-filled valence band. We have

$$p = n, \quad (2.8)$$

where  $p$  and  $n$  are hole and electron concentrations, respectively. Some semiconductors are called intrinsic semiconductors where there are free carriers as a result of thermal excitation.

If there are impurity atoms or structural defects in a crystal, there is a breakdown in the periodicity of the crystalline structure and it becomes possible for electrons to possess energies. One result of this is the generation of new optical absorption bands, sometimes giving the crystal a coloured appearance.

To explain the impurity states in a crystal, Ge and Si are good examples. If atoms of the elements ( such as phosphorus, arsenic and antimony) having five valence electrons with an  $s^2p^3$  electron configuration substitute a silicon or germanium atom, only four valence

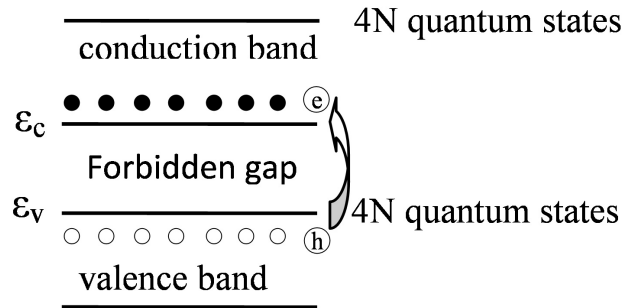
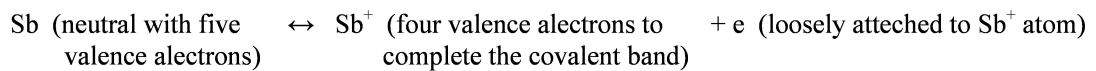


Figure 2.9: Intrinsic conductivity occurs in a semiconductor as a result of thermal excitation of electrons from the valence band to conduction band.

electrons form the covalent bond with neighboring Si or Ge atoms. One electron is relatively free to move in the crystal. This situation can be summarized as follows:



The various energies  $\epsilon_c$ ,  $\epsilon_v$  and  $\epsilon_d$  are the energy of the conduction-band edge, the energy of the valence-band edge and the energy of the donor level, respectively. The word "donor" refers to those impurities that are capable of donating an excess electron to the conduction band. The donor ionization energy is  $\epsilon_c - \epsilon_d$ . This energy is needed for the excess electron from Sb atom. If the thermal energy  $kT$  is sufficiently large compared to the donor ionization energy, practically all donors can be ionized. The donors give their electrons to the conduction band. This process is indicated in figure 2.10 and figure 2.11.

If atoms of the elements (such as boron, aluminum, gallium and indium) having three valence electrons with an  $s^2p$  electron configuration substitute a silicon or germanium atom, four valence electrons form the covalent bond with neighboring Si or Ge atoms. In order to complete the covalent bond, one electron must be accepted somewhere with neighboring Si atoms. The hole is created as a result of the missing electron. This process can be summarized as follows:

As a summary electrons in donor states jump into conduction band when there is thermal

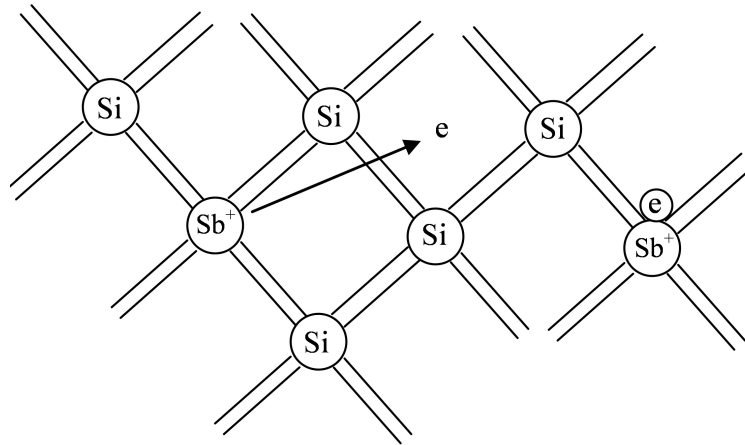


Figure 2.10: Substitution of antimony atom into silicon. Antimony atoms act as donor impurity.

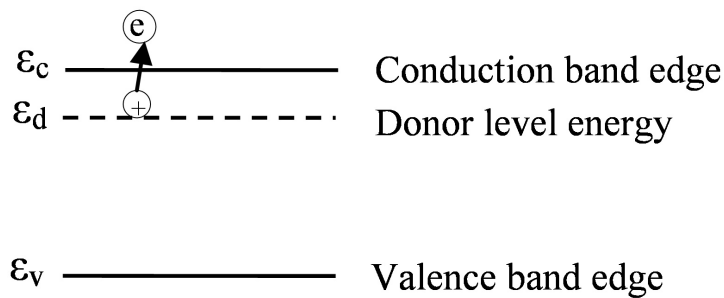
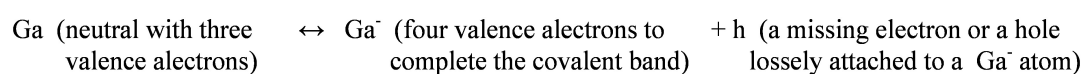


Figure 2.11: Energy levels of Si created by substitution of antimony atoms.

excitation and they become free carriers. These electrons ionized from donor states contribute to electric conduction since there are many vacant states. On the other hand, the acceptors need an electron to complete the covalent band. The acceptors can capture the electron from the valence band. After the electron excess, vacant state stay in the valence band. As a result of this, electrons in the valence band can move. Electrons in the acceptor level energy contribute the electric conduction. The vacant states in the valence band are called holes. This process is indicated in figure 2.12 and figure 2.13. Therefore, electric conduction is carried by electrons in the conduction band and holes in the valence band. If in a semiconductor, current



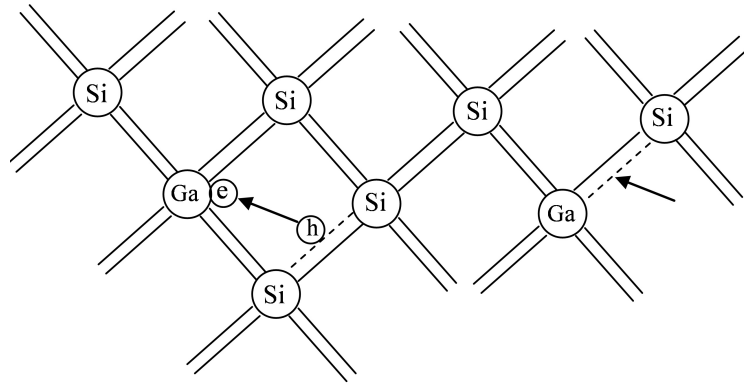


Figure 2.12: Substitution of gallium atom into silicon. Gallium atoms act as acceptor impurity.

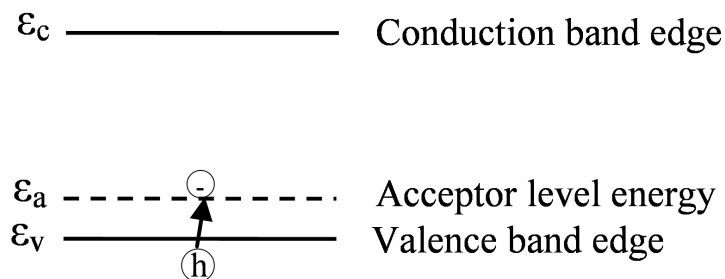


Figure 2.13: Energy levels of Si created by substitution of gallium atoms.

carriers are predominantly electrons, it is called n type semiconductor. If the current carriers are predominantly holes, it is called p type semiconductor. The term n type refers to charge carriers type, negative type meaning electrons and p type refers to positive type meaning holes. The dominance of one type of carriers is caused by substitution foreign atoms ( impurities ) to the semiconductor. Such semiconductors are called extrinsic semiconductors. Without impurities, where  $p=n$ , these type of semiconductors are called as intrinsic semiconductors.

#### 2.1.4 Structural Defects in Semiconductors

Defects are very important for modern science and technology. To mention the areas of defects, batteries, fuel cells displays, data storage and computer memories are some examples for them. A defect can be considered as mistake. The mistake could be a missing atom or an



impurity in a normal atom [34].

Defects are usually associated with crystalline solids because of regular repetition of atoms throughout its volume. A disturbance in this regularity causes the defect. Although crystal type, concentration and distribution are controlled in laboratory, they may have defects. Some properties such as density and elastic constants are proportional to the concentration of defects. Very small concentration of defect have very small effect on these properties. Other properties such as conductivity of a semiconductor crystal, may be more sensitive to the presence of small numbers of defects.

A point defect in a semiconductor is represented as an energy level on band diagrams. Energy levels lying in the band gap are very important for electronic and optical properties. The effect of these impurities on the electronic properties of semiconductor depend on the how closer to the bottom of the conduction band or top of the valence band. The energy levels lie near the valence and conduction band are called shallow levels. If they lie near to the center of the band gap they are called as deep levels.

Shallow levels are very important for electronic conductivity. Shallow donor levels are close to the conduction band to produce n-type semiconductor whereas shallow acceptor levels are close to the valence band to produce p-type semiconductor.

The same considerations may apply to vacancies. Donor levels are created as a result of anion vacancies and this causes n-type semiconductors. Acceptor levels are created as a result of cation vacancies and this causes p-type semiconductors.

## **2.2 Theoretical Approach to Experiments**

### **2.2.1 X-Ray Diffraction Experiment**

X-rays were discovered by the German Physicist Roentgen in 1895. They were named as X-rays since their nature was not known at that time. X-rays have the same nature as light but they have very much shorter wavelength. X-rays have the wavelength 10 to 0.01 nm and energies 120 eV to 120 keV. X-rays used in diffraction have wavelengths lying approximately in the range of 0.05-0.25 nm. In 1912, the X-ray diffraction (XRD) was discovered. After the discovery, the nature of the X-rays were proved clearly.

X-rays are produced when any electrically charged particle of sufficient kinetic energy is rapidly decelerated. In general, electrons are used for this purpose. X-ray tube contains two metal detectors and a source of electrons. The high voltage (some tens of thousands of volts) is created between these detectors and as a result of this, electrons strike in a very high speed to the target. X-rays are produced at the point of impact and radiate in all directions.

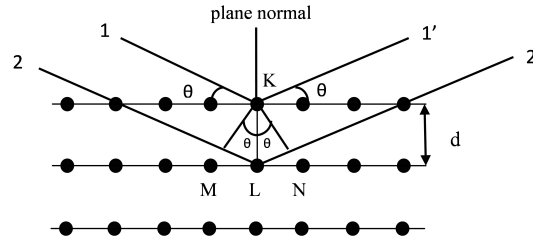


Figure 2.14: Representation of X-ray diffraction by a crystal lattice.

When X-rays strike a crystal, they will be diffracted by the crystal. A diffracted beam may be defined as a beam composed of a large number of scattered rays mutually reinforcing one another. Atoms in the crystal scatter incident X-rays in all directions and in some of these directions the scattered beams will be completely in phase. In figure 2.14 the deflection of incident X-rays are shown. If rays 1 and 2 are scattered by atoms K and L, the path difference for rays 1K1' and 2L2' is

$$ML + LN = d \sin \theta + d \sin \theta = 2d \sin \theta. \quad (2.9)$$

Scattered rays 1' and 2' will be completely in phase if the path difference is equal to a whole number  $n$  of wavelengths, or if

$$n\lambda = 2d \sin \theta. \quad (2.10)$$

This relation was first formulated by W. L. Bragg and it is known as the Bragg law [35] where  $n$  is the order of reflection; it may be take any integral value,  $\lambda$  is the wavelength of the X-rays,  $\theta$  is Bragg angle between the incident beam and the particular crystal planes,  $d$  is the interplanar spacings [36]. After XRD analysis, the information is obtained about crystal lattice structure such as interplanar spacings ( $d$ ), lattice constants ( $a$ ,  $b$  and  $c$ ), the Miller indices ( $h$ ,  $k$  and  $l$ ) and the angles ( $\alpha$ ,  $\beta$  and  $\gamma$ ).

Table 2.1 shows the seven types of cells and corresponding formulas of interplanar spacings, lattice constants, Miller indices and the angles for lattice structures.

Table 2.1: Seven types of crystal cells and corresponding formulas for interplanar spacings [37].

System	a: b: c	Axial Angles	$d_{hkl}$
1. Cubic	1: 1: 1	$\alpha = \beta = \gamma = 90^\circ$	$\frac{a_0}{\sqrt{h^2+k^2+l^2}}$
2. Tetragonal	1: 1: c	$\alpha = \beta = \gamma = 90^\circ$	$\frac{a_0}{\sqrt{h^2+k^2+\frac{l^2}{c^2}}}$
3. Orthorhombic	a: 1: c	$\alpha = \beta = \gamma = 90^\circ$	$\frac{b_0}{\sqrt{\frac{h^2}{a^2}+k^2+\frac{l^2}{c^2}}}$
4. Hexagonal	1: 1: c	$\alpha = \beta = 90^\circ, \gamma = 120^\circ$	$\frac{a_0}{\sqrt{\frac{4}{3}(h^2+hk+k^2)+\frac{l^2}{c^2}}}$
5. Rhombohedral	1: 1: 1	$\alpha = \beta = \gamma \neq 90^\circ$	$\frac{a_0 \sqrt{1+2 \cos^3 \alpha - 3 \cos^2 \alpha}}{\sqrt{(h^2+k^2+l^2) \sin^2 \alpha + 2(hk+hl+kl)(\cos^2 \alpha - \cos \alpha)}}$
6. Monoclinic	a: 1: c	$\alpha = \gamma = 90^\circ, \beta \neq 90^\circ$	$\frac{b_0}{\sqrt{\frac{(h/a)^2+(\frac{l}{c})^2-2\frac{hl}{ac} \cos \beta}{\sin^2 \beta}+k^2}}$
7. Triclinic	a: 1: c	$\alpha \neq \beta \neq \gamma \neq 90^\circ$	$\frac{b_0}{\sqrt{\begin{vmatrix} \frac{h}{a} & \frac{h}{a} \cos \gamma & \frac{h}{a} \cos \beta \\ k & 1 & \cos \alpha \\ \frac{l}{c} & \cos \alpha & 1 \end{vmatrix} + k^2 \begin{vmatrix} 1 & \cos \gamma & \cos \beta \\ \cos \gamma & 1 & \cos \alpha \\ \cos \beta & \cos \alpha & 1 \end{vmatrix}}}$

### 2.2.2 Energy Dispersive Spectral Analysis (EDSA) Experiments

Energy dispersive spectral analysis (EDSA) is also called as energy X-ray dispersive spectroscopy (EDS) is used to analyze the elements of the crystal or chemical characterization. It is based on X-ray Fluorescence emission of the characteristic X-rays coming from the crystal. The crystal is excited by high energy X-rays, gamma rays or high energetic particles such as electrons and protons. The incident beam coming to the atoms of the crystal may eject the electron from the inner shell. The electron in the outer shell fill the hole created by ejected electron. The energy difference between these two shells may be released in the X-ray form. The X-ray created by the energy difference between the two shells is called characteristic X-rays. The number and energy of X-rays emitted from the specimen can be measured by an EDS system. As a result of this analysis the elemental composition of the crystal can be identified. Since every elements have their own atomic structure and allow characteristic X-rays. It helps to identify the element from the others.

There are a number of EDS systems exist but mainly the set up consists of four primary components : the beam source; the X-ray detector; the pulse processor; and the analyzer. But in general, EDS systems are found on scanning electron microscopes. The main equipments for scanning electron microscopes are a cathode and magnetic lenses. Cathode is used to create electrons having energy from a few hundred eV to 40 keV and magnetic lenses are used to focus a beam of electrons. These lenses focused to a spot about 0.4 nm to 5.0 nm in diameter. A detector is used to convert X-ray energy into voltage signals after that this information is sent to a pulse processor, which measures the signals and passes them onto an analyzer for data display and analysis.

### 2.2.3 Optical Absorption, Transmission and Reflection Spectroscopy

Ultraviolet-Visible-Near Infrared spectroscopy is useful to characterize the absorption, transmission and reflectivity of a variety of technologically important materials such as pigments, coatings, windows and filters. This application is very important for characterization of the optical or electronic properties of materials.

#### 2.2.3.1 Absorption

Absorbance spectroscopy is generally called as spectrophotometry. In this technique, the amount of light which is absorbed by a sample at a given wavelength is measured. Absorption occurs in a semiconductor when incoming light energy is higher than the band gap energy of the semiconductor. Electrons in the lower energy states are excited by the incoming light energy and transfer to the upper energy states. Some incoming light energy is absorbed by the semiconductor. The light intensity passes through the semiconductor can be explained by using the Lamber-Beer-Bouger Law [38, 39]

$$I = I_0 \exp(-\alpha d), \quad (2.11)$$

where  $I_0$  is incident light intensity,  $I$  is the light intensity after propagation from the sample having thickness  $d$  and  $\alpha$  is the absorption coefficient which is related to the transition probabilities between the electronic energy levels in the material. It can be defined as,

$$\alpha = \frac{4\pi k}{\lambda}. \quad (2.12)$$

Here  $k$  is the absorption index of the material and  $\lambda$  is the light wavelength. The dependence of the absorption on photon energy  $h\nu$  and band gap energy  $E_g$  of the material are expressed in the following equation [40]

$$\alpha h\nu = A(h\nu - E_g)^p, \quad (2.13)$$

where  $A$  is constant depends on the transition probability and  $p$  is an index which characterizes the optical absorption process. The value of  $p$  is generally equal to 2 and 1/2 for indirect and direct transitions, respectively.

### 2.2.3.2 Reflection

Reflection spectroscopy is the study of light has been reflected from a solid, liquid or gas. The reflection coefficient is the ratio of reflected wave intensity to that of the incident wave intensity. The reflection coefficient for normal incident of light is given by [1]

$$r = \frac{1 - n^*}{1 + n^*} = \frac{1 - n + ik}{1 + n - ik}. \quad (2.14)$$

Here  $n^*$  is the complex refractive index and defined as

$$n^* = n - ik, \quad (2.15)$$

where  $n$  is refractive index of an optical or dielectric medium.

The reflectance  $R$  is then defined by Fresnel equation

$$R = |r|^2 = \left| \frac{1 - n + ik}{1 + n - ik} \right|^2 = \frac{(1 - n)^2 + k^2}{(1 + n)^2 + k^2}. \quad (2.16)$$

At angles other than normal, the reflectance is a complex trigonometric function involving the polarization direction of the incident beam. When absorption index is zero the reflectance becomes

$$R = \frac{(1 - n)^2}{(1 + n)^2}. \quad (2.17)$$

### 2.2.3.3 Transmission

Transmission spectroscopy is the study of the light that has been passed through the solid, liquid or gas. In the Lambert-Beer-Bauguer Law (see equation 2.11) the term  $I/I_0$  is called

transmittance. The overall transmission is given by [41]

$$T = \frac{(1 - R)^2 \exp(-\alpha d)}{1 - R^2 \exp(-2\alpha d)}. \quad (2.18)$$

If  $\alpha d$  is large the second term in the denominator can be neglected; then

$$T \approx (1 - R)^2 \exp(-\alpha d). \quad (2.19)$$

The relation in equation 2.19 can be solved for  $\alpha$ , if  $R$  and  $d$  are known. If  $R$  is not known, the transmittance of two samples having different thicknesses  $d_1$  and  $d_2$  can be measured. Then  $\alpha$  is obtained from

$$\frac{T_1}{T_2} \approx \exp(-\alpha(d_2 - d_1)), \quad (2.20)$$

where  $T_1 = \frac{I_1}{I_0}$  and  $T_2 = \frac{I_2}{I_0}$ . It is clear that  $\frac{T_1}{T_2}$  is equal to  $\frac{I_1}{I_2}$  and does not depend on incident intensity of light.

Further, if the sample thickness is known and is thin enough to create interference fringes in the transmission spectra, the refractive index of the sample can be determined using the following equation

$$n = \frac{1}{(\frac{1}{\lambda_2} - \frac{1}{\lambda_1})2d}, \quad (2.21)$$

where  $\lambda_1$  and  $\lambda_2$  are the wavelengths at which two adjacent maxima occur and  $d$  is the sample thickness.

The refractive index can be expressed in terms of photon energy  $h\nu$ , the simple oscillator energy  $E_{s0}$  and the dispersion energy  $E_d$ , which is a measure of the strength of interband optical transition, by the relation

$$n^2(h\nu) = 1 + \frac{E_{so}E_d}{E_{so}^2 - (h\nu)^2}. \quad (2.22)$$

In the above expression the refractive index absorption data is analyzed in  $h\nu < E_g$  range according to the single-effective-oscillator model which was proposed by Wemple and DiDomenico [42, 43].

Plotting  $(n^2 - 1)^{-1}$  versus  $(h\nu)^2$  allows the determination of the lower parameters by fitting a linear function to the lower energy data range. The zero-frequency refractive index  $n_0$  is obtained on the expression

$$n_0^2 = 1 + \frac{E_d}{E_{so}}. \quad (2.23)$$

The oscillator energy  $E_{so}$  is an "average" energy gap and it is approximately equals to two times of the lowest direct band gap  $E_{gd}$  ( $E_{so} \approx 2.0E_{gd}$ ) [44]-[47].

The oscillator strength  $S_{so}$  can be found by the refractive index analysis. The refractive index at low energies can be represented by a single Selmeir oscillator [48]

$$\frac{(n_{\infty}^2 - 1)}{(n^2 - 1)} = 1 - \left(\frac{\lambda_{so}}{\lambda}\right)^2. \quad (2.24)$$

Here  $\lambda_{so}$  is the oscillator wavelength and  $n_{\infty}$  is the infinite wavelength refractive index. The above equation can be rewritten in terms of  $S_{so} = (n_{\infty}^2 - 1)/\lambda_{so}^2$  as

$$(n^2 - 1)^{-1} = \frac{1}{S_{so}\lambda_{so}^2} - \frac{1}{S_{so}\lambda^2}. \quad (2.25)$$

$S_{so}$  and  $\lambda_{so}$  can be obtained as a result of  $(n^2 - 1)^{-1}$  vs  $\lambda^{-2}$  analysis.

#### 2.2.4 Photoluminescence Experiments

When a material is exposed to radiation, some of the energy may be absorbed and re-emitted as light of a longer wavelength (Stoke's Law). This is the process of luminescence. The re-emitted light is related to the characteristic of the material.

There are various luminescence types. The names are given them according to their type of excitation. Some of the luminescence types are photoluminescence (excited by optical or ultra-violet light), radioluminescence (excited by nuclear radiations, i.e.,  $\gamma$  rays,  $\beta$  rays, X-rays, etc.) and cathodoluminescence (electron beam). Luminescence can be created by not only radiation but also chemical energy (chemiluminescence), mechanical energy (triboluminescence), electrical energy (electroluminescence), biochemical energy (bioluminescence) and sound waves (sonoluminescence) [32].

Photoluminescence (PL) process is the inverse of the absorption process of photons. The electrons in the ground state may be excited by photons to the allowed excited states. When they combine from the excited states to the ground states, the excess energy is in the form of radiative.

There are mainly three steps in PL [49]

- (i) Firstly, there is an excitation step creating electron and hole pairs by photons.

(ii) Secondly, there is a thermalization step. In this step excited electron and hole pairs relax towards quasi-thermal equilibrium distributions.

(iii) Finally, there is a recombination step. In this step, thermalized pairs recombine radiatively (PL occurs) (figure 2.15).

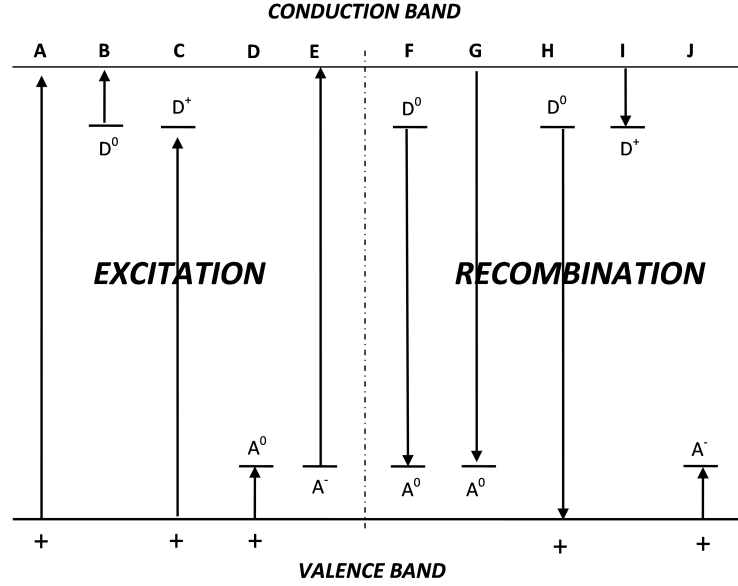


Figure 2.15: Excitation and recombination process in a PL experiment.

The most important step dealing with us is the recombination step since the emission process occur and it gives us information about some characteristic features of studied materials.

#### 2.2.4.1 Recombination Mechanisms

There are mainly three types of optical transitions that occur in the semiconductors when they are excited by photons.

##### i) Band to band transitions

An electron occupying a higher energy state can make a transition to an empty lower-energy state and the energy difference between the two states can be emitted as electromagnetic radiation. These types of transitions are sometimes called as free to free transitions since this



process occurs between free electrons and holes. The radiation rate created by the transition from upper states to the lower states is determined by the probability  $P_{ul}$  for 1 carrier/cm<sup>3</sup> in the upper state to make a radiative transition to 1 vacancy/cm<sup>3</sup> in the lower state:

$$R = n_u n_l P_{ul}. \quad (2.26)$$

The above equation is similar to the equation for absorption coefficient

$$\alpha(h\nu) = A \sum (P_{if} n_i n_f), \quad (2.27)$$

where  $\alpha$  is the absorption coefficient for a given photon energy  $h\nu$ ,  $P_{if}$  is the probability for transition from the initial state to the final states,  $n_i$  is the density of the electrons in the initial state and  $n_f$  is the density of the available (empty) final states.

In a direct-gap semiconductors, the radiated photon energy is given by the equation:

$$h\nu = E_u - E_l, \quad (2.28)$$

where  $E_u$  is the upper state energy and  $E_l$  is the lower state energy (figure 2.16). Threshold emission energy is  $h\nu = E_g$  where  $E_g$  is the direct band gap of the semiconductor. In an

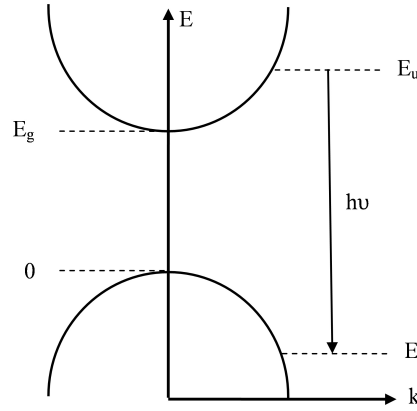


Figure 2.16: Direct band to band transition.

indirect band-gap semiconductors, the radiated photon energy is given by the equation:

$$h\nu = E_u - E_l \pm E_p, \quad (2.29)$$

where  $E_p$  is the energy of the phonon (figure 2.17). The threshold emission energy is  $h\nu = E_g - E_p$  for indirect band gap semiconductors.

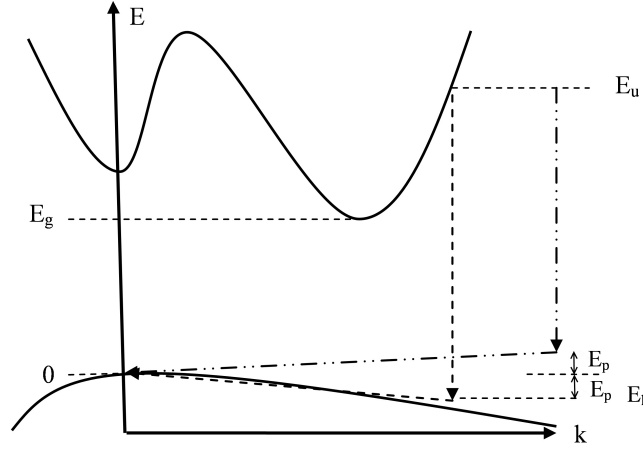


Figure 2.17: Indirect band to band transition.

## ii) Free to Bound Transition

a) Shallow Transitions: The shallow transitions to neutralize donors and acceptors are shown in figure 2.15.I and figure 2.15.J, respectively. These transitions could be radiative in far field infrared.

b) Deep Transitions: Deep transitions occur between electrons in the conduction band and acceptor state or valence band and donor state (figure 2.15.G and figure 2.15.H). Deep transitions emit a photon  $h\nu = E_g - E_i$  for direct transitions and  $h\nu = E_g - E_i - E_p$  for indirect transitions having a photon energy  $E_p$ , where  $E_i$  is the energy level lying for acceptors or donors and  $E_g$  is the band gap energy.

## iii) Donor-Acceptor Transitions

Donor and acceptor transitions are shown in figure 2.15.F) and in figure 2.18. When both donor and acceptor impurities are present in a semiconductor, coulomb interaction between donor and acceptor modifies the binding energies such that energy separating the paired donor and acceptor states is (see figure 2.19),

$$h\nu = E_g - E_a - E_d + \frac{q^2}{\epsilon r}. \quad (2.30)$$

For distant pairs the coulomb interaction term  $\frac{q^2}{\epsilon r}$  is very small. As a result of this, the lowest possible photon energy is obtained in case of there is no phonon emission.

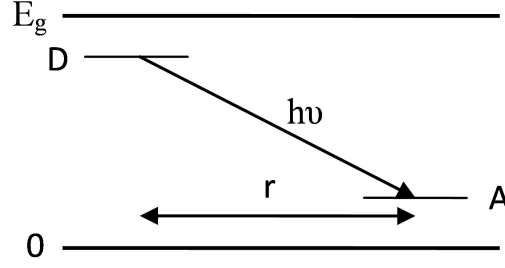


Figure 2.18: Donor to acceptor transition.

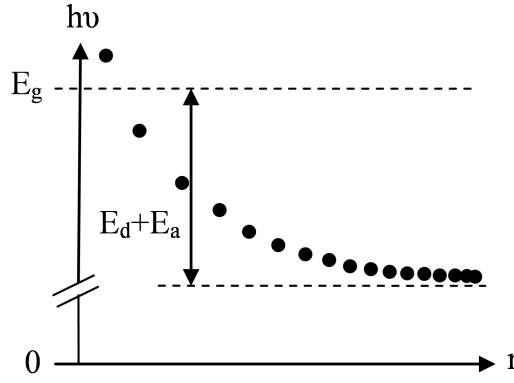


Figure 2.19: Effect of coulomb interaction on emission energy ( $r$  is the donor-acceptor separation).

If the impurities are separated by distances greater than the effective Bohr radius, the transition occur by a tunneling process. A transition between distant pairs is more probable than a transition between nearer pairs. Therefore, while pair separation decreases, the emission intensity decreases as  $r$  decreases.

#### 2.2.4.2 Laser Excitation Power Dependence of Photoluminescence of Semiconductors

The dependence of the laser excitation power with the PL intensity gives information about recombination mechanisms. The relation between PL intensity and laser excitation power is following [50]-[53]

$$I \propto L^\gamma, \quad (2.31)$$

where  $I$  is PL intensity,  $L$  is laser excitation power and  $\gamma$  is a constant. If the  $\gamma$  values are between 1 and 2, it shows free- and bound- exciton emission, whereas if the  $\gamma$  values are between 0 and 1, means that free to bound and donor-acceptor pair recombination [54, 55].

Not only dependence of the peak intensity with laser excitation power is important to obtain information about recombination process but also dependence of the peak energy with laser excitation power is very important. Before saying the importance, the relation for the laser power and peak energy should be presented.

In the work done by E. Zacks and A. Halperin [56], they consider a crystal of dielectric constant  $\epsilon$  with donor and acceptor concentrations  $N_d$  and  $N_a$ , respectively. They assumed that one of the impurities is in minority ( $N_d \ll N_a$ ) and thermal ionization of donors or acceptors is negligible since the temperature of the crystal is low. An ionized donor-acceptor pair of separation  $r$  are created due to pair recombination. Excitation causes by the ionized impurities and turns them back to the neutral state. Recombination of pairs has separation between  $r$  and  $r + dr$  should be proportional to the concentration of neutral minority impurities  $N_d P(r)$  to the number of majority impurities in the volume element  $4\pi r^2 dr$ , and to the rate of recombination of the pairs  $W(r)$  which is,

$$W(r) = \frac{1}{\tau(r)}. \quad (2.32)$$

$\tau(r)$  is lifetime of the pairs. The intensity is

$$I(r) = 4\pi N_a N_d r^2 \frac{P(r)}{\tau(r)}, \quad (2.33)$$

where,  $P(r)$  is fraction of neutral donors. At steady state ,

$$P(r) = \frac{\tau(r)}{\tau(r) + T(r)}, \quad (2.34)$$

where  $T(r)$  is the lifetime of the unexcited pair. Using the equations 2.33 and 2.34 , the intensity is obtained;

$$I(r) = \frac{4\pi N_a N_d r^2}{\tau(r) + T(r)}. \quad (2.35)$$

From the binding energies such that energy separation the paired donor and acceptor states (see section 2.2.4)  $h\nu = E_g - E_d - E_a - \frac{e^2}{\epsilon r}$  and when we take the zero energy as  $E_g - E_d - E_a$ , the energy becomes

$$E(r) = -\frac{e^2}{\epsilon r}, dE = \frac{e^2}{\epsilon r^2} dr, \quad (2.36)$$

so that equation 2.35 becomes,

$$I(E) = \frac{4\pi N_a N_d (\frac{e^2}{\epsilon})^3}{E^4(\tau(E) + T(E))}. \quad (2.37)$$

If there is an assumption such that one of the impurities produces a shallow hydrogenic energy level and the other a much deeper one, the recombination rate is given by the following approximation [57]

$$W(r) = W(0)e^{\frac{-2r}{R_B}}. \quad (2.38)$$

Here,  $W(0)$  is a constant and  $R_B$  is the shallow impurity Bohr radius. Using equation 2.32 and  $E_B = \frac{e^2}{\epsilon R_B}$ , the recombination rate is obtained in terms of energy as

$$W(E) = \frac{1}{\tau(E)} = W(0)e^{\frac{-2E_B}{E}}. \quad (2.39)$$

The dependence of the capture cross section on separation [57]-[59] has been estimated to be

$$\sigma(r) = Ar^2. \quad (2.40)$$

The rate of the excitation has following relation,

$$W_{exc} = \frac{1}{T(r)} = M\sigma(r) = MAr^2, \quad (2.41)$$

where  $T(r)$  is the lifetime of the unexcited pair under the given conditions of excitation,  $M$  is a constant flux which is produced in a steady state by a given intensity of exciting light.

Using equations 2.41, 2.39 and 2.36 and equating to zero the derivative of 2.37 with respect to  $E$  the below equations are obtained as following :

$$\frac{dI}{dE} = 4\pi N_a N_d (\frac{e^2}{\epsilon})^3 [-4E^3(\tau(E) + T(E)) - E^4 \frac{d}{dE}[\tau(E) + T(E)]] = 0 \quad (2.42)$$

$$\frac{d\tau}{dE} = \frac{1}{W_0} (\frac{-2E_B}{E^2}) e^{\frac{2E_B}{E}} = (\frac{-2E_B}{E^2})(\tau E), \quad (2.43)$$

$$\frac{dT}{dE} = (\frac{\partial T}{\partial r})(\frac{\partial r}{\partial E}) = \frac{1}{MA} (\frac{-2}{r^3}) \frac{\epsilon r^2}{e^2} = \frac{-2\epsilon}{r e^2 MA} = \frac{-2\epsilon r}{r^2 e^2 MA} = \frac{2}{r^2 MAE} = \frac{2T}{E} \quad (2.44)$$

$$4[\tau(E) + T(E)] + E[(\frac{-2E_B}{E^2})\tau(E) + \frac{2T}{E}] = 0. \quad (2.45)$$

For the energy of the maximum intensity  $E_m$ ,

$$\tau(E_m)(4 - 2\frac{E_B}{E_m}) + 6T(E_m) = 0, \quad (2.46)$$

$$\frac{T(E_m)}{\tau(E_m)} = \frac{1}{3} \left( \frac{E_B}{E_m} - 2 \right). \quad (2.47)$$

By inserting  $T(E_m) = \frac{(E_m)^2 \epsilon^2}{e^4 MA}$  and  $\tau(E_m) = \frac{1}{W_0} e^{\frac{2E_B}{E_m}}$  which are derived from equations 2.41 and 2.39 into equation 2.47 following equations are obtained, respectively.

$$3T(E_m) = \left( \frac{E_B}{E_m} - 2 \right) \tau(E_m), \quad (2.48)$$

$$\frac{3(E_m)^2 \epsilon^2}{e^4 MA} = \frac{E_B - 2E_m}{E_m} \frac{1}{W_0} e^{\frac{2E_B}{E_m}}, \quad (2.49)$$

$$M = \frac{3\epsilon^2 E_m^3 e^{-\frac{2E_B}{E_m}}}{e^4 A W_0 (E_B - 2E_m)}. \quad (2.50)$$

Since,  $M$  is proportional to the excitation intensity  $J$ , the following equation can be written,

$$J = D \frac{E_m^3}{E_B - 2E_m} \exp \frac{-2E_B}{E_m}, \quad (2.51)$$

where  $D$  is a proportionality factor.

Comparing with experimental results, the measured photon energies is used instead of  $E(r)$ , so that  $E_m = h\nu_m - h\nu_\infty$ . Rewriting equation 2.51 gives

$$J = D \frac{(h\nu_m - h\nu_\infty)^3}{h\nu_B + h\nu_\infty - 2h\nu_m} \exp \frac{-2(h\nu_B - h\nu_\infty)}{h\nu_m - h\nu_\infty}, \quad (2.52)$$

where  $h\nu_B$  is the emitted photon energy of a close donor-acceptor pair separated by  $R_B$ ,  $h\nu_\infty$  is the emitted photon energy of an infinitely distant donor-acceptor pair and  $h\nu_m$  is the emission energy of band maxima.

#### 2.2.4.3 Temperature Dependence of Photoluminescence of Semiconductors

The temperature dependence of PL spectra is used to obtain information about electronic energy levels in crystals. While the temperature of semiconductors are increased, the PL intensity is decreased because of thermal ionization. If the probability of the radiative transitions is assumed to be independent of temperature, the luminescence efficiency can be written as following [41]

$$\eta = \frac{P_r}{P_r + P_{nr}}, \quad (2.53)$$

where  $P_r$  is the probability for a radiative transition and  $P_{nr}$  is the probability for a nonradiative transition. The  $P_{nr}$  has temperature dependence

$$P_{nr} = P_{nr0} \exp \frac{-E_t}{k_B T} \quad (2.54)$$

where  $P_{nr0}$  independent of the temperature is a coefficient,  $k_B$  is the Boltzman constant,  $T$  is temperature and  $E_t$  is the thermal activation energy. As a result of this, the temperature dependence of the luminescence efficiency can be expressed as following

$$\eta = \frac{1}{1 + C \exp[\frac{-E_t}{k_B T}]}, \quad (2.55)$$

where  $C$  is a constant and its value is equal to the ratio of probability of the nonradiative transition to the radiative one. The above equation can be used to express the temperature dependence of the band peak intensity

$$I = \frac{I_0}{1 + \alpha \exp[\frac{-E_t}{k_B T}]}, \quad (2.56)$$

where  $I_0$  is proportionality constant and  $\alpha$  is the rate parameter.

In the temperature dependence PL measurements, there is a relation between full width at half maxima (FWHM) of the emission spectra and temperature [60, 61]

$$W = W_0 [\coth \frac{h\nu_e}{2k_B T}]^{1/2}, \quad (2.57)$$

where  $W_0$  is a constant, and  $h\nu_e$  is the vibrational mode of the excited state.

In most crystals, while the temperature increases, the emission band maxima which is energy of emitted photon decreases. This process is related with the band gap variation with the temperature [62]. The relation between band gap energy and temperature is following [63]

$$E_g(T) = E_g(0) + \frac{\gamma T^2}{T + \beta}. \quad (2.58)$$

Here,  $E_g(0)$  is the band gap at zero temperature,  $\gamma = \frac{dE_g}{dT}$  is the rate of the change of the band gap with temperature and  $\beta$  is approximately the Debye temperature.

### 2.2.5 Thermally Stimulated Current Measurements

When a semiconductor is exposed to radiation at low temperatures, the energy levels in the band gap of the semiconductor are filled. As a result of this, electrons or holes emitted by

heating to a higher energy. To drive the electrons or holes, a force which is electric field is required. This process is called thermally stimulated current (TSC). TSC measurements are used to obtain information on trap states using some experimental methods [64]-[71].

In TSC measurements, the purpose is to achieve the information about the trapping centers and their distribution in crystals.

### 2.2.5.1 Traps and Recombination Centers

When a crystal is exposed to radiation, the electron in the valence band makes transition to the conduction band (figure 2.20 (a)). This ionization creates free electron-hole pairs. After some time, they become localized at defect centers. This results in the trapping of electrons (figure 2.20 (b)) and/or of holes (figure 2.20 (e)). When the crystal is again exposed to some energy which may be thermal (for TSC), the traps are once again free to move through the crystal.

Second process which may occur for free electrons and holes is that they may recombine with a charge carrier of opposite sign, either directly (figure 2.20 (h)) or indirectly (figure 2.20 (d) and (g)). If these transitions occur radiatively the luminescence results.

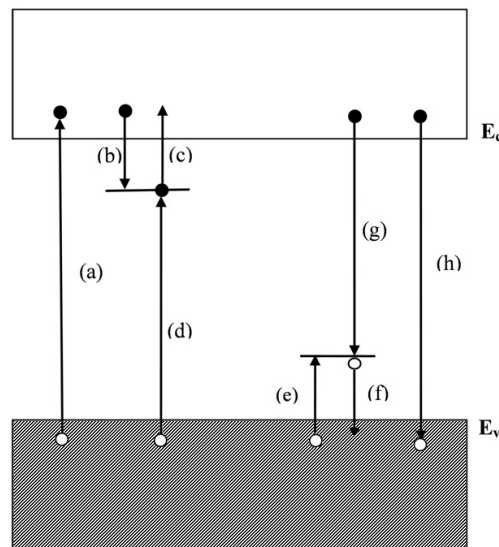


Figure 2.20: Electronic transitions in semiconductors. Solid circles are electrons and open circles are holes.



Thus, localized defect centers can be trap or recombination centers. To distinguish between these two types of localized energy levels relative probabilities of recombination and thermal excitation are important. As an example, if transition (c) probability is greater than transition (d) probability, then the center is called as a trap center. Contrast to this process, if transition (d) probability is greater than transition (c) probability then the center is called as a recombination center. Similar processes are valid for (g) and (f) transition.

The probability of a charge carrier which is thermally released from its trap is exponentially related to  $-\frac{E}{kT}$ , where  $E$  is 'trap depth' which is defined as the energy difference between trap and delocalized energy difference (the energy difference between  $E_c$  and  $D_e$ , see figure 2.21). For a given temperature those centers of small  $E$  are more likely to be traps than centers of large  $E$ . For this reason, the traps are localized near the edges whereas the recombination centers are localized towards the middle of the forbidden gap. As a result of this, a trap at one temperature may become a recombination center at a lower temperature and vice versa. So at a given temperature the transmission probabilities of traps and recombination centers are equal to each other. This energy level is called as demarcation level and represented as  $D$ . If the energy depth  $E$  is greater than  $D$ , the center would be recombination center whereas if the energy depth  $D$  is greater than  $E$  the center would be a trap center.

The demarcation levels for electrons  $D_e$  and for holes  $D_h$  are shown in figure 2.21.

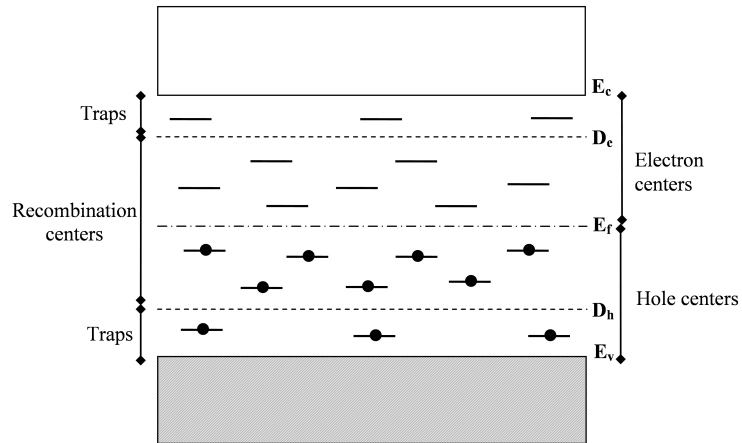


Figure 2.21: Energy levels in an insulator in equilibrium at absolute zero. The below  $E_f$  are full of electrons whereas those above are empty [32].

### 2.2.5.2 First and Second Order Kinetics

When the transition (b) occurs in figure 2.20 at a temperature  $T$ ,  $E$ , the energy depth, is such that  $E \gg$  several  $kT$  where  $k$  is Boltzmann's constant then the electron in trap level is likely to stay there for a considerable period. In this situation, if we assume a Maxwellian distribution of energies, the probability  $p$  per unit time for thermal excitation from the trap is exponentially depend on temperature as following,

$$p = \nu \exp \frac{-E}{kT}, \quad (2.59)$$

where  $\nu$  is a constant in unit of reciprocal time. The time between excitation and relaxation back to the valence band is delayed by the residence of electron in the metastable state  $m$ .

The rate of the thermal excitation of electrons from metastable level  $m$  to the conduction band is

$$\frac{-dn}{dt} = np = n\nu \exp \frac{-E}{kT}. \quad (2.60)$$

Where  $n$  is the concentration of electrons in level  $m$  [64]-[72]. The negative sign shows loss of electrons. If there is no retrapping which means that the transition from delocalized energy levels to the trap levels, the luminescence intensity  $I$  which is created from the decay of electrons from trap level to the valence band is ;

$$I(t) = -\eta \frac{dn}{dt} = \eta n \nu \exp \left( \frac{-E}{kT} \right), \quad (2.61)$$

where  $\eta$  is a constant. When we integrate the equation 2.60

$$\int \frac{-dn}{dt} = \int pn = - \int \frac{dn}{n} = \int p dt \implies n(t) = n(0) \exp(-pt) \quad (2.62)$$

and multiply the both sides with  $\eta p$  in equation 2.62

$$\eta p n(t) = \eta p n(0) \exp(-pt), \quad (2.63)$$

then the following equation is obtained

$$I(t) = I_0 \exp(-pt). \quad (2.64)$$

Where  $I_0$  is the initial intensity at  $t = 0$

Randal and Wilkins [73] ( later Garlick and Gibson [74] ) suggested that the probability for electrons in the excited state to be retrapped into level  $m$  may be equal to recombine into

ground level (recombination sites)

$$I(t) = -\eta \frac{dn}{dt} = \alpha n^2, \quad (2.65)$$

where  $\alpha$  is a constant. Integration yields;

$$I(t) = \frac{I_0}{(n_0 \alpha t + 1)^2}. \quad (2.66)$$

In equations 2.60 and 2.61, the decay rate is proportional to  $n$ , that means it is first order process whereas in equation 2.65 the decay rate is proportional to  $n^2$  that means it is second order process.

$\nu$ , which is the attempt-to-escape frequency, can be written as [75, 76]:

$$\nu = \sigma \vartheta N_s, \quad (2.67)$$

where  $\sigma$  is the capture cross section,  $N_s$  is the effective density of states in the delocalized energy level (conduction band) and  $\vartheta$  is the free carrier thermal velocity.  $\vartheta$  and  $N_s$  have a temperature dependence as following;

$$N_s(T) = 2 \left( \frac{kT m_e^*}{2\pi \hbar^2} \right)^{3/2}, \quad (2.68)$$

and

$$\vartheta = \sqrt{\frac{3kT}{m_e^*}}, \quad (2.69)$$

where  $m_e^*$  is the electron effective mass.

#### Adirovitch Theory

Adirovitch used three differential equations for transition of electron between the traps ( $N$ ) and recombination centers ( $m$ ) in 1956 [77]. This process is shown in figure 2.22. The first equation about the emission intensity  $I$  is proportional to concentration of free electrons in the conduction band  $n_c$  and concentration of holes in centers  $m$  and equal to the rate of the change of  $m$  with minus sign as following:

$$I = -\frac{dm}{dt} = A_m m n_c. \quad (2.70)$$

Where  $A_m$  is recombination probability.  $A_m = \sigma_m \vartheta$  where  $\sigma_m$  is the cross section for recombination in a center and  $\vartheta$  is the thermal velocity of free carriers.

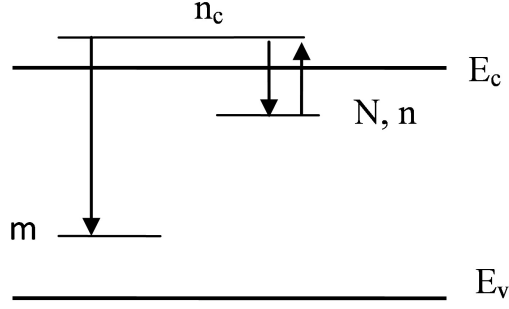


Figure 2.22: Energy levels in a solid.  $n$ ,  $m$  and  $n_c$  are the concentrations of trapped electrons, holes in the centres and free electrons in the conduction band, respectively.  $N$  is total concentration of traps even filled and empty [78].

Another equation was firstly derived by Randall and Wilkins [72] for transitions of electrons between the traps and the conduction band is following;

$$I = -\frac{dn}{dt} = vn \exp\left(\frac{-E}{kT}\right) - n_c(N - n)A_n. \quad (2.71)$$

Where  $A_n$  is retrapping probability.  $A_n = \sigma_n \vartheta$  where  $\sigma_n$  is the cross section for retrapping and  $\vartheta$  is the thermal velocity of free electrons.

The third equation is related with the charge neutrality which is;

$$m = n + n_c. \quad (2.72)$$

. When we take the derivative of equation 2.72 with respect to time  $t$  and using equations 2.71 and 2.70 the following equation is obtained as

$$\frac{dn_c}{dt} = vn \exp\left(\frac{-E}{kT}\right) - n_c[A_m m + (N - n)A_n]. \quad (2.73)$$

There is two basic assumptions firstly made by Adirovich and Halperin and Braner [77, 79] as following [80]-[83]

$$\frac{|dn_c|}{|dt|} \ll \frac{|dn|}{|dt|}, \quad (2.74)$$

$$n_c \ll n. \quad (2.75)$$

The meaning of  $n_c \ll n$  is that the concentration of free carriers in the conduction band or valence band is much smaller than the concentration of that of in the trap. The meaning of

$\frac{|dn_c|}{|dt|} \ll \frac{|dn|}{|dt|}$  is that the rate of the change of the free carriers in the conduction or valence band is much smaller than that of other recombination and retrapping. As a result of these assumptions. Following equations can be written as;

$$\frac{dm}{dt} = \frac{dn}{dt} \text{ since } \frac{dn_c}{dt} \longrightarrow 0. \quad (2.76)$$

Using equation 2.73 following expression can be written;

$$n_c = \nu n \exp\left(\frac{-E}{kT}\right) \frac{1}{[A_m m + (N - n)A_n]}. \quad (2.77)$$

When we substitute the above equation into 2.71, the following equations are obtained:

$$\frac{-dn}{dt} = \nu n \exp\left(\frac{-E}{kT}\right) - \nu n \exp\left(\frac{-E}{kT}\right) \frac{(N - n)A_n}{[A_m m + (N - n)A_n]}, \quad (2.78)$$

$$\frac{-dn}{dt} = \nu n \exp\left(\frac{-E}{kT}\right) \left[1 - \frac{(N - n)A_n}{[A_m m + (N - n)A_n]}\right], \quad (2.79)$$

$$\frac{-dn}{dt} = \frac{-dm}{dt} = \nu n \exp\left(\frac{-E}{kT}\right) \left[\frac{mA_m}{[A_m m + (N - n)A_n]}\right], \quad (2.80)$$

#### First Order Kinetics

As mentioned before first order kinetics means that if an electron released from trap level it recombine quickly with a hole centre. As a result of this the following case is valid

$$A_m m \gg A_n (N - n). \quad (2.81)$$

Using the above relation, the term  $\frac{mA_m}{(N-n)A_n + mA_m}$  in equation 2.80 goes 1. As a result of this the following equation is obtained as

$$I = \frac{-dn}{dt} = \nu n \exp\left(\frac{-E}{kT}\right). \quad (2.82)$$

When we integrate the both sides of above equation using  $\beta = \frac{dT}{dt}$  where  $\beta$  is heating rate

$$\frac{-dn}{n} = \nu dt \exp\left(\frac{-E}{kT}\right) = \nu \frac{dT}{\beta} \exp\left(\frac{-E}{kT}\right), \quad (2.83)$$

$$\ln n = \frac{-\nu}{\beta} \int_{T_0}^T \exp\left(\frac{-E}{kT'}\right) dT' + \ln n_0, \quad (2.84)$$

$$n = n_0 \exp\left(\frac{-\nu}{\beta} \int_{T_0}^T \exp\left(\frac{-E}{kT'}\right) dT'\right), \quad (2.85)$$

and multiply the both sides with  $\nu \exp(\frac{-E}{kT})$ , the current is obtained as

$$I = n\nu \exp(\frac{-E}{kT}) = n_0\nu \exp(\frac{-E}{kT}) \exp(\frac{-\nu}{\beta} \int_{T_0}^T \exp(\frac{-E}{kT'}) dT'). \quad (2.86)$$

For the above equation, we obtain the condition for maximum when  $\frac{dI}{dT} = 0$

$$\frac{E}{kT^2} \exp \frac{-E}{kT} \exp(\frac{-\nu}{\beta} \int_{T_0}^T \exp(\frac{-E}{kT'}) dT') = \exp \frac{-2E}{kT} (\frac{\nu}{\beta}) \exp(\frac{-\nu}{\beta} \int_{T_0}^T \exp(\frac{-E}{kT'}) dT'), \quad (2.87)$$

$$\frac{E}{kT_m^2} = \frac{\nu}{\beta_m} \exp(\frac{-E}{kT_m}), \quad (2.88)$$

where  $\beta_m$  is the instantaneous heating rate at the maximum and  $T_m$  is the maximum temperature. This equation is used for different heating rate methods which will be discussed later.

### Second Order Kinetics

The condition for second order kinetics is that electrons are thermally excited several times before recombining into the center. As a result of this

$$A_n(N - n) \gg A_m m. \quad (2.89)$$

When we rewrite the equation 2.80

$$I = \nu n \exp(\frac{-E}{kT}) \frac{1}{[1 + \frac{(N-n)A_n}{A_m m}]}, \quad (2.90)$$

using the equation 2.89, the current is obtained as;

$$I = \nu n \exp(\frac{-E}{kT}) \frac{A_m m}{A_n(N - n)}. \quad (2.91)$$

Since,  $N \gg n$  and  $m = n$ ,  $A_m = A_n$  current becomes

$$I = \frac{-dn}{dt} = \frac{\nu}{N} n^2 \exp(\frac{-E}{kT}). \quad (2.92)$$

When we integrate the both sides using  $\beta = \frac{dT}{dt}$

$$\frac{-dn}{n^2} = \frac{\nu}{N\beta} \int_{T_0}^T \exp(\frac{-E}{kT'}) dT', \quad (2.93)$$

$$\frac{1}{n} = \frac{1}{n_0} + \frac{\nu}{N\beta} \int_{T_0}^T \exp(\frac{-E}{kT'}) dT', \quad (2.94)$$

$$n = \frac{N\beta n_0}{\nu n_0 \int_{T_0}^T \exp(\frac{-E}{kT'}) dT'} + N\beta, \quad (2.95)$$

$$n = \frac{N\beta n_0}{N\beta[1 + \frac{\nu n_0}{N\beta} \int_{T_0}^T \exp(\frac{-E}{kT'}) dT']}, \quad (2.96)$$

and substitute  $n^2$  into equation 2.92, the current is obtained for second order kinetics as

$$I = \frac{\nu}{N} n_0^2 \exp(\frac{-E_t}{kT}) [1 + \frac{n_0 \nu}{\beta N} \int_{T_0}^T \exp(\frac{-E}{kT'}) dT']^{-2}. \quad (2.97)$$

The above expression is used to define second order process in TSC luminescence.

### 2.2.5.3 Isothermal Decay Method

This method is based on the shape of the TSC curve with respect to time. In this process the sample is heated until a temperature value  $T_p$  and keeps constant at that temperature. The thermally stimulated current can be written as [73, 78]

$$I = I_0 \exp(-\nu \exp(\frac{-E_t}{kT_p})t), \quad (2.98)$$

where  $I_0$  is initial current value at time zero. The equation 2.98 is checked that whether it is valid or not by plotting  $\ln I$  vs  $t$  graph. The criteria is to observe a straight line. After this process, the measurements are repeated at different temperatures. The slopes  $\gamma = -\nu \exp(\frac{-E_t}{kT_p})$  are obtained. Then, the slope of  $\ln \gamma$  vs  $1/T_p$  gives  $E_t/k$  value.

### 2.2.5.4 Initial Rise Method

This method is the simplest method to evaluate the thermal activation energy  $E_t$ . In this method, the traps and recombination centers can be considered as constant at low temperatures. As a result of this in this temperature region the TSC intensity is an exponential function of temperature  $T$

$$I(T) = C \exp(\frac{-E_t}{kT}). \quad (2.99)$$

The above equation was firstly derived by Garlick and Gibson [74]. The equation 2.99 can be rewritten by taking the logarithmic of it;

$$\ln I(T) = C_1 - \frac{E_t}{kT}. \quad (2.100)$$

The slope of the  $\ln I$  vs  $1/T$  graph gives the  $-E_t/k$  value.

### 2.2.5.5 The Various Heating Rates Method

If the heating rate  $\beta$  increases the maximum temperature  $T_m$  shifts to higher temperatures. The condition for this process is only keeping the other parameters such as initial trap occupancy  $n_0$ , constant. The expression for the various heating rates methods was evaluated in section 2.2.5.2 where

$$\frac{E}{kT_m^2} = \frac{\nu}{\beta_m} \exp\left(\frac{-E}{kT_m}\right). \quad (2.101)$$

When the above equation is written according to  $\beta$  the following expression is obtained;

$$\beta = \frac{\nu k}{E_t} T_m^2 \exp\left(\frac{-E}{kT_m}\right). \quad (2.102)$$

Since the term  $T_m^2 \exp(\frac{E_t}{kT_m})$  is an increasing function of  $T_m$ , the  $\beta$  value also increases. As a result of this, there is a shift in TSC spectra towards  $T_m$ .

### 2.2.5.6 Curve Fitting Method

Slow retrapping (monomolecular condition)

In the conductivity measurements, there is a relation between conductivity,  $\sigma(T)$  for bulk crystals and concentration of free carriers  $n_c(T)$  as following

$$\sigma = e\mu n_c, \quad (2.103)$$

where  $e$  is the electronic charge and  $\mu$  is the mobility. Using equations 2.70 and 2.76, the following expression is obtained as,

$$-A_m m n_c = \frac{-n_c}{\tau} = \frac{dn}{dt}. \quad (2.104)$$

Where  $\tau$  is  $\frac{1}{mA_m}$ , lifetime of free electrons. When the equations 2.82 and 2.85 are substituted into equation 2.104 the following equation is obtained as

$$n_c(T) = \tau n_0 \nu \exp\left(\frac{-E}{kT}\right) \exp\left(\frac{-\nu}{\beta} \int_{T_0}^T \exp\left(\frac{-E}{kT'}\right) dT'\right). \quad (2.105)$$

Using the above equation we obtain the conductivity as following

$$\sigma = e\mu \tau n_0 \nu \exp\left(\frac{-E}{kT}\right) \exp\left(\frac{-\nu}{\beta} \int_{T_0}^T \exp\left(\frac{-E}{kT'}\right) dT'\right). \quad (2.106)$$



When the voltage  $V$  is applied to bulk crystal the thermally stimulated current is obtained using ohms law as;

$$I = \frac{VA}{L}\sigma = \frac{VA}{L}e\mu\tau n_0 \nu \exp\left(\frac{-E}{kT}\right) \exp\left(\frac{-\nu}{\beta} \int_{T_0}^T \exp\left(\frac{-E}{kT'}\right) dT'\right) \quad (2.107)$$

where  $A$  and  $L$  are area and length of the crystal used for TSC. The variation  $\mu$  and  $\tau$  with  $T$  can be ignored over the temperature span of TSC curve so equation 2.106 can be written as

$$\sigma = A \exp(-t + B \int_{t_0}^t \exp(-t) t^{-2} dt). \quad (2.108)$$

Where  $t = \frac{E_t}{kT}$  and  $A$  and  $B$  are constants:  $A = n_0 \tau e \mu \nu$ ,  $B = \frac{\nu E_t}{\beta k}$ . If the integral part of equation 2.108 is taken integration by parts, the following equation is obtained leading to a convergent series;

$$\sigma = A \exp(-t + B(\exp(-t)t^{-2} - 2 \exp(-t)t^{-3} + 3 * 2 \exp(-t)t^{-4} \dots))_{t_0}^t. \quad (2.109)$$

By making approximation taking the first term is remaining

$$\sigma \simeq A \exp(-t + B(\exp(-t)t^{-2}))_{t_0}^t, \quad (2.110)$$

$$\sigma \simeq \sigma_0 + A \exp(-t + B(\exp(-t)t^{-2})), \quad (2.111)$$

where  $\sigma_0$  is the conductivity at  $t = t_0$ . If there are more than one peak;

$$\sigma(T) = \sum_{i=1}^m \sigma_i(T), \quad (2.112)$$

where  $\sigma_i(T)$  is thermally stimulated conductivity for each peaks,  $m$  is total number of observed peaks.

Fast retrapping (bimolecular condition)

when the equation 2.103 is rewritten by inserting equation 2.104, the conductivity  $\sigma$  is obtained as following

$$\sigma = e\mu\left(\frac{-dn}{dt}\tau\right). \quad (2.113)$$

By using equations 2.92 and 2.108, the conductivity is obtained as,

$$\sigma = e\mu\tau \frac{\nu}{N} n_0^2 \exp\left(\frac{-E_t}{kT}\right) \left[1 + \frac{n_0 \nu}{\beta N} \int_{T_0}^T \exp\left(\frac{-E}{kT'}\right) dT'\right]^{-2}. \quad (2.114)$$

If we assume that  $\nu$  is independent of  $T$ , the variation  $\mu$  and  $\tau$  with  $T$  can be ignored and  $n_0 = N$  that means all the traps are filled, equation 2.114 can be written as;

$$\sigma = A \exp(-t) [1 - B \int_{t_0}^t \exp(-t) t^{-2} dt]^{-2}. \quad (2.115)$$

Where  $t = \frac{E_t}{kT}$ ,  $A = n_0 e \tau \mu \nu$  and  $B = \frac{\nu E_t}{k\beta}$ . A convergent infinite series are obtained by repeating integration by parts of the integral in equation 2.115 then we obtain the conductivity,

$$\sigma = \frac{A \exp(-t)}{(1 + B(\exp(-t)t^{-2} - 2 \exp(-t)t^{-3} + 3 * 2 \exp(-t)t^{-4} \dots))_{t_0}^t}. \quad (2.116)$$

By dropping all terms in series except first term since  $t$  is large in practice;

$$\sigma \simeq \frac{A \exp(-t)}{(1 + B(\exp(-t)t^{-2}))_{t_0}^t}. \quad (2.117)$$

If  $t_0$  is much greater than other  $t$  values the bottom limit can be ignored and conductivity becomes,

$$\sigma \simeq \frac{A \exp(-t)}{(1 + B(\exp(-t)t^{-2}))^2}. \quad (2.118)$$

If there are more than one peak overlapping each other, the conductivity for fast retrapping can be found by equation 2.112.

#### 2.2.5.7 Traps Distribution Method

This method was successfully applied into TSC curves by Serpi and Macciotta in 1972 [84]. If an exponential distribution of traps is assumed, the density of traps at energy  $E$  can be written as [85]

$$N(E) = A \exp(-\alpha E), \quad (2.119)$$

where  $A$  is a constant and  $\alpha$  is the energy parameter which characterizes the traps distribution. After this assumption the following expression can be written for the traps filled at the excitation temperature  $T_e$

$$n_0(T_e) = A \exp(-\alpha E) \exp\left[\frac{(E - E_f)}{kT_e}\right], \quad (2.120)$$

in the above equation  $E$  is the fermi energy level in darkness and  $E_f$  is the quasi-Fermi level energy during light excitation.  $E$  and  $E_f$  can be written as

$$E = kT_m \ln\left(\frac{N_c}{n_m}\right), \quad (2.121)$$

$$E_f = kT_m \ln\left(\frac{N_c}{n_e}\right), \quad (2.122)$$

where  $n_e$  and  $n_m$  are the densities of free electrons during light excitation and in darkness, respectively.  $T_m$  is the temperature of thermocurrent peak in darkness. Using the equations 2.120, 2.121 and 2.122 the following expression is obtained,

$$S_0\left(\frac{I_m}{I_e}\right) \propto A \exp(\alpha E). \quad (2.123)$$

$S_0$ , the area of the thermocurrent peak, is directly proportional to  $n_0$  where  $I_m$  is the darkness current at peak temperature and  $I_e$  is the current during light excitation at peak temperature, respectively. If the areas of the curves and  $E$  values for each different light excitations are calculated and plotted  $\ln S_0\left(\frac{I_m}{I_e}\right)$  vs  $E$  graph, the  $\alpha$  value corresponding the variation of traps for every decade can be obtained.

#### 2.2.5.8 Trap Concentration Determination

The trap concentration is [86]

$$N_t = \frac{Q}{ALeG}. \quad (2.124)$$

Here,  $Q$  is amount of charge released during the TSC measurement and it can be calculated from the TSC peak area and  $G$  is the photoconductivity gain calculated from [87]

$$G = \frac{\tau}{t_{tr}} = \frac{\tau\mu V_2}{L^2}, \quad (2.125)$$

where,  $\tau$  is the carrier lifetime and  $t_{tr}$  is the carrier transit time between electrodes. To find the carrier life times, photoconductivity experiments were carried out [88]. After termination of light pulse  $t=t_0$ , the current decays. Using the following equation, the carrier lifetime  $\tau$  is determined.

$$V = V_0 + C \exp\left(\frac{-t}{\tau}\right) \quad (2.126)$$

Where  $V_0$  is voltage at  $t = \infty$  and  $C$  is a constant.

## CHAPTER 3

### EXPERIMENTAL DETAILS

In this chapter, the details of experiments such as XRD, EDSA, Transmission, Reflection, PL, TSC and photoconductivity decay, conducted to examine the structural, optical and electrical transport properties of  $\text{Ti}_2\text{In}_2\text{S}_3\text{Se}$ ,  $\text{TiInSeS}$  and  $\text{Ti}_2\text{In}_2\text{SSe}_3$  crystals, will be given. The experimental details of Bridgman method used to grow these layered crystals will also be given.

#### 3.1 XRD Experiments

In the X-ray powder diffraction experiment which is shown in figure 3.1, a "Rigaku Miniflex" diffractometer with  $\text{Cu K}\alpha$  radiation ( $\lambda = 0.154049 \text{ nm}$ ) were utilized at a scanning speed of  $0.02 \text{ s}^{-1}$  in the  $10\text{-}70^\circ$  diffraction angle range ( $2\theta$ ). "DICVOL 04", a least-squares computer program was used to obtain the lattice parameters from XRD spectra.

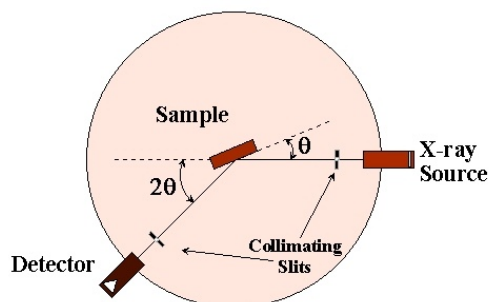


Figure 3.1: The simple schematic representation of XRD experiment.

### 3.2 EDSA Experiments

The chemical composition of studied crystals was determined by energy dispersive spectroscopic analysis (EDSA). In EDSA, the JSM-6400 electron microscope was used in the energy range of 0-10 keV. To analyze the chemical composition of the studied crystals, basic equipments are NORAN System6 X-ray Microanalysis System and Semafore Digitizer.

### 3.3 Transmission and Reflection Experiments

”Shimadzu” UV-1201 model spectrophotometer were used for transmission and reflection experiments. The spectrophotometer consisted of 20 W halogen lamp, holographic grating, and silicon photodiode. The transmission measurements were carried out under normal incidence of light with polarization direction along the (001) plane, which is perpendicular to the  $c$ -axis of the crystal. The schematic representation of room temperature transmission experiment is shown in figure 3.2. For room temperature reflection experiments shown in figure 3.3, the specular reflectance measurement attachment was utilized with  $5^\circ$  incident angle. The resolution of the spectrophotometer was 5 nm. ” To decrease the temperature from 300 K to 10 K, an ”Advanced Research Systems, Model CSW-202” closed-cycle helium cryostat was used temperature was controlled within an accuracy of  $\pm 0.5$  K. Temperature-dependent transmission setup is presented in figure 3.4.

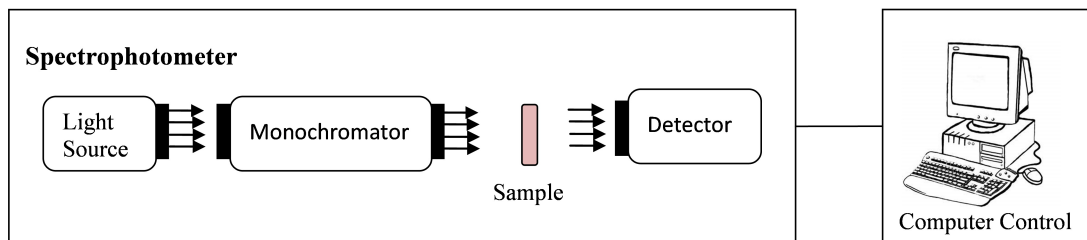


Figure 3.2: Schematic representation of room temperature transmission experiment set-up.

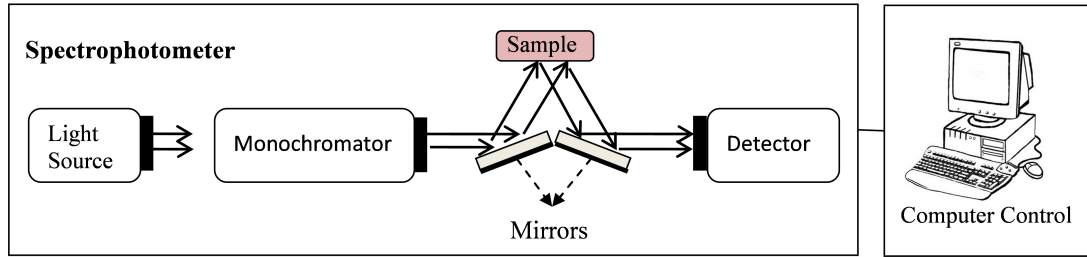


Figure 3.3: Schematic representation of reflection experiment set-up.

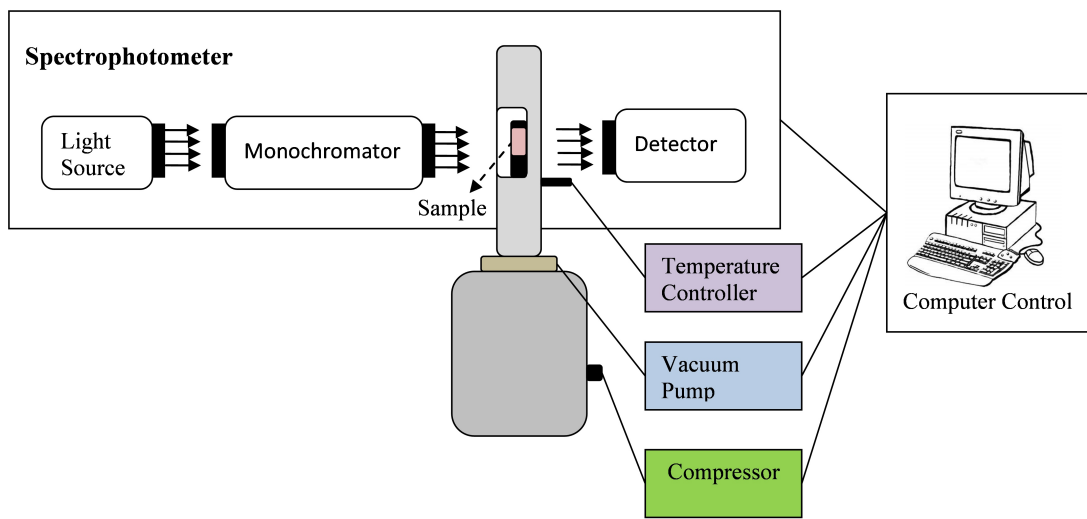


Figure 3.4: Schematic representation of temperature-dependent transmission experiment set-up.

### 3.4 PL Experiments

The schematic representation of PL experiment is shown in figure 3.5. A frequency-doubled YAG:Nd<sup>3+</sup> laser having the  $\lambda = 532$  nm was used as a light source for excitation. The PL light was collected from the sample in the direction to the normal of it. To decrease the temperature from 300 K to low temperatures, a "CTI-Cryogenics M-22" closed cycle helium cryostat was used. The PL spectra was analyzed using a "Oriel MS-257" grating monochromator and "Hamamatsu S7010-1008" FFT-CCD Image Sensor with single stage electric cooler. Sets of neutral density filters were used to adjust the exciting laser intensity.

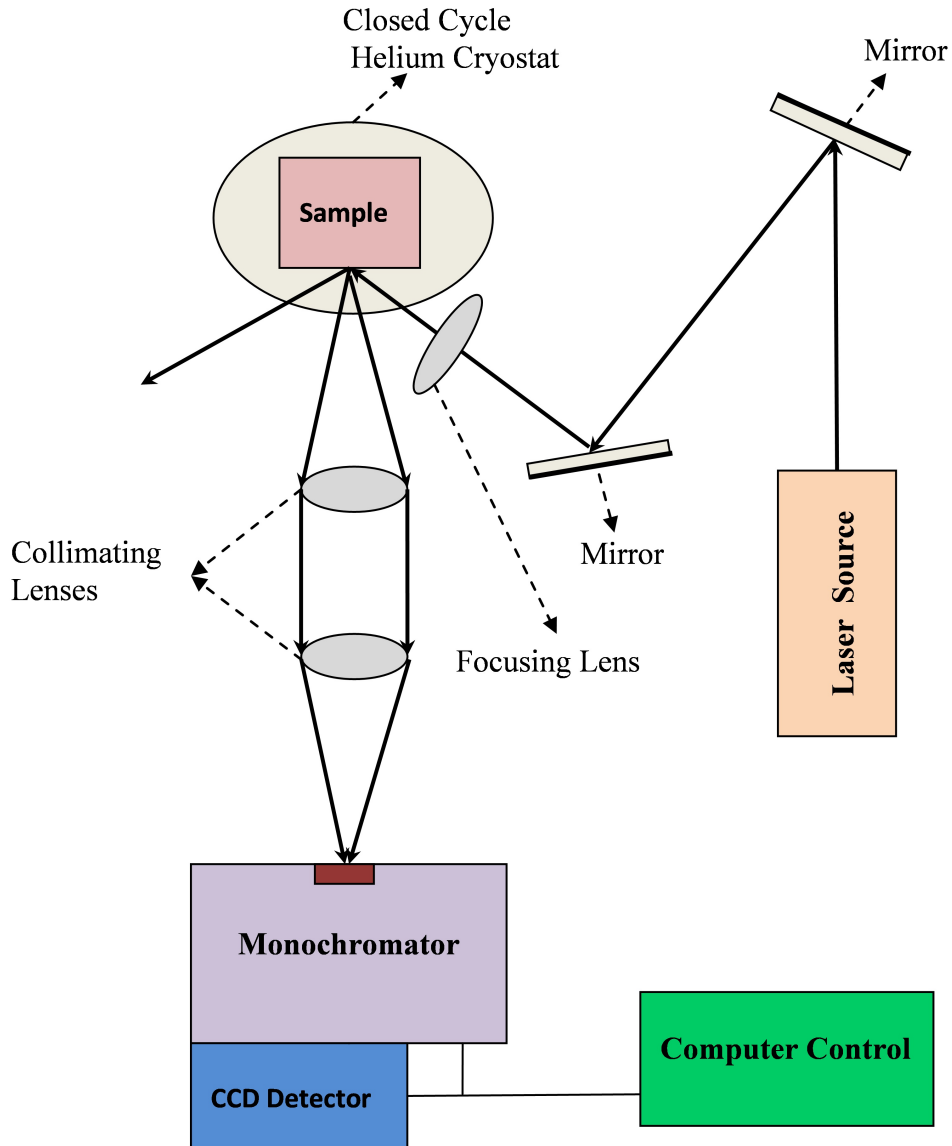


Figure 3.5: Schematic representation of PL experiment set-up.

### 3.5 TSC Experiments

To conduct the TSC experiments, the silver paste was used to attach the sample to the copper holder. According to sandwich geometry shown in figure 3.6, the electrodes were made. One electrode was made on the front of the sample and the other one was at the back of it and it covered the whole surface of the sample to maintain electrical and thermal conductivity. In the sample layer, the conductivity is about four orders of magnitude higher than normal of the

sample [6]. As a result of this, the electric field lines covered the whole volume of the sample. To make the contacts, thin copper wires were used. The copper holder was mounted on the cold finger of the cryostat and the back side was grounded through the sample holder. A closed cycle helium cryostat was used in the TSC measurements. To obtain constant heating, a Lake-Shore 331 temperature controller was used. A Keithley 228 A voltage/current source and a Keithley 6435 picoammeter were employed for TSC measurements. To excite the carriers, a light emitting diode was used. It generates light with an energy of 2.6 eV (see figure 3.7).

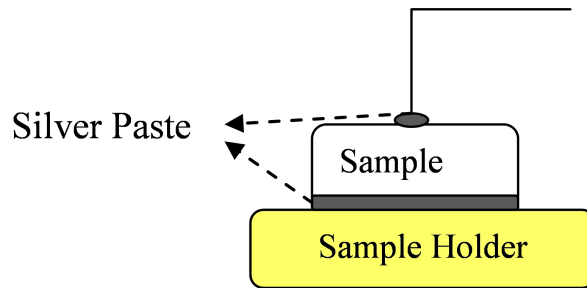


Figure 3.6: The representation of sample attached to sample holder in sandwich geometry.

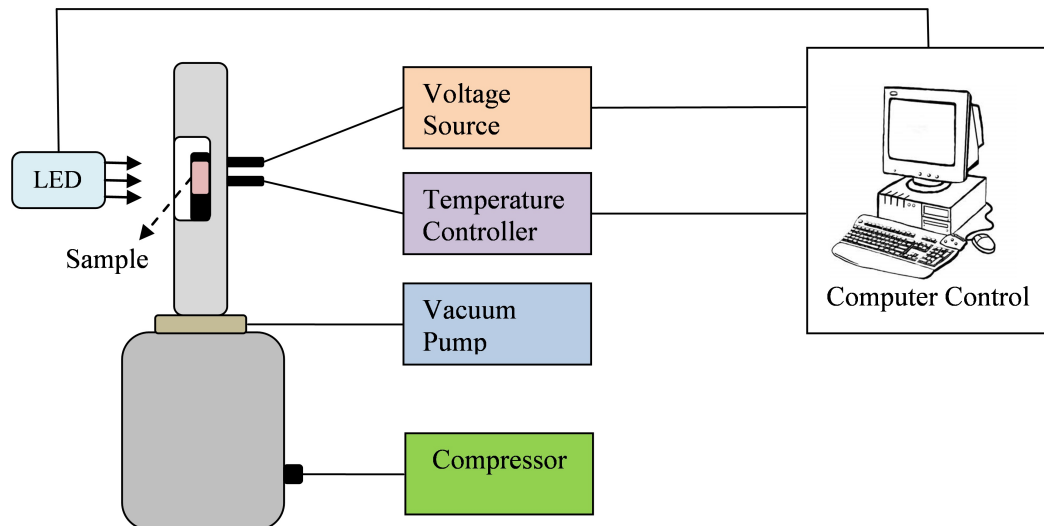


Figure 3.7: Schematic representation of TSC experiment set-up.



### 3.6 Photoconductivity Decay Experiments

The photoconductivity (PC) decay measurements were done to find carrier life time. The PC experiments were carried out as follows. A coplanar structure on the sample with ohmic electrodes separated by a small gap were formed and illumination was occurred by a high efficiency blue light emitting diode. The controller operator was a digital signal generator operating square waves. A fast current-voltage converter circuit was used the PC amplification. A fast digital voltmeter was used to record the signal. After the light pulse, the current decays were observed nearly exponential. The diagram of PC experiment was shown in figure 3.8.

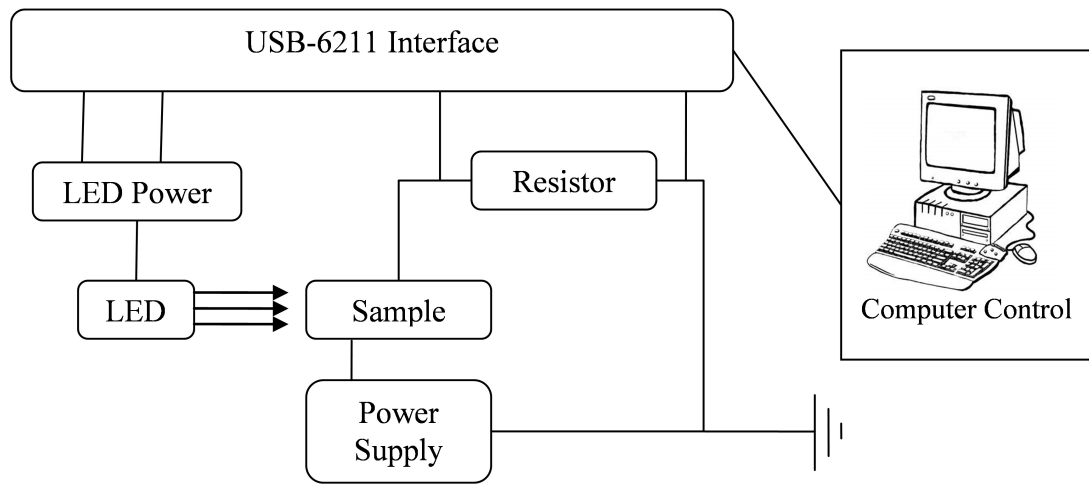


Figure 3.8: Schematic representation of PC experiment set-up.

### 3.7 Bridgman Method

$\text{Ti}_2\text{In}_2\text{S}_3\text{Se}$ ,  $\text{TlInSeS}$  and  $\text{Ti}_2\text{In}_2\text{SSe}_3$  polycrystals were synthesized from high-purity elements (at least 99.999%) taken in stoichiometric proportions. The single crystals were grown from synthesized polycrystals by the Bridgman method in evacuated ( $10^{-5}$  Torr) silica tubes with a tip at the bottom. The ampoule was moved in a vertical furnace through a thermal gradient of  $30\text{ }^\circ\text{C cm}^{-1}$ , between the temperatures  $760$  and  $410\text{ }^\circ\text{C}$ , at a rate of  $1.0\text{ mm h}^{-1}$ .

## CHAPTER 4

### RESULTS AND DISCUSSION

In this chapter, the results of XRD, EDSA, Transmission, Reflection, PL and TSC experiments, conducted to examine the structural, optical and electrical transport properties of  $\text{Tl}_2\text{In}_2\text{S}_3\text{Se}$ ,  $\text{TlInSeS}$  and  $\text{Tl}_2\text{In}_2\text{SSe}_3$  layered single crystals, will be presented and discussed.

#### 4.1 Introduction

The ternary semiconducting chalcogenides with the formula  $\text{TlBX}_2$  (B and X represent metal and chalcogen atoms, respectively) have been studied intensively in recent years [2, 3, 10]. They have both layered ( $\text{TlGaS}_2$ ,  $\text{TlGaSe}_2$ ,  $\text{TlInS}_2$ ) and chain ( $\text{TlInSe}_2$ ,  $\text{TlInTe}_2$ ,  $\text{TlGaTe}_2$ ) structures. The quaternary  $\text{Tl}_2\text{In}_2\text{S}_3\text{Se}$ ,  $\text{TlInSeS}$  and  $\text{Tl}_2\text{In}_2\text{SSe}_3$  crystals belong to the group of layered semiconductors. These compounds have structural similarities to  $\text{TlInS}_2$  crystal with the difference that some part of the sulfur atoms are replaced by selenium ones. The lattice structure of these compounds composed of rigorously periodic two-dimensional layers arranged parallel to the (001) plane (see figures 4.1 and 4.2), and each such consecutive layer is rotated by a right angle with respect to the previous one. Interlayer bonding is formed between Tl and Se(S) atoms while the bonding between In and Se(S) atoms is an intralayer type.

$\text{Tl}_2\text{In}_2\text{S}_3\text{Se}$ ,  $\text{TlInSeS}$  and  $\text{Tl}_2\text{In}_2\text{SSe}_3$  layered crystals are all n-type crystals as determined from hot probe technique.

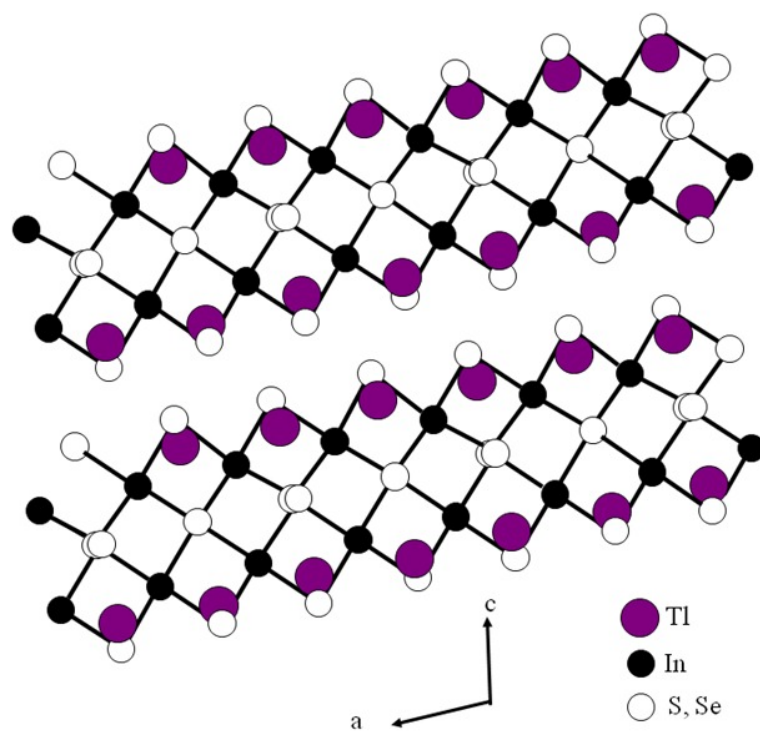


Figure 4.1: Projection of the crystal structure of thallium and indium chalcogenides on the  $ac$ - plane.

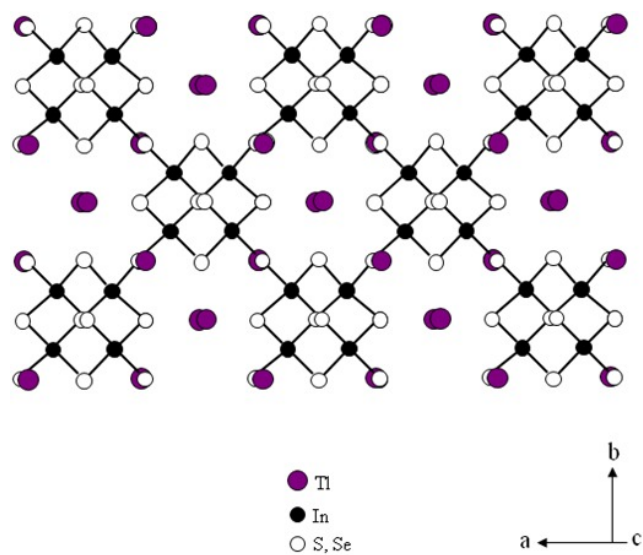


Figure 4.2: Projection of the crystal structure of thallium and indium chalcogenides on the  $ab$ - plane.

## 4.2 Structural, Optical and Electrical Transport Properties of $\text{Tl}_2\text{In}_2\text{S}_3\text{Se}$ Layered Crystals

### 4.2.1 Results of X-ray Experiments and Energy Dispersive Spectral Analysis

For  $\text{Tl}_2\text{In}_2\text{S}_3\text{Se}$  crystals, the resulting ingot were orange in color and the freshly cleaved surfaces were mirror-like. The structure of  $\text{Tl}_2\text{In}_2\text{S}_3\text{Se}$  crystal were analyzed by XRD. The Miller indices ( $hkl$ ), the observed and calculated interplanar spacings ( $d$ ) and the relative intensities ( $I/I_0$ ) of the diffraction lines for  $\text{Tl}_2\text{In}_2\text{S}_3\text{Se}$  crystal were found. These structural parameters are listed in table 4.1. Figure 4.3 presents the X-ray diffractogram of  $\text{Tl}_2\text{In}_2\text{S}_3\text{Se}$  crystal. "DICVOL 04", a least-squares computer program, was used to calculate the lattice parameters of the monoclinic unit cell,  $a = 0.8912$ ,  $b = 0.3981$ ,  $c = 0.8501$  nm, and  $\beta = 119.49^\circ$  [89].

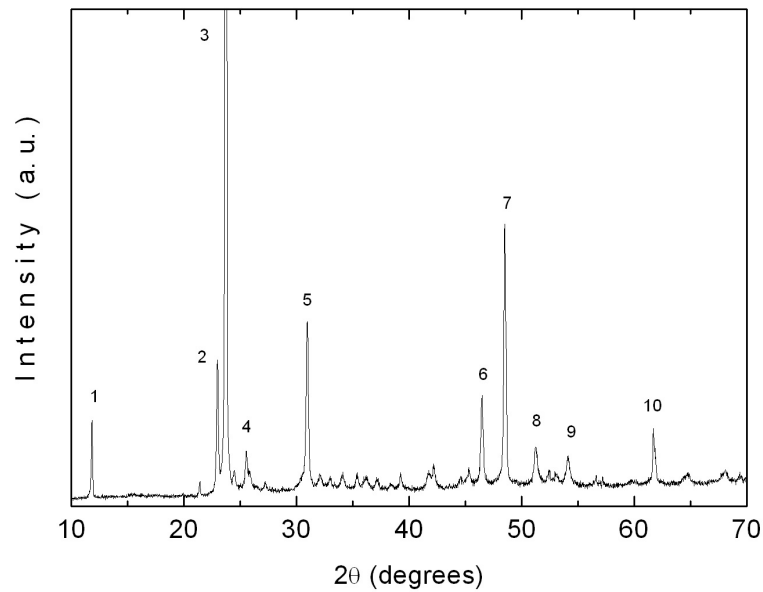


Figure 4.3: X-ray diffraction pattern of  $\text{Tl}_2\text{In}_2\text{S}_3\text{Se}$  powder sample.

By the help of EDSA, the chemical composition of  $\text{Tl}_2\text{In}_2\text{S}_3\text{Se}$  crystals was determined as 25.9 : 26.1 : 35.9 : 12.1, respectively [89]. The spectrum obtained from EDSA is shown in figure 4.4.

Table 4.1: X-ray powder diffraction data for  $\text{Tl}_2\text{In}_2\text{S}_3\text{Se}$  crystals.

No.	$hkl$	$d_{obs}$ (nm)	$d_{calc}$ (nm)	$I/I_0$
1	1 0 -1	0.7481	0.7492	5.0
2	2 0 0	0.3874	0.3874	9.0
3	2 0 -2	0.3751	0.3750	100.0
4	1 1 0	0.3487	0.3486	2.8
5	3 0 -2	0.2890	0.2888	11.5
6	0 2 0	0.1954	0.1953	6.8
7	4 0 -4	0.1876	0.1876	21.9
8	1 2 1	0.1783	0.1784	2.8
9	5 0 -1	0.1694	0.1694	2.2
10	1 1 4	0.1502	0.1502	5.0

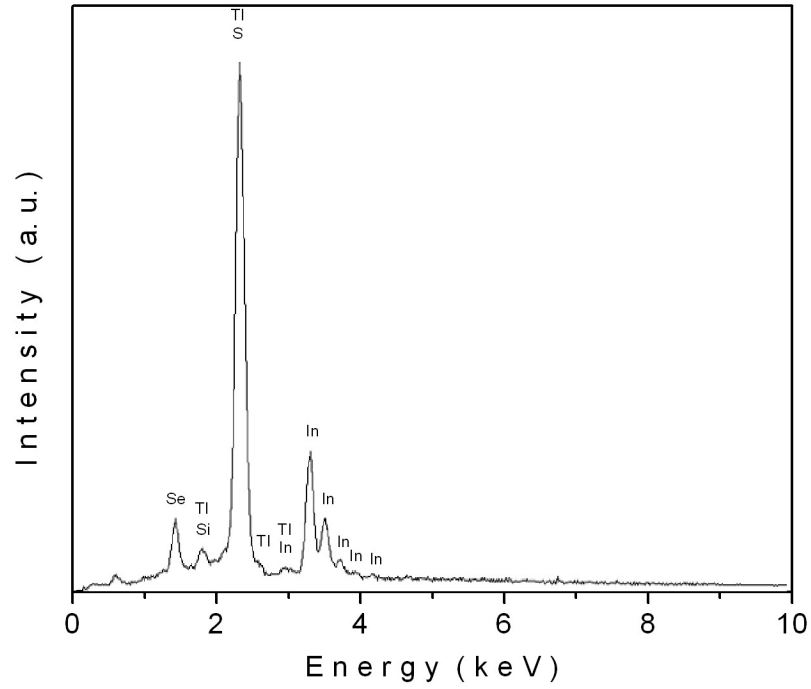


Figure 4.4: Energy dispersive spectroscopic analysis of  $\text{Tl}_2\text{In}_2\text{S}_3\text{Se}$  crystal.

#### 4.2.2 Results of Transmission and Reflection Experiments

For  $\text{Tl}_2\text{In}_2\text{S}_3\text{Se}$  single crystals, the transmittance ( $T$ ) and reflectivity ( $R$ ) spectra were recorded in the wavelength ( $\lambda$ ) range of 450-1100 nm (figure 4.5). The reflectivity of the material with refractive index  $n$  and absorption coefficient  $\alpha$  was given as

$$R = |r|^2 = \left| \frac{1 - n + ik}{1 + n - ik} \right|^2 = \frac{(1 - n)^2 + k^2}{(1 + n)^2 + k^2}, \quad (4.1)$$

where  $k = \alpha\lambda/4\pi$ . The transmittance, in the absence of interference fringes, is represented by the relation

$$T = \frac{(1 - R)^2 \exp(-\alpha d)}{1 - R^2 \exp(-2\alpha d)}, \quad (4.2)$$

where  $d$  is the sample thickness. As a result of these relations, from the analysis of transmission and reflection measurements, refractive index and absorption coefficient can be obtained.

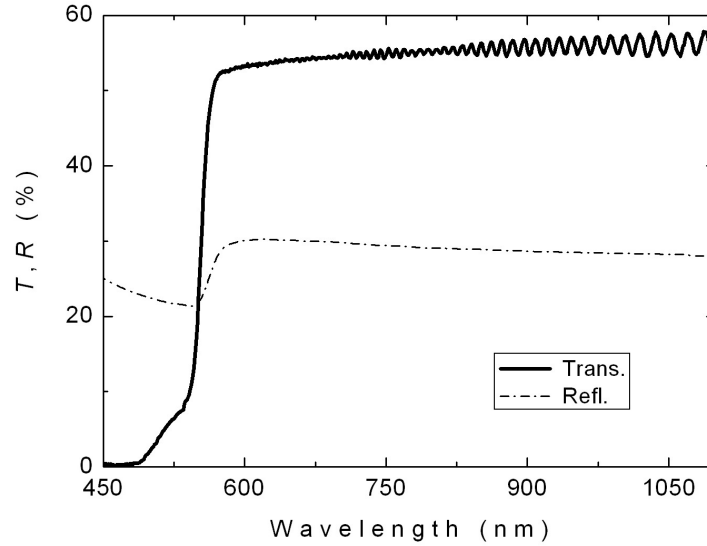


Figure 4.5: The spectral dependence of transmittance and reflectivity for  $\text{Tl}_2\text{In}_2\text{S}_3\text{Se}$  crystal at room temperature.

In the reflection measurements, the samples having thickness such that  $\alpha d \gg 1$  were used whereas in the transmission measurements, the sample thickness was reduced by using transparent tape and determined from transmission interference fringes. The long wavelength where the transmission were very high values were used (figure 4.5). Using the the long wavelength value of the refractive index  $n = 3.25$  in the equation 2.21, the thickness of the sample was calculated. Mostly, the sample thickness was of the order of  $10 \mu\text{m}$  [89].

The dependence of absorption coefficient with photon energy is very important to obtain detailed information about energy band gaps. This relation was analyzed in the high absorption regions.  $\alpha$  can be represented by the relation

$$\alpha h\nu = A(h\nu - E_g)^p. \quad (4.3)$$

In this equation,  $A$  is a constant depends on the transition probability and  $p$  is an index that

characterizes the optical absorption process. If  $p$  is theoretically equal to 2 and 1/2 it corresponds to indirect and direct allowed transitions, respectively. Figure 4.6 shows the variation of  $\alpha$  from 40 to 4260  $\text{cm}^{-1}$  with increasing photon energy from 2.15 to 2.60 eV. From the analysis of the experimental data it was shown that, the absorption coefficient was proportional to  $(h\nu - E_g)^p$  with  $p = 2$  and 1/2 for ranges 2.18-2.29 eV and 2.46-2.58 eV, respectively. Insets 1 and 2 of figure 4.6 display the dependencies of  $(\alpha h\nu)^{1/2}$  and  $(\alpha h\nu)^2$  on photon energy  $h\nu$ , respectively. The circles are the experimental data and the solid lines were fitted to a linear equation to find the band gaps. The linear dependencies for the relations  $(\alpha h\nu)^{1/2}$  and  $(\alpha h\nu)^2$  versus  $h\nu$  suggests the realization of indirect and direct allowed transitions, respectively. The extrapolations of straight lines, indirect band gap energy  $E_{gi} = 2.16 \pm 0.02$  eV and direct band gaps energy  $E_{gd} = 2.42 \pm 0.02$  eV were calculated, respectively [89]. Indirect and direct inter-band edge transitions can exist for thallium containing layered crystals because of specific features of the prevailing  $p$ -anionic upper valence band and  $s$ -Tl states [90].

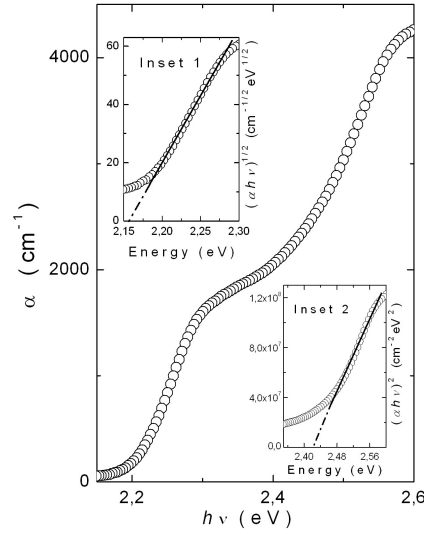


Figure 4.6: The variation of absorption coefficient as a function of photon energy for  $\text{Tl}_2\text{In}_2\text{S}_3\text{Se}$  crystal at  $T = 300$  K. Circles represent the experimental data that were fitted to a linear equation (the solid lines) to find the band gaps. Insets 1 and 2 represent the dependencies of  $(\alpha h\nu)^{1/2}$  and  $(\alpha h\nu)^2$  on photon energy, respectively.

Figure 4.7 shows the transmission spectra in the temperature range of 10-300 K for  $\text{Tl}_2\text{In}_2\text{S}_3\text{Se}$  crystal. Thick samples (300  $\mu\text{m}$ ) were used in the low temperatures. If the thin layered samples were used at low temperatures, they broken into pieces. Since they are very fragile.

Technical reasons did not allow us a direct measurement of the reflection at low temperatures. The point is that the specular reflectance attachment for a Shimadzu UV-1201 model spectrophotometer which is not adapted for the low-temperature reflection measurements via a closed-cycle helium cryostat. Therefore, for the calculation of absorption coefficient  $\alpha$  at low temperatures, the spectral dependence of room temperature reflectivity was uniformly shifted in energy according to the blue shift of the absorption edge. For this reason, the temperature dependence of indirect band gap energy ( $E_{gi}$ ) was only analyzed. The value of indirect transition energy gap decreases from 2.28 to 2.16 eV with increasing temperature from 10 to room temperature. This variation was illustrated in the inset of figure 4.7. The temperature dependence of the energy band gap can be represented by the relation

$$E_{gi}(T) = E_{gi}(0) + \frac{\gamma T^2}{T + \beta} . \quad (4.4)$$

Here,  $E_{gi}(0)$  is the band gap at zero temperature,  $\gamma = dE_{gi}/dT$  is the rate of the change of the band gap with temperature and  $\beta$  is approximately the Debye temperature. The experimental data for the dependence of  $E_{gi}$  on temperature (10-300 K) were fitted using equation 4.4 as shown in the inset of figure 4.7 (solid line corresponds to the theoretical fit). From the analysis,  $E_{gi}(0) = 2.28$  eV,  $\gamma = -6.1 \times 10^{-4}$  eV K<sup>-1</sup>, and  $\beta = 135$  K were found. The Debye temperature,  $\beta$ , were estimated using Lindemann's melting rule [91] from the analysis of X-ray results. Melting temperature  $T_m = 1048$  K was used for this calculation and  $\beta = 142$  K was found.

The obtained refractive index  $n$  as a function of wavelength is shown in figure 4.8. As seen from the figure, the refractive index in the energy region of  $h\nu < E_g$  gradually decreases from 3.45 to 3.25 with increasing wavelength in the region 616-1100 nm. To analyze the data, the single-effective-oscillator model proposed by Wemple and DiDomenico [42, 43] was used. This model could be applied to the ternary TlGaSe<sub>2</sub> and TlGaS<sub>2</sub> layered crystals successfully, [92, 93]. There is a relation between the refractive index and photon energy in the following equation

$$n^2(h\nu) = 1 + \frac{E_{so}E_d}{E_{so}^2 - (h\nu)^2} , \quad (4.5)$$

where  $E_{so}$  is the single oscillator energy and  $E_d$  is the dispersion energy. From the analysis of  $(n^2 - 1)^{-1}$  on  $(h\nu)^2$ , the oscillator parameters were obtained by fitting a linear function to the lower energy data range (1.13-2.02 eV). It is presented in inset of figure 4.8. The zero frequency refractive index  $n_0$  was estimated from equation 4.5.  $E_{so}$  and  $E_d$  were found 4.78



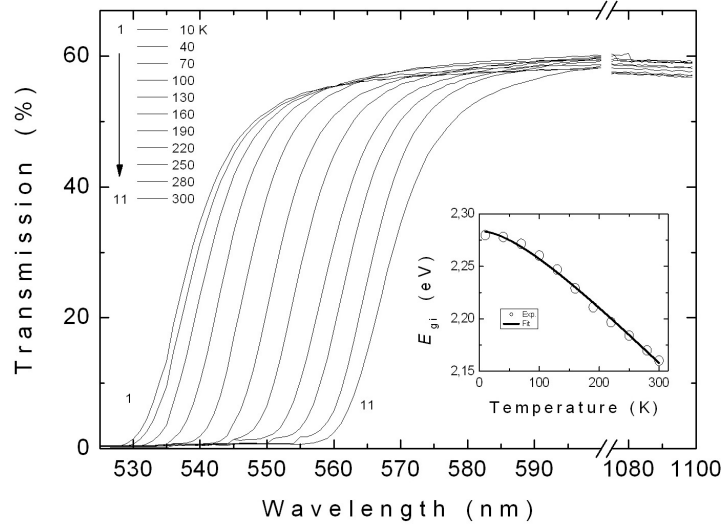


Figure 4.7: The spectral dependence of transmittance for  $\text{Tl}_2\text{In}_2\text{S}_3\text{Se}$  crystal in the temperature range of 10-300 K. Inset: The indirect band gap energy as a function of temperature. The solid line represents the fit using equation 4.4.

eV and 43.58 eV, respectively (see inset of figure 4.8). The zero-frequency dielectric constant  $\epsilon_0 = n_0^2 = 10.12$  and refractive index  $n_0 = 3.18$  were obtained from the equation 4.5. The oscillator energy  $E_{so}$  is an "average" energy gap and can be found from the relationship  $E_{so} \approx 2.0 E_{gd}$  where  $E_{gd}$  is the lowest direct band gap [44, 47]. The ratio  $E_{so}/E_{gd}$  was found to be 1.97 [89].

The oscillator strength  $S_{so}$  for  $\text{Tl}_2\text{In}_2\text{S}_3\text{Se}$  crystal can be obtained by the help of the refractive index  $n$  analysis. At low energies, there is a representation for the refractive index by a single Sellmeier oscillator [48]

$$\frac{(n_\infty^2 - 1)}{(n^2 - 1)} = 1 - \left(\frac{\lambda_{so}}{\lambda}\right)^2, \quad (4.6)$$

where  $\lambda_{so}$  is the oscillator wavelength and  $n_\infty$  is infinite wavelength refractive index. Rearranging of equation 4.6 gives

$$(n^2 - 1)^{-1} = \frac{1}{S_{so}\lambda_{so}^2} - \frac{1}{S_{so}\lambda^2}. \quad (4.7)$$

Here,  $S_{so} = (n_\infty^2 - 1)/\lambda_{so}^2$ . The values of  $S_{so}$  and  $\lambda_{so}$ , calculated from the plots of  $(n^2 - 1)^{-1}$  versus  $\lambda^{-2}$ , were found to be  $13.18 \times 10^{13} \text{ m}^{-2}$  (204.80 eV<sup>2</sup>) and  $2.60 \times 10^{-7} \text{ m}$ , respectively [89]. The obtained oscillator strength values are in the same order with those obtained for ZnS, ZnSe, Ag<sub>2</sub>S, GeSe<sub>2</sub> and TlGaS<sub>2</sub> crystals [43, 46, 93, 94].

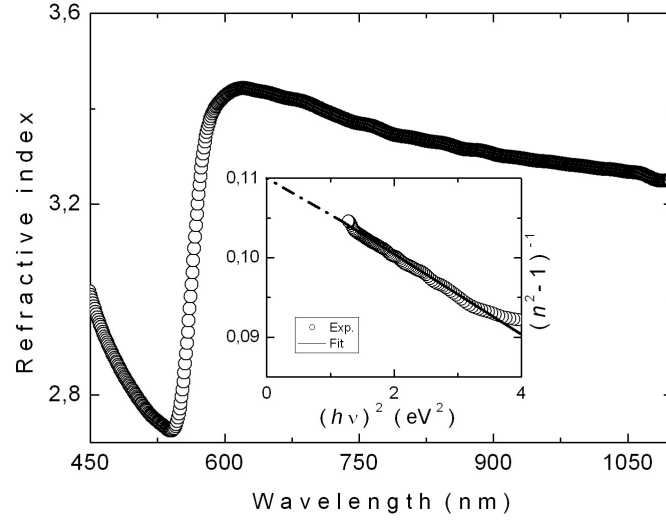


Figure 4.8: The dependence of refractive index on the wavelength for  $\text{Tl}_2\text{In}_2\text{S}_3\text{Se}$  crystal. Inset: Plot of  $(n^2 - 1)^{-1}$  versus  $(h\nu)^2$ . The solid line represents the fit using equation 4.5.

#### 4.2.3 Results of Photoluminescence Experiments

Crystals used for PL measurements had dimensions of  $6 \times 3 \times 1 \text{ mm}^3$ . In PL experiments, the sample were illuminated in a direction close to the layer. The temperature was decreased from 300 K to 22 K and it was controlled within an accuracy of  $\pm 0.5 \text{ K}$ . The PL spectra of the sample was analyzed in the wavelength region of 535-725 nm. To adjust the exciting laser intensity from 16 to  $516 \text{ mW cm}^{-2}$ , sets of neutral density filters were used. PL spectra have been corrected for the spectral response of the optical apparatus [95].

Figure 4.9 presents the PL spectra of  $\text{Tl}_2\text{In}_2\text{S}_3\text{Se}$  crystals in 22-58 K temperature range at the constant laser excitation intensity  $L = 78 \text{ mW cm}^{-2}$ . All spectra were analyzed using a fitting procedure to decompose the overlapped bands. A typical result of fitting two Gaussian peaks to A- and B- bands is shown in figure 4.10. The procedure yielded the peak position, full-width at half-maximum (FWHM) and intensity of the bands. The observed emission bands were centered at 564 nm (2.20 eV, A-band) and 642 nm (1.93 eV, B-band) at  $T = 22 \text{ K}$ . As seen from figure 4.9, emissions bands change as temperature is increased: the peak positions show several degrees of red shift, the FWHM increases and the peak intensities decrease. With increasing temperature, the FWHM rised from 0.15 to 0.20 eV and from 0.42 to 0.52 eV with increasing temperature in the range of 22-58 K for A- and B- bands, respectively [95].

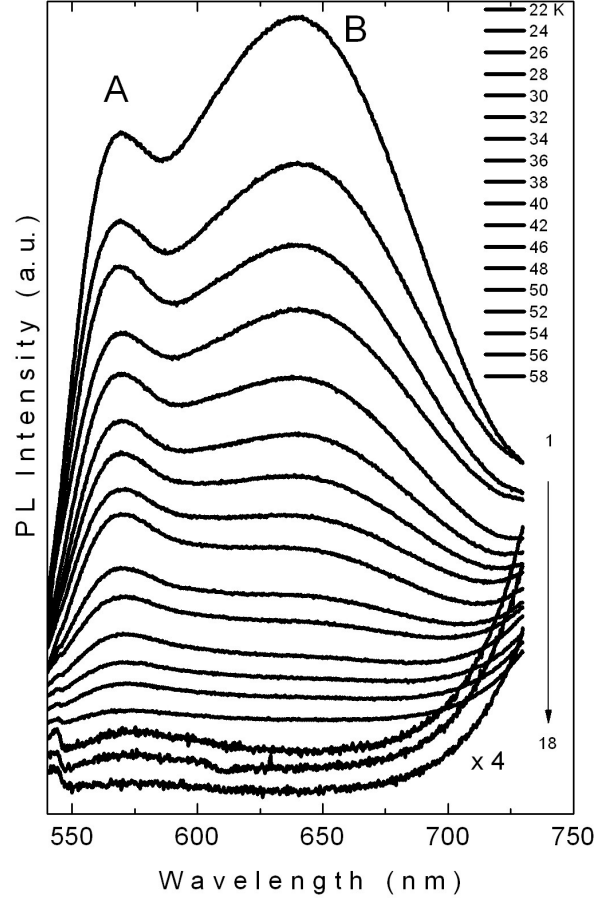


Figure 4.9: Temperature dependence of PL spectra from  $\text{Tl}_2\text{In}_2\text{S}_3\text{Se}$  crystal at excitation laser intensity  $L = 78 \text{ mW cm}^{-2}$ . Note that for curves 16-18, intensities have been multiplied by a factor of four.

There is a shift in the peak energies towards the lower energies with increasing temperature (see the inset of figure 4.11). It is known from the work [49] that when the temperature increases, the donor-acceptor pair transition energy decreases. The experimental data for the temperature dependence of PL bands intensities were fitted by the following expression:

$$I = \frac{I_0}{1 + \alpha \exp[(-E_t/k_B T)]}, \quad (4.8)$$

where  $I_0$  is a proportionality constant,  $E$  is the thermal activation energy,  $k$  is the Boltzmann constant and  $\alpha$  is the recombination process rate parameter. Figure 4.11 shows the temperature dependence of the emission band maximum intensities as a function of the reciprocal temperature in the 22-58 K range. The best fits using equation 4.8, demonstrated by the solid curves in figure 4.11, have been achieved with parameters  $I_{0A} = 3.5$ ,  $E_A = 0.02 \text{ eV}$ ,  $\alpha_A =$

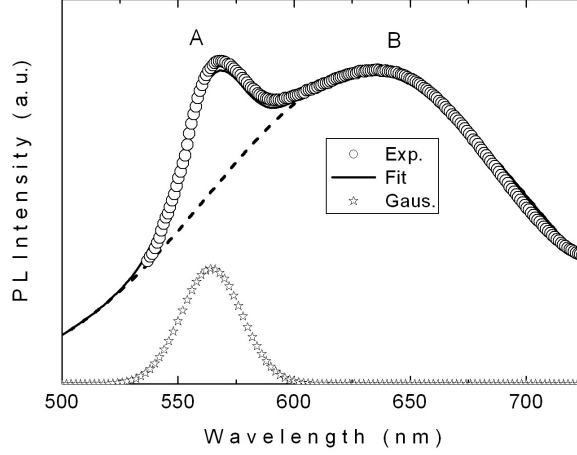


Figure 4.10: Decomposition of the PL spectrum from  $\text{Tl}_2\text{In}_2\text{S}_3\text{Se}$  crystal into two Gaussian lineshapes ( $T = 22 \text{ K}$ ,  $L = 516 \text{ mW cm}^{-2}$ ).

1128.3 and  $I_{0B} = 26.7$ ,  $E_B = 0.01 \text{ eV}$ ,  $\alpha_B = 141.8$  for A- and B- bands, respectively. Since  $\text{Tl}_2\text{In}_2\text{S}_3\text{Se}$  crystal is an  $n$ -type semiconductor, it is believed that these levels are shallow donor levels located at  $E_{dA} = 0.02 \text{ eV}$  and  $E_{dB} = 0.01 \text{ eV}$  below the bottom of the conduction band. These shallow levels can be point defects. They were created because of deviations in stoichiometry or uncontrolled impurities. The latter may be attributed to the presence of Si impurities introduced into  $\text{Tl}_2\text{In}_2\text{S}_3\text{Se}$  during the crystal growth process in ungraphitized ampoules [95].

The laser excitation intensity dependence of PL spectra is also important to obtain information about the recombination mechanism. The PL spectra at different 16 laser intensities were shown in figure 4.12 at  $T = 22 \text{ K}$ . From the analysis of the spectra, we obtained the information about the peak energy position and intensity for emission bands at different laser excitation intensities. It is revealed that the peak energy position of A-band ( $E_{pA}$ ) does not change with laser excitation intensity, while that of B- band ( $E_{pB}$ ) shifts slightly towards higher energies with increasing excitation intensity (blue shift). Referring to work [95], it means that there are inhomogeneously distributed donor-acceptor pairs. As obtained from the data analysis, B-band maximum shifts higher energies ( $\Delta E_{pB} = 30 \text{ meV}$ ) with increasing excitation laser intensities from 16 to  $516 \text{ mW cm}^{-2}$  (i.e., 20 meV per decade of exciting radiation intensity). The observed blue shift is typical of ternary and quaternary compounds such as  $\text{CdGeAs}_2$  (10-15 meV per decade of intensity of exciting radiation)[96],  $\text{HgInGaS}_4$

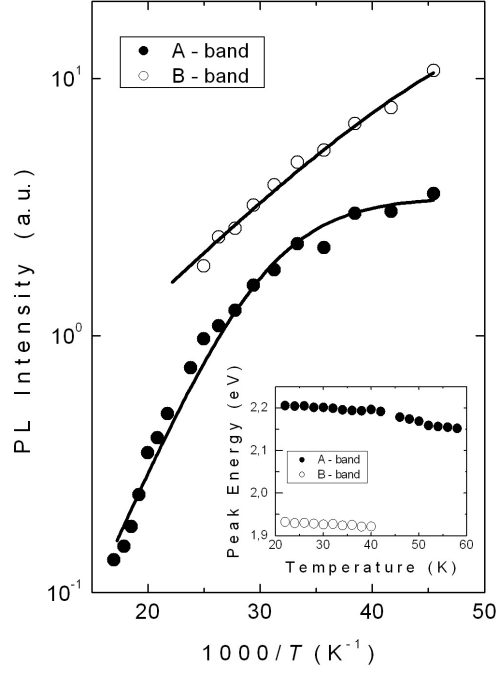


Figure 4.11: Temperature dependences of PL bands intensities for  $\text{Tl}_2\text{In}_2\text{S}_3\text{Se}$  crystal. Circles are the experimental data. Solid curves show the theoretical fits using equation 4.8. The inset: temperature dependences of emission A- and B-bands peak energies.

(20 meV per decade of intensity of exciting radiation) [97],  $\text{Tl}_2\text{InGaS}_4$  (20 meV per decade of intensity of exciting radiation)[98],  $\text{CuIn}_{1-x}\text{Ga}_x\text{Se}_2$  (15 meV per decade of intensity of exciting radiation) [99].

”At low excitation laser intensities only a small fraction of the donor and acceptor levels trap carriers. This leads to recombination from distant pairs only. At high enough excitation laser intensities all donors and acceptors are excited, which leads to a contribution from closer pairs as well. The energy of the emitted photon during a donor-acceptor pair transition has a positive contribution from a Coulombic interaction between ionized impurities. This contribution increases as the separation between the pairs decreases [49]. Furthermore, radiative transition probabilities for different pair separations are different and decrease exponentially as a function of the pair distance [49]. Distant pair recombination (contributing to the low part energy part of a donor-acceptor pair emission band) saturates at high excitation laser intensities, whereas close pairs have a larger transition probability and can accommodate more carriers. Therefore, it was observed a shift of the emission band peak energy to a higher energy as the

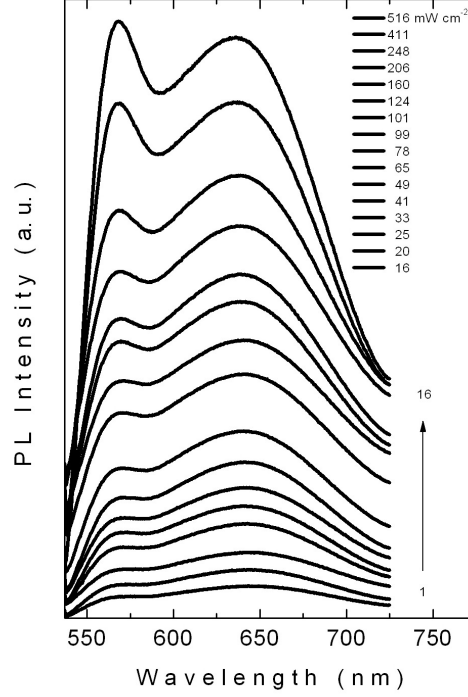


Figure 4.12: PL spectra of  $\text{Tl}_2\text{In}_2\text{S}_3\text{Se}$  crystal as a function of excitation laser intensity at  $T = 22$  K.

excitation laser intensity increases [95]” [91].

The dependence of the B- band peak energy ( $E_{pB}$ ) at  $T = 22$  K as a function of excitation laser intensity ( $L$ ) is given in figure 4.13. The experimental data in figure 4.13 were then fitted by the following expression:

$$L(E_{pB}) = L_0 \frac{(E_{pB} - E_\infty)^3}{E_B + E_\infty - 2E_{pB}} \exp \frac{-2(E_B - E_\infty)}{E_{pB} - E_\infty}, \quad (4.9)$$

where  $L_0$  is a proportionality constant,  $E_B$  is the emitted photon energy of a close donor-acceptor pair separated by a shallow impurity Bohr radius ( $R_B$ ), and  $E_\infty$  is the emitted photon energy of an infinitely distant donor-acceptor pair [56]. By using a nonlinear least square fit to the experimental data,  $E_\infty$  and  $E_B$  were found as 1.82 eV and 2.07 eV, respectively. These energy values are in good agreement with the band gap energy ( $E_{gi} = 2.27$  eV) and the observed values of the peak energy position (i.e.,  $E_\infty < 1.91$  eV  $< E_{pB} < 1.94$  eV  $< E_B < E_{gi}$ ) at  $T = 22$  K. The indirect band gap energy  $E_{gi} = 2.27$  eV at  $T = 22$  K was evaluated using the temperature coefficient of  $E_{gi}$ , reported in 4.2.2 for  $\text{Tl}_2\text{In}_2\text{S}_3\text{Se}$  crystal ( $dE_{gi}/dT = -6.1 \times 10^{-4}$  eV K $^{-1}$ ) [95].

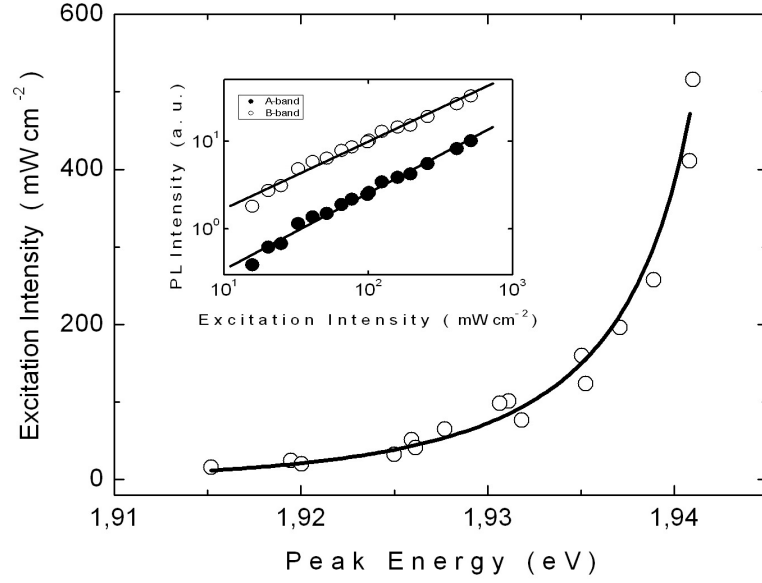


Figure 4.13: Excitation laser intensity versus emission peak energy for  $\text{Tl}_2\text{In}_2\text{S}_3\text{Se}$  crystal for B-band at  $T = 22$  K. The solid curve represents the theoretical fit using equation 4.9. Inset: Dependence of PL intensities at the emission maximums versus excitation laser intensity for A- and B-bands at  $T = 22$  K. The solid lines show the theoretical fits using equation 4.10.

In PL spectra of  $\text{Tl}_2\text{In}_2\text{S}_3\text{Se}$  crystal, the increase in the peak intensities of A- and B- bands with increase in the laser excitation intensity was also observed. The logarithmic plot of PL intensities versus laser excitation intensities are given in the inset of figure 4.13. Experimental data were fitted by a simple power law of the following form (see equation 2.31):

$$I \propto L^\gamma, \quad (4.10)$$

where,  $I$  is PL intensity,  $L$  is excitation laser intensity and  $\gamma$  is a dimensionless constant. Using the above expression the value of  $\gamma = 0.87$  and  $0.76$  for A- and B- bands were found, respectively. It is well known from the work [54, 55], laser photon energy must be greater than the band gap energy. If the  $\gamma$  values are between 1 and 2, free- and bound-exciton emission occurs. If the  $\gamma$  values are smaller or equal to 1 free-to-bound and donor-acceptor pair recombination occurs.

As a result of PL spectra analysis with respect to temperature and excitation laser intensity, there is a possible scheme for the states located in the forbidden energy gap. In the proposed scheme, shallow donor levels  $d_A$  and  $d_B$  were located at  $E_{dA} = 0.02$  eV and  $E_{dB} = 0.01$  eV below the bottom of the conduction band, respectively. The sum of the donor ( $E_{dB}$ ) and

acceptor ( $E_{aB}$ ) levels for the emission B- band can be written as [49]:

$$E_{dB} + E_{aB} = E_{gi} - E_{\infty} = 2.27 \text{ eV} - 1.82 \text{ eV} = 0.45 \text{ eV} \quad (4.11)$$

Considering that the donor level  $d_B$  was located at  $E_{dB} = 0.01 \text{ eV}$  below the bottom of the conduction band, the above energy sum suggests that the acceptor level  $a_B$  involved in the emission B- band was placed at  $E_{aB} = 0.44 \text{ eV}$  above the top of the valence band. For the A-band, the shallow donor level at  $E_{dA} = 0.02 \text{ eV}$  and the observed peak energy at  $T = 22 \text{ K}$  ( $E_{pA} = 2.20 \text{ eV}$ ), results in an acceptor level, which was located at  $E_{aA} = 0.05 \text{ eV}$  above the top of the valence band. Taking into account the above considerations, the observed emission A- and B- bands in the PL spectra have been attributed to the radiative transitions from the donor level  $d_A$  to the acceptor level  $a_A$  and from the donor level  $d_B$  to the acceptor level  $a_B$ , respectively [95].

#### 4.2.4 Results of Thermally Stimulated Current Experiments

The TSC experiments were performed in the temperature range of 10-170 K. The sample was cooled from 300 K to 10 K. Temperature controller was utilized to provide constant heating rates in the range of  $0.4\text{-}1.5 \text{ K s}^{-1}$ . A light emitting diode was used to excite the carriers. The diode light has a maximum peak of 2.6 eV. The traps were filled at  $T_0 = 10 \text{ K}$  under a bias voltage  $V_1 = 10 \text{ V}$  for about 750 s. However for the revealing of traps distribution they were filled at different illumination temperatures ( $T_{0i} = 20, 30, 37$  and  $40 \text{ K}$ ). Then the excitation was turned off. The bias voltage  $V_2$  was applied to the sample and the temperature was increased at a constant rate, after an expectation time 300 s. The bias voltage  $V_2 = 100 \text{ V}$  could be applied to the sample since the dark current contribution was low in  $\text{Ti}_2\text{In}_2\text{S}_3\text{Se}$ . The figure 4.14 shows the illumination and heating parameters of the optimum TSC conditions for  $\text{Ti}_2\text{In}_2\text{S}_3\text{Se}$  crystal .

While the illumination of the sample, positive and negative charge carriers are created. According to bias voltage, one type of carriers is driven but the other type of carriers is collected quickly. As a result of this, driven carriers are trapped. Figure 4.15 shows the TSC spectra of  $\text{Ti}_2\text{In}_2\text{S}_3\text{Se}$  for two biasing polarities at a constant rate of  $\beta = 1.2 \text{ K s}^{-1}$  in the range of 40-120 K. The peak intensity is highest when the illumination surface has negative polarity. It means that the electrons are distributed in the crystal and then trapped. As a result of this, the peak in the TSC spectra of  $\text{Ti}_2\text{In}_2\text{S}_3\text{Se}$  crystal can be considered as electron traps [100].



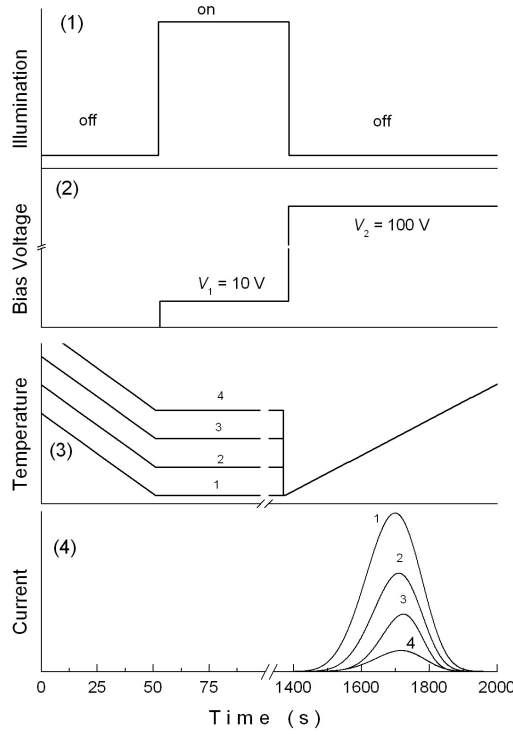


Figure 4.14: Principles of the TSC experiment for  $\text{Tl}_2\text{In}_2\text{S}_3\text{Se}$  crystals; (1) time period of applied illumination; (2) variation of bias voltage; (3) temperature variation with time for four different light illumination temperatures; (4) TSC spectra for four different light illumination temperatures: 20 (1), 30 (2), 37 (3) and 40 K (4).

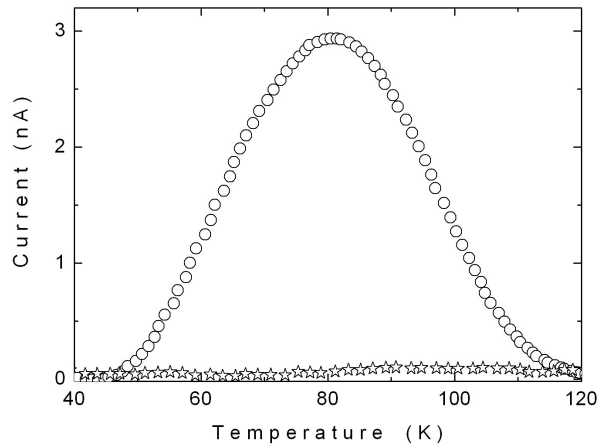


Figure 4.15: Typical experimental TSC curve of  $\text{Tl}_2\text{In}_2\text{S}_3\text{Se}$  crystals under bias voltage. Circles and stars show the experimental data obtained when the polarity of illuminated surface was negative and positive, respectively.

It is important to determine the type of trapping kinetics to analyze the TSC spectra. To analyze the TSC spectra, relative magnitudes of capture cross sections  $S_t$  and  $S_r$  of the trapping and recombination centers, respectively, are very important. If  $S_t \ll S_r$ , the process is monomolecular, i.e., slow re trapping occurs. The cases  $S_t = S_r$  and  $S_t \gg S_r$  are bimolecular and fast re trapping, respectively. For slow re trapping (monomolecular condition), electrons thermally excited from traps have greater probability of recombining with holes than being re trapped. In this case, the initial density of filled traps has no effect on both the shape and peak position of the TSC curve. Figure 4.16 shows the TSC spectra of  $\text{Tl}_2\text{In}_2\text{S}_3\text{Se}$  crystal registered for different illumination time (50-900 s) at a constant heating rate of  $\beta = 1.0 \text{ K s}^{-1}$  [100]. We obtained that the minimum illumination time as 750 s by plotting the maximum values of TSC ( $I_{\max}$ ) versus illumination time (inset of figure 4.16). To vary the initial density of filled traps, illumination time changed and it was observed that there was no change for both the shape and the peak position of the TSC curve. This fact indicates that the traps may be considered under monomolecular condition.

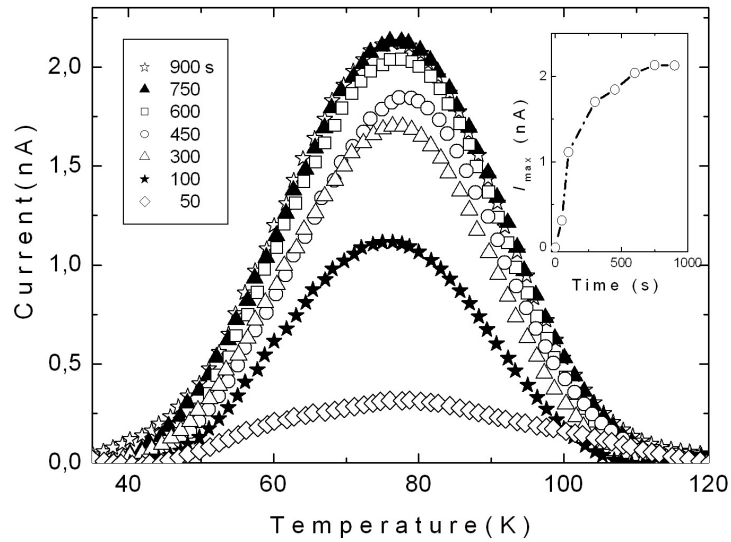


Figure 4.16: TSC spectra of the  $\text{Tl}_2\text{In}_2\text{S}_3\text{Se}$  crystals for various illumination times at a constant heating rate of  $\beta = 1.0 \text{ K s}^{-1}$ . Inset: maximum thermally stimulated currents as a function of illumination time. The dash-dotted line is only guide for the eye.

Figure 4.17 presents TSC spectra of the  $\text{Tl}_2\text{In}_2\text{S}_3\text{Se}$  crystals measured at six heating rates of  $\beta = 0.4\text{-}1.5 \text{ K s}^{-1}$  in the temperature range of 30-125 K [100]. As expected, thermally stimulated current gradually increases, and the peak maximum ( $T_m$ ) shifts to a high temperature with

increasing the heating rate.

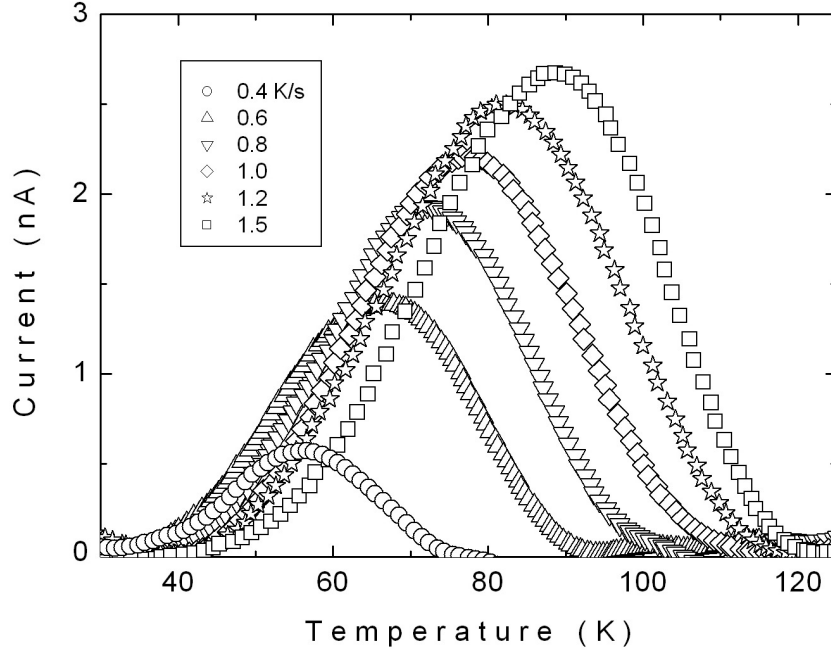


Figure 4.17: The experimental TSC spectra of  $\text{Tl}_2\text{In}_2\text{S}_3\text{Se}$  crystals at different heating rates.

To reveal the traps distribution in  $\text{Tl}_2\text{In}_2\text{S}_3\text{Se}$  crystals, the sample was excited by light for 750 s at different illumination temperatures ( $T_{0i}$ ) ranging from 20 to 40 K. Then the light source was switched off and the sample was cooled down to 10 K. After that, in order to excite the trapped electrons to the conduction band, the sample was heated at a constant rate  $\beta = 1.2 \text{ K s}^{-1}$ . The experimental TSC spectra of  $\text{Tl}_2\text{In}_2\text{S}_3\text{Se}$  crystal at different illumination temperatures ( $T_{0i} = 20, 30, 37$ , and 40 K) are shown in figure 4.18. The intensity of the TSC spectra decreased and the maximum values of peak shifted towards higher temperatures with increasing illumination temperatures. This situation supports the validity of a quasi-continuous traps distribution [85, 97, 101, 102].

The area enclosed under the curve obtained with illumination at temperature  $T_{0i}$  is proportional to the total number of carriers released from the traps during the heating process. In order to obtain the energetic traps distribution in the studied crystals the peak was calculated from the area difference of two successive experimental TSC spectra for the pairs of illumination temperatures  $T_{0i}$  and  $T_{0i+1}$ : 20 and 30 K, 30 and 37 K, 37 and 40 K. The maximum

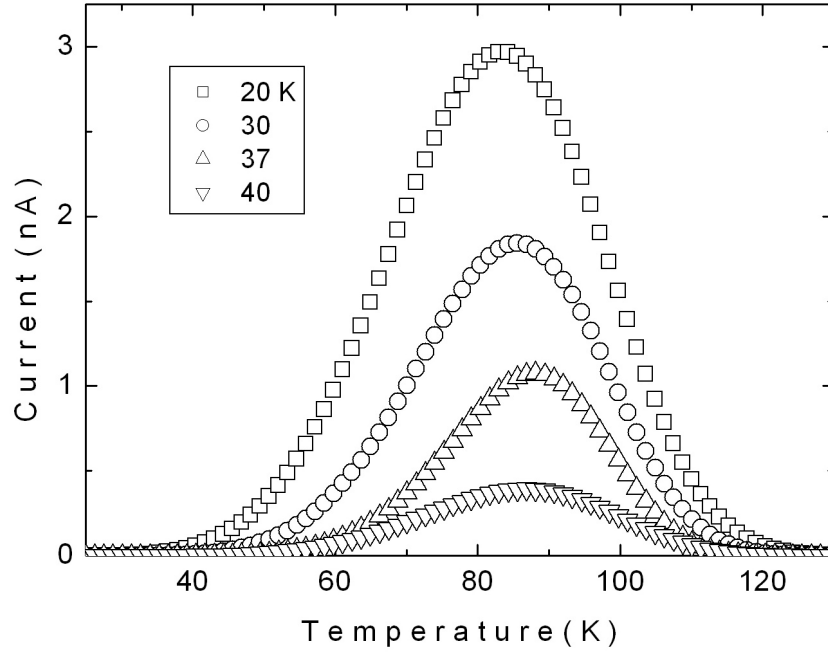


Figure 4.18: The TSC spectra of  $\text{Tl}_2\text{In}_2\text{S}_3\text{Se}$  crystals at different illumination temperatures  $T_0$ .

temperatures ( $T_{mi}$ ) and areas ( $Q_i$ ) of peak, evaluated from the subtracted two successive TSC curves related to different pairs of illumination temperatures, are listed in the table 4.2. Since the difference in the current value during heating is due to the trap levels above a certain energy level, the mean activation energy of those traps can be found with the help of the initial rise method previously defined in 2.2.5.4. In this method only the initial part of the subtracted TSC curves were analyzed for the peaks. When the traps start to empty with temperature, the TSC is directly proportional to  $\exp(-E_t/k)$ . Therefore, a semi-logarithmic plots of the currents versus  $1/T$  gives the straight lines with the slopes of  $(-E_{ti}/k)$  for the peak as shown in figure 4.19. The mean activation energies of traps calculated for the curves are presented table 4.2.

Inset of figure 4.19 presents the plots of  $\ln(Q_i)$  (the amount of the released charge during the heating process) as a function of the mean activation energies. The dependence is well approximated by the exponent, which suggests the presence of an exponential distribution of the traps. The exponential distribution is consistent with the presence of fluctuations in the crystal potential, caused by structural defects, which give rise to localized states acting as

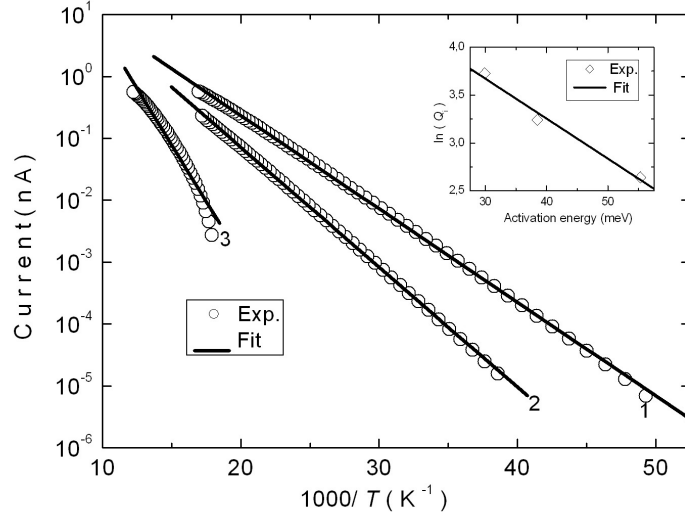


Figure 4.19: Thermally stimulated currents versus  $1000/T$  for the TSC spectra of  $\text{Tl}_2\text{In}_2\text{S}_3\text{Se}$  crystals, calculated from the difference of two successive experimental TSC spectra for the selective pairs of temperatures 20-30 K, 30-37 K and 37-40 K (curves from 1 to 3). Solid lines present the theoretical fits according to the initial rise method. Inset: The logarithmic plot of released charge as a function of activation energy. Squares show the experimental data for the peak. Solid line is theoretical fit according to equation 4.12.

traps for the carriers [101].

The following expression can be written for the traps filled at the illumination temperature  $T_{0i}$  by assuming an exponential traps distribution, whose density at energy  $E_{ti}$  will be given by  $N_{ti} = A \exp(-\alpha E_{ti})$ , [85]

$$Q_i \propto A \exp(-\alpha E) . \quad (4.12)$$

Here,  $\alpha$  is the energy parameter that characterizes the traps distribution. From the analysis of the graph  $\ln(Q_i)$  versus mean activation energies, the value of  $\alpha = 0.094 \text{ meV}^{-1}$ , corresponding to 25 meV/decade were found, respectively (inset of figure 4.19).

The obtained values of  $E_{ti}$  and  $T_{mi}$  were used to calculate the attempt-to-escape frequencies  $\nu_i$  from the following expression

$$\nu_i = \frac{\beta E_{ti}}{k T_{mi}^2} \exp\left(\frac{E}{k T_{mi}}\right) , \quad (4.13)$$

The capture cross section of the traps was determined using the following equation

$$S_{ti} = \frac{\nu_i}{N_c \vartheta_{th}} , \quad (4.14)$$

Table 4.2: The illumination temperatures of two successive experimental TSC curves ( $T_{0i}$ - $T_{0i+1}$ ); maximum temperature ( $T_{mi}$ ) and area ( $Q_i$ ) of calculated TSC curves ; mean activation energy ( $E_{ti}$ ), capture cross section ( $S_{ti}$ ), attempt-to-escape frequency ( $\nu_i$ ) and concentration ( $N_{ti}$ ) of traps in  $\text{Ti}_2\text{In}_2\text{S}_3\text{Se}$  crystal.

$T_{0i} - T_{0i+1}$ (K)	$T_{mi}$ (K)	$Q_i$ ( $\mu\text{C}$ )	$E_{ti}$ (meV)	$S_{ti}$ ( $\text{cm}^2$ )	$\nu_i$ ( $\text{s}^{-1}$ )	$N_{ti}$ ( $\text{cm}^{-3}$ )
20-30	78.8	41.5	30	$3.5 \times 10^{-25}$	0.9	$2.6 \times 10^{12}$
30-37	81.0	25.6	39	$8.5 \times 10^{-25}$	2.9	$2.8 \times 10^{12}$
37-40	88.5	14.0	55	$3.6 \times 10^{-24}$	13.5	$1.7 \times 10^{12}$

where  $N_c = 2(2\pi m^* ekT/h^2)^{3/2}$  is the effective density of states in the conduction band and  $\vartheta_{th}$  is the thermal velocity of a free electron. The effective mass  $m_e^* = 0.14 m_0$  [103] was utilized to calculate  $N_c$  and  $\vartheta_{th}$ . Using the latter values, the capture cross section of the traps in  $\text{Ti}_2\text{In}_2\text{S}_3\text{Se}$  crystals were estimated (table 4.2). It will be noted that the obtained magnitudes of attempt-to-escape frequency and capture cross section of the traps for all studied crystals are low, which suggests a strong repulsive barrier to capture the carriers [104].

The concentration of the traps was estimated using the relation [105]

$$N_{ti} = \frac{Q_i}{ALeG} . \quad (4.15)$$

Here,  $Q_i$  is amount of charge released during the TSC measurement that can be calculated from the area of the TSC peak and  $G$  is the photoconductivity gain calculated from [87]

$$G = \frac{\tau}{t_{tr}} = \frac{\tau \mu V_2}{L^2} . \quad (4.16)$$

In this equation,  $\tau$  is the carrier lifetime and  $t_{tr}$  is the carrier transit time between the electrodes. The carrier lifetime were determined from the PC decay experiments [88].

After termination of light pulse at  $t = t_0$ , the current decays are nearly exponential .The carrier lifetime  $t_{tr}$  is determined by the corresponding output voltage equation

$$V = V_0 + C \exp\left(\frac{-t}{\tau}\right) , \quad (4.17)$$

where  $V_0$  is voltage at  $t = \infty$  and  $C$  is a constant. The theoretical fit (solid line) using equation 4.17 to the experimental data for  $\text{Ti}_2\text{In}_2\text{S}_3\text{Se}$  crystals is shown in figure 4.20. From the decay of photocurrent, carrier lifetime was obtained as  $\tau = 13.6$  ms. The corresponding photoconductivity gain was found to be  $G = 2498$  from the equation 4.16 utilizing  $V_2 = 100$  V and  $\mu = 28 \text{ cm}^2 \text{ V}^{-1} \text{ sec}^{-1}$  [103]. The trap concentrations ( $N_{ti}$ ) were calculated using the equation 4.15 as  $2.6 \times 10^{12}$ ,  $2.8 \times 10^{12}$  and  $1.7 \times 10^{12} \text{ cm}^{-3}$ .

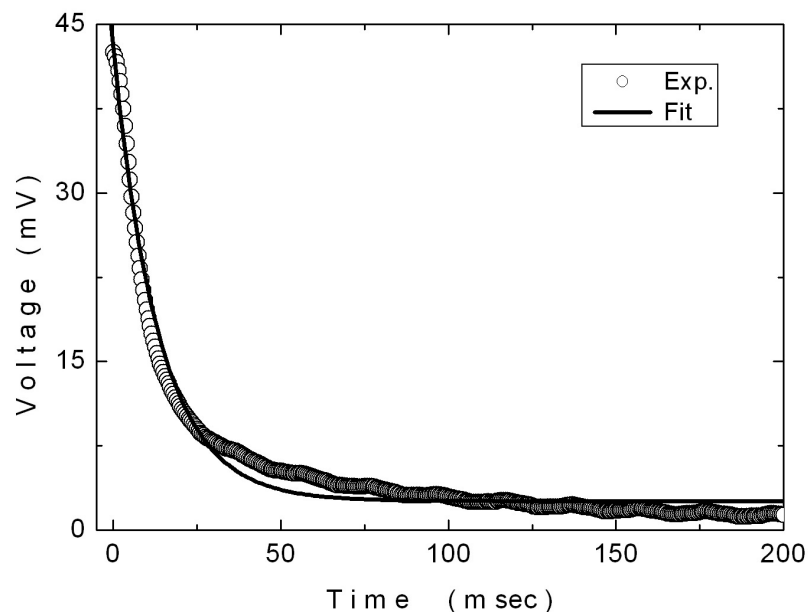


Figure 4.20: The photoconductivity decay curve for the  $\text{Tl}_2\text{In}_2\text{S}_3\text{Se}$  crystals.

### 4.3 Structural, Optical and Electrical Transport Properties of $\text{TlInSeS}$ Layered Crystals

#### 4.3.1 Results of X-ray Experiments and Energy Dispersive Spectral Analysis

For  $\text{TlInSeS}$  crystals, the resulting ingot were red in color and the freshly cleaved surfaces were mirror-like. The X-ray diffractogram of  $\text{TlInSeS}$  crystal are shown in figure 4.21. In table 4.3, the Miller indices ( $hkl$ ), the observed and calculated interplanar spacings ( $d$ ), and the relative intensities ( $I/I_0$ ) of the diffraction lines are presented. Using "DICVOL 04", the lattice parameters of the monoclinic unit cell,  $a = 0.72850$ ,  $b = 0.45380$ ,  $c = 0.78357$  nm, and  $\beta = 106.22^\circ$ , were obtained [106].

By the help of EDSA, the chemical composition of  $\text{TlInSeS}$  crystals was determined as  $\text{Tl} : \text{In} : \text{Se} : \text{S}$ , 25.7 : 25.9 : 24.3 : 24.1, respectively [106]. The spectrum obtained from EDSA is shown in figure 4.22.

Table 4.3: X-ray powder diffraction data for TlInSSe crystals.

No.	<i>hkl</i>	$d_{obs}(nm)$	$d_{calc}(nm)$	$I/I_0$
1	1 1 0	0.38834	0.38866	43.7
2	2 0 0	0.37588	0.37625	66.5
3	0 0 2	0.34998	0.34981	30.6
4	2 1 0	0.28984	0.28965	100.0
5	1 1 2	0.24327	0.24313	13.3
6	3 0 1	0.21759	0.21758	17.2
7	3 1 1	0.19629	0.19620	39.2
8	1 1 3	0.18824	0.18833	11.4
9	2 0 -4	0.17884	0.17883	16.3
10	4 0 1	0.17010	0.17013	12.7
11	0 2 3	0.16261	0.16263	24.5

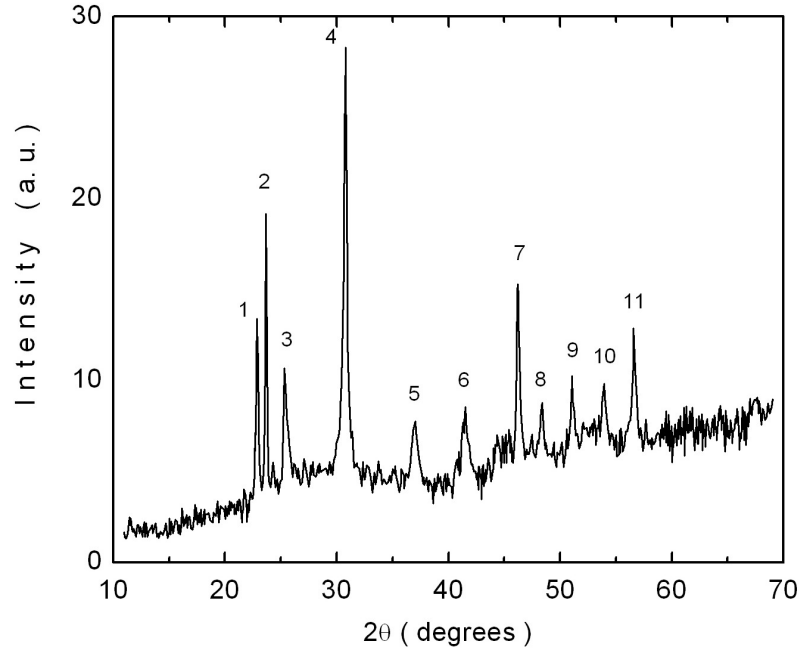


Figure 4.21: X-ray diffraction pattern of TlInSeS powder sample.

#### 4.3.2 Results of Transmission and Reflection Experiments

The transmittance ( $T$ ) and reflectivity ( $R$ ) spectra of TlInSeS single crystals were recorded in the wavelength ( $\lambda$ ) range of 500-1100 nm (figure 4.23). The absorption coefficient  $\alpha$  and refractive index  $n$  were obtained from the equations 4.1 and 4.2. The reflection measurements were done using specimens with natural cleavage planes and a thickness such that  $\alpha d \gg 1$ . In the reflection measurements, the samples having thickness such that  $\alpha d \gg 1$  were



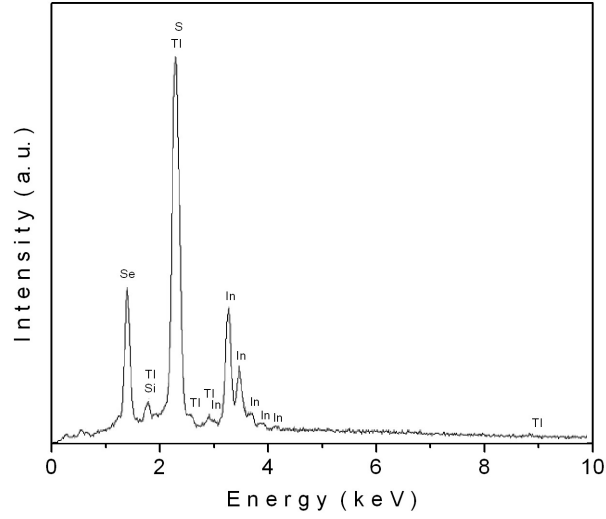


Figure 4.22: Energy dispersive spectroscopic analysis of TlInSeS crystal.

used whereas in the transmission measurements, the sample thickness was reduced by using transparent tape and determined from transmission interference fringes at wavelength slightly longer than the intrinsic absorption edge, i.e. in a region with relatively high transmission (figure 4.23). Using the the long wavelength value of the refractive index  $n = 3.30$  in the equation 2.21, the thickness of the sample was calculated. Mostly, the sample thickness was of the order of  $20\ \mu\text{m}$  [106].

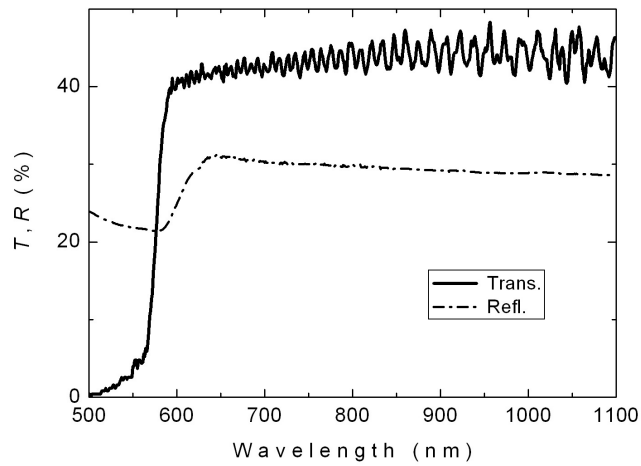


Figure 4.23: The spectral dependence of transmittance and reflectivity for TlInSeS crystal at room temperature.

The  $\alpha$  can be represented by the equation 4.3. Figure 4.24 shows the variation of  $\alpha$  from 190 to 5100  $\text{cm}^{-1}$  with increasing photon energy from 1.90-2.50 eV. From the analysis of the experimental data it was shown that, the absorption coefficient was proportional to  $(h\nu - E_g)^p$  with  $p = 2$  and  $1/2$  for ranges 2.09-2.21 and 2.26-2.43 eV, respectively. Insets 1 and 2 of figure 4.24 display the dependencies of  $(\alpha h\nu)^{1/2}$  and  $(\alpha h\nu)^2$  on photon energy  $h\nu$ , respectively. The circles show the experimental data. They were fitted to a linear equation (the solid lines) to find the energy band gaps. The linear dependencies for the relations  $(\alpha h\nu)^{1/2}$  and  $(\alpha h\nu)^2$  versus  $h\nu$  suggests the realization of indirect and direct allowed transitions, respectively. The extrapolations of straight lines, indirect band gap energy  $E_{gi} = 2.05 \pm 0.02$  eV and direct band gaps energy  $E_{gd} = 2.21 \pm 0.02$  eV were calculated, respectively [106]. Indirect and direct inter-band edge transitions can exist for thallium containing layered crystals [106] because of specific features of the prevailing  $p$ -anionic upper valence band and  $s$ -Tl states [90].

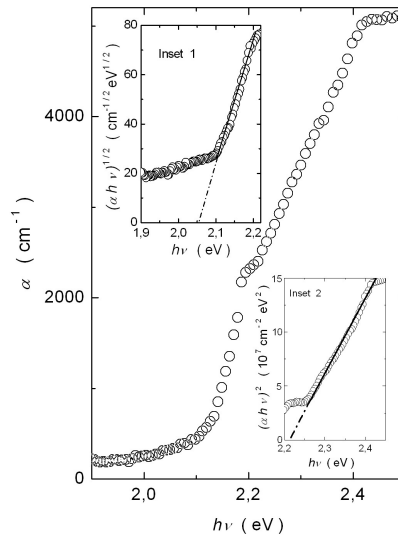


Figure 4.24: The variation of absorption coefficient as a function of photon energy for TlInSeS crystal at  $T = 300$  K. Circles represent the experimental data that were fitted to a linear equation (the solid lines) to find the band gaps. Insets 1 and 2 represent the dependencies of  $(\alpha h\nu)^{1/2}$  and  $(\alpha h\nu)^2$  on photon energy, respectively.

Figure 4.25 shows the transmission spectra of TlInSeS crystal that was registered in the temperature range of 10-300 K. Thick samples (300  $\mu\text{m}$ ) were used in the low temperatures. If the thin layered samples were used at low temperatures, they broken into pieces. Since they are very fragile. The value of indirect transition energy gap obtained by the analysis decreases

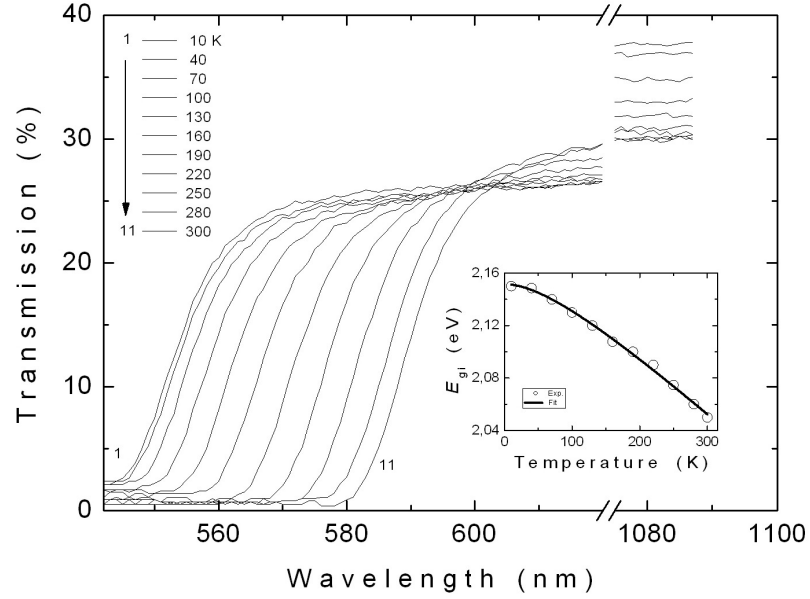


Figure 4.25: The spectral dependence of transmittance for TIInSeS crystal in the temperature range of 10-300 K. Inset: The indirect band gap energy as a function of temperature. The solid line represents the fit using equation 4.4.

from 2.15 to 2.05 eV with increasing temperature from 10 to 300 K, as illustrated in the inset of figure 4.25. The temperature dependence of the energy band gap can be represented by the relation 4.4. The experimental data for the dependence of  $E_{gi}$  on temperature (10-300 K) were fitted using equation 4.4 as shown in the inset of figure 4.25 (solid line corresponds to the theoretical fit). From the analysis,  $E_{gi}(0) = 2.15$  eV,  $\gamma = -4.7 \times 10^{-4}$  eV K<sup>-1</sup>, and  $\beta = 130$  K were found. The Debye temperature,  $\beta$ , were estimated using Lindemann's melting rule [91] from the analysis of X-ray results. Melting temperature  $T_m = 1045$  K was used for this calculation and  $\beta = 141$  K was found [106].

The obtained refractive index  $n$  as a function of wavelength is shown in figure 4.26. As seen from this figure, the refractive index in the energy region of  $h\nu < E_g$  gradually decreases from 3.54 to 3.30 with increasing wavelength in the region 645-1100 nm. To analyze the data, the single-effective-oscillator model proposed by Wemple and DiDomenico [42, 43] was used. This model could be applied to the ternary TlGaSe<sub>2</sub> and TlGaS<sub>2</sub> layered crystals successfully, [92, 93]. There is a relation between the refractive index and photon energy ( see the equation 4.5). From the analysis of  $(n^2 - 1)^{-1}$  on  $(h\nu)^2$ , the oscillator parameters were obtained by fitting a linear function to the lower energy data range (1.13-1.94 eV). It is presented in inset

of figure 4.26. The zero frequency refractive index  $n_0$  was estimated from equation 4.5, i.e. according to the equation 2.23 [106]. From the analysis of the inset of figure 4.26 the values of the parameters  $E_{so}$  and  $E_d$  were found to be 4.46 eV and 41.74 eV, respectively. The zero-frequency dielectric constant  $\epsilon_0 = n_0^2 = 10.36$  and refractive index  $n_0 = 3.22$  were evaluated by means of equation 4.5 [106]. The oscillator energy  $E_{so}$  is an "average" energy gap and can be found from the relationship  $E_{so} \approx 2.0 E_{gd}$  where  $E_{gd}$  is the lowest direct band gap [44, 47]. The ratio  $E_{so}/E_{gd}$  was found to be 2.0.

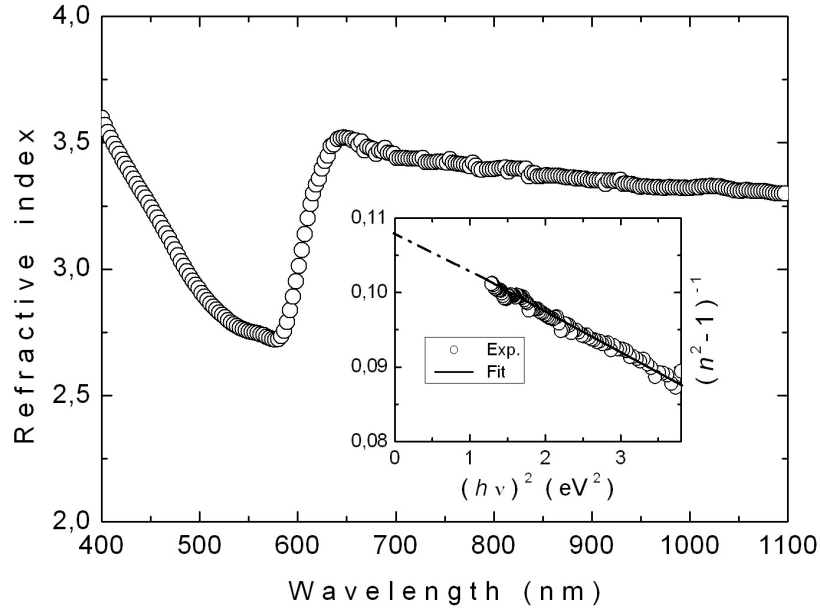


Figure 4.26: The dependence of refractive index on the wavelength for TIInSeS crystal. Inset: Plot of  $(n^2 - 1)^{-1}$  versus  $(h\nu)^2$ . The solid line represents the fit using equation 4.5.

The oscillator strength  $S_{so}$  for TIInSeS crystal can be obtained by the help the refractive index  $n$  analysis using the equations 4.6 and 4.7. The values of  $S_{so}$  and  $\lambda_{so}$ , calculated from the plots of  $(n^2 - 1)^{-1}$  versus  $\lambda^{-2}$ , were found to be  $1.21 \times 10^{14} \text{ m}^{-2}$  (188.02 eV<sup>2</sup>) and  $2.78 \times 10^{-7} \text{ m}$  respectively [106]. The obtained oscillator strength values are in the same order with those obtained for ZnS, ZnSe, Ag<sub>2</sub>S, GeSe<sub>2</sub> and TlGaS<sub>2</sub> crystals [43, 46, 93, 94].

### 4.3.3 Results of Photoluminescence Experiments

The photoluminescence spectra of TIInSeS layered crystals have been studied in the wavelength region of 500-700 nm and temperature region of 10-65 K and reported in Ref. [91].

The observed emission band, centered at 584 nm (2.122 eV) at  $T = 10$  K, was assigned to donor-acceptor pair recombination. The variation of the PL band intensity versus excitation laser intensity has also been investigated. The red and blue shifts of this band have been observed with increasing temperature and increasing laser excitation intensity, respectively. The PL was found to be due to radiative transitions from the shallow donor level located at 0.023 eV below the conduction band to the moderately deep acceptor level at 0.064 eV located above the valence band.

#### 4.3.4 Results of Thermally Stimulated Current Experiments

The TSC experiments were performed in the temperature range of 10-180 K. The sample was cooled from 300 K to 10 K. The temperature controller was utilized to provide constant heating rates in the range of 0.2-1.0 K s<sup>-1</sup>. A light emitting diode was used to excite the carriers. The diode light has a maximum peak of 2.6 eV. The traps were filled at  $T_0 = 10$  K under a bias voltage  $V_1 = 10$  V for about 600 s. However for the revealing of traps distribution they were filled at different illumination temperatures ( $T_{0i} = 30, 45, 52$  and  $57$  K). Then the excitation was turned off. The bias voltage  $V_2$  was applied to the sample and the temperature was increased at a constant rate, after an expectation time 60 s. The bias voltage  $V_2 = 100$  V could be applied to the sample since the dark current contribution was low in TlInSeS. The figure 4.27 shows the illumination and heating parameters of the optimum TSC conditions for TlInSeS crystal [107].

Figure 4.28 shows the TSC spectra of TlInSSe for two biasing polarities at a constant heating rate  $\beta = 0.8$  K s<sup>-1</sup> in the temperature range of 10-180 K. Since, the polarity of the illuminated surface is negative, the intensity of the peak is highest. The peak appearing in the TSC spectra of TlInSeS crystal can be considered as electron traps [107].

Figure 4.29 shows the TSC spectra of TlInSeS crystal registered for different illumination time (50-600 s) at a constant heating rate  $\beta = 0.8$  K s<sup>-1</sup>. We obtained that the minimum illumination time as 600 s by plotting the maximum values of TSC ( $I_{max}$ ) versus illumination time (inset of figure 4.29). To vary the initial density of filled traps, illumination time changed and it was observed that there was no change for both shapes and peak positions of the TSC curve. This fact indicates that the traps may be considered under monomolecular condition.

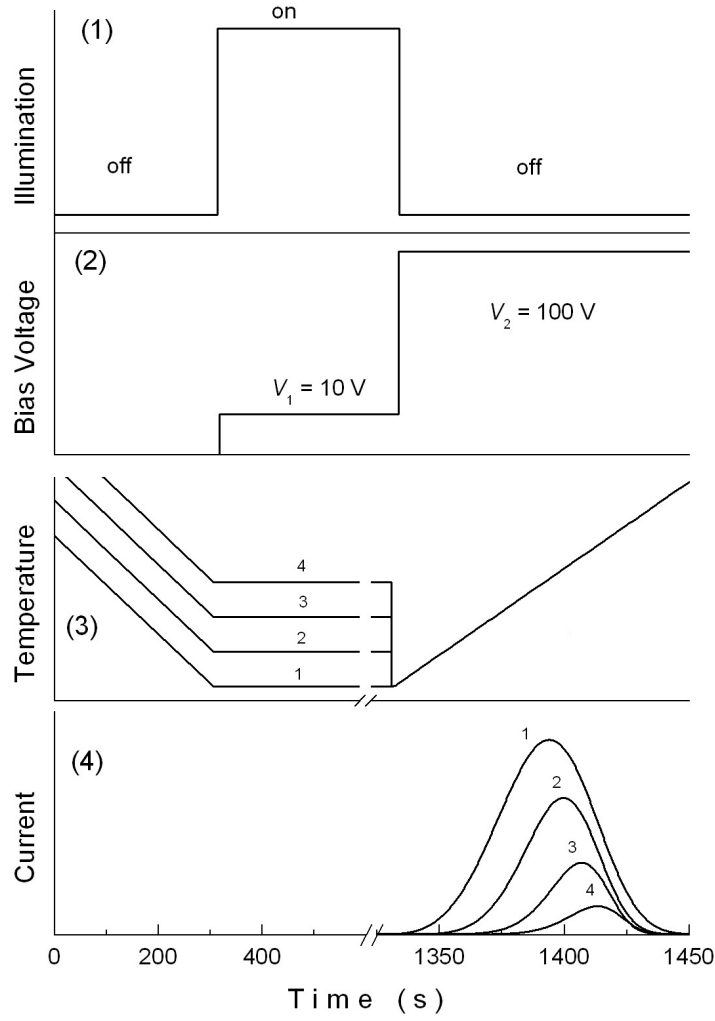


Figure 4.27: Principles of the TSC experiment for TIInSeS crystals; (1) time period of applied illumination; (2) variation of bias voltage; (3) temperature variation with time for four different light illumination temperatures; (4) TSC spectra for four different light illumination temperatures: 30 (1), 45 (2), 52 (3) and 57 K (4).

To estimate the mean activation energy of the traps, we used the isothermal decay method defined in subsection 2.2.5.3. In this method the sample was heated from  $T_0$  to  $T_p$  at a constant rate. After that, the sample was held at  $T_p$  until complete detrapping. For this process, the TSC can be described by (see equation 2.98)

$$I = I_0 \exp(-\gamma t), \quad (4.18)$$

where  $I_0$  is initial current at time  $t = 0$  and  $\gamma = \nu \exp(-E_t/kT_p)$ . The TSC decay measurement on the TIInSeS crystals were repeated at  $T_p = 50, 55, 60, 65, 70, 75$  and  $80$  K at a constant

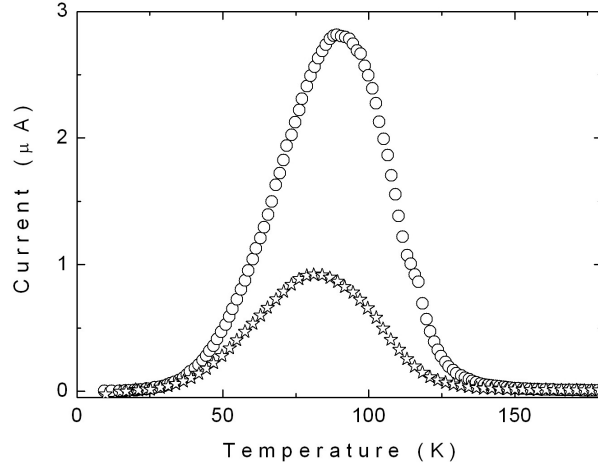


Figure 4.28: Typical experimental TSC curve of TIInSeS crystals under bias voltage. Circles and stars show the experimental data obtained when the polarity of illuminated surface was negative and positive, respectively.

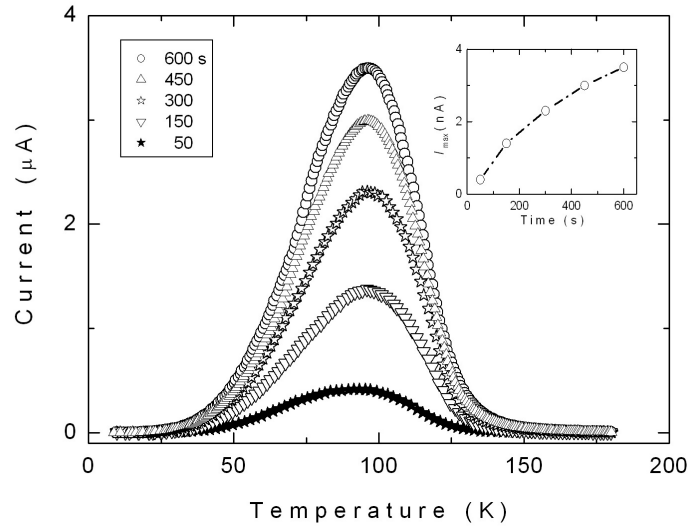


Figure 4.29: TSC spectra of the TIInSeS crystals for various illumination times at a constant heating rate of  $\beta = 0.8 \text{ K s}^{-1}$ . Inset: maximum thermally stimulated currents as a function of illumination time. The dash-dotted line is only guide for the eye.

heating rate  $0.8 \text{ K s}^{-1}$  (figure 4.30). From the analysis of  $\ln(I)$  versus time  $t$  the were obtained for each temperature  $T_p$ . By the help of  $\ln \gamma$  values versus  $1000/T_p$  graph (inset of figure 4.30) the mean activation energy  $E_t$  was obtained as 25 meV [107].

Figure 4.31 presents TSC spectra of the TIInSeS crystals measured at six heating rates of  $\beta =$

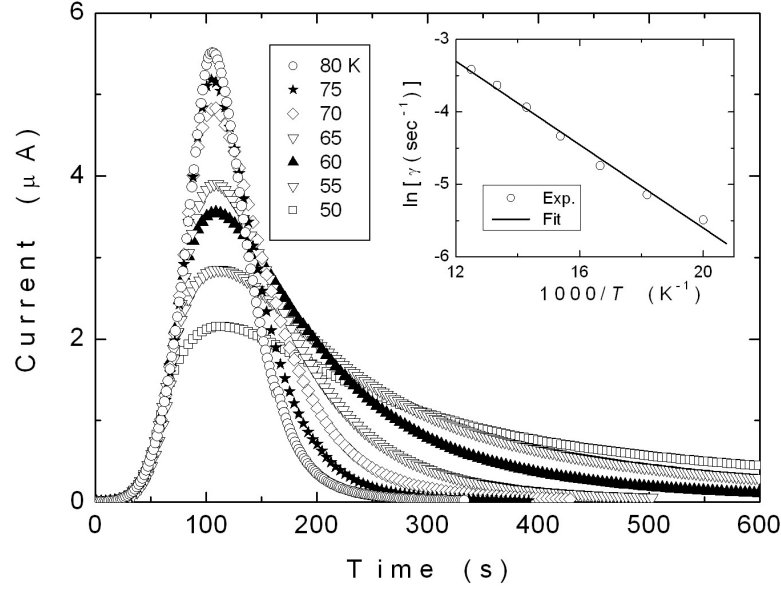


Figure 4.30: Experimental TSC spectra of TIInSeS crystals at different temperatures  $T_p = 50, 55, 60, 65, 70, 75$  and  $80$  K. Inset:  $\gamma = \nu \exp(-E_t/kT_p)$  plot as a function of  $1000/T_p$ .  $\nu$  is the attempt-to-escape frequency of a trapped carrier.

$0.2\text{-}1.0 \text{ K s}^{-1}$  with step  $0.2 \text{ K s}^{-1}$  in the temperature range of  $10\text{-}180 \text{ K}$ . As expected, while the heating rate increases, TSC increases and there is a shift in peaks maximum ( $T_m$ ) to higher temperatures [107].

The analysis of the TSC data gives information about the characteristic features of the traps distribution. For this reason, the sample was excited by light at different illumination temperatures ( $T_{0i}$ ) ranging from  $30$  to  $57 \text{ K}$ . The sample was illuminated at  $T_{0i}$  for  $600 \text{ s}$  then the light source was switched off and the sample was cooled down to  $10 \text{ K}$ . Thereafter, the sample was heated at a constant rate  $\beta = 0.8 \text{ K s}^{-1}$  to excite the trapped electrons to the conduction band. The experimental TSC spectra of TIInSSe crystal at different illumination temperatures ( $T_{0i} = 30, 45, 52,$  and  $57 \text{ K}$ ) are shown in figure 4.32. The intensity of the TSC spectra decreased and the peak maximum shifted towards higher temperatures with increasing light illumination temperatures. This fact supports the validity of a quasi-continuous traps distribution [85, 97, 101, 102].

The area enclosed under the curve obtained with illumination at temperature  $T_{0i}$  is proportional to the total number of carriers released from the traps during the heating process. In order to obtain the energetic traps distribution in the designated temperature region, the total



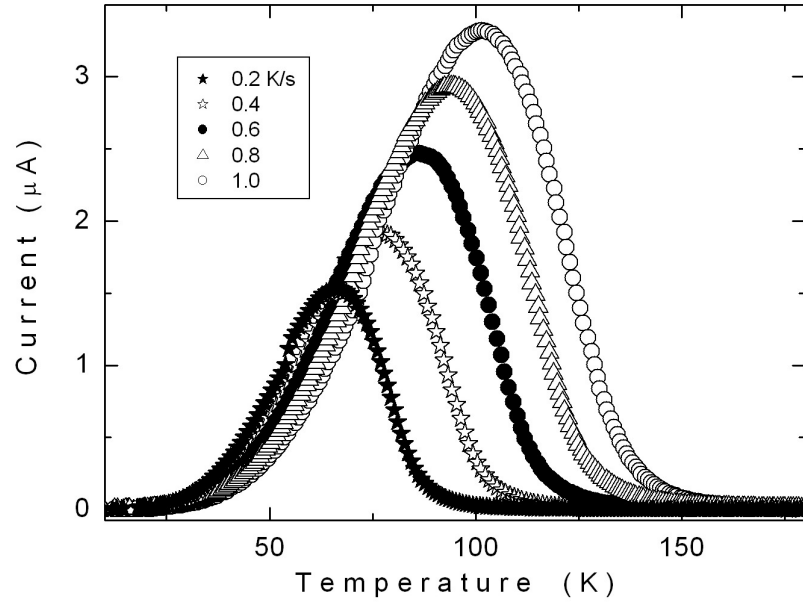


Figure 4.31: The experimental TSC spectra of TlInSeS crystals at different heating rates.

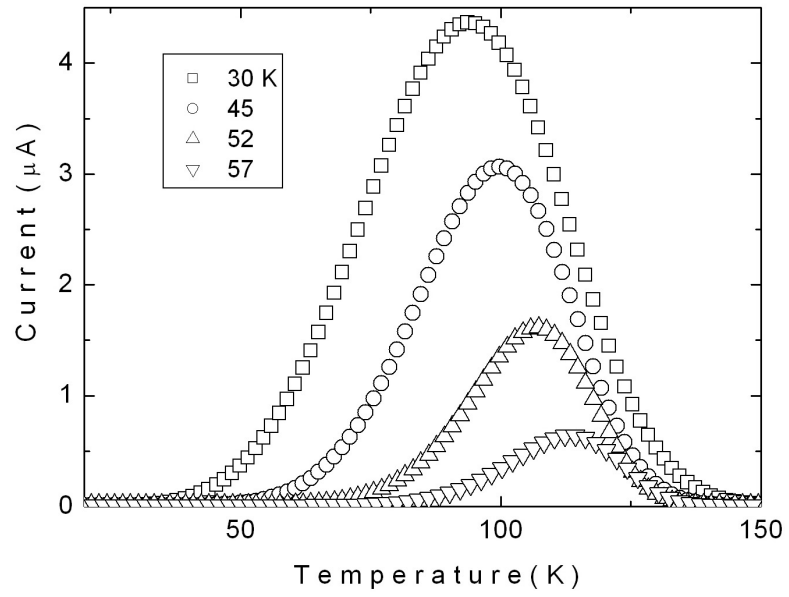


Figure 4.32: The TSC spectra of TlInSeS crystals at different illumination temperatures  $T_0$ .

charge released from the traps is calculated from the area difference of two successive experimental TSC spectra related to the pairs of illumination temperatures  $T_{0i}$  and  $T_{0i+1}$ : 30 and 45 K, 45 and 52 K and 52 and 57 K. The maximum temperatures ( $T_{mi}$ ) of calculated TSC curves

with corresponding peak areas ( $Q_i$ ) are listed in table 4.4. Since the difference in the current value during heating is due to the trap levels above a certain energy level, the mean activation energy of those traps can be found with the help of the initial rise method. A semi-logarithmic plots of the currents versus  $1/T$  gives the straight lines with the slopes of  $(-E_{ti}/k)$  for the peak as shown in figure 4.33. The mean activation energies of traps calculated for the curves are presented table 4.4.

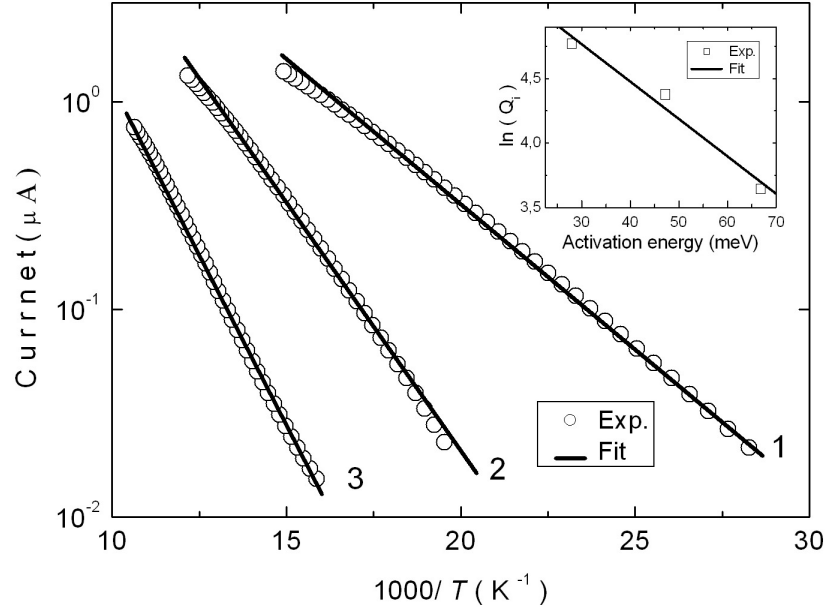


Figure 4.33: Thermally stimulated currents versus  $1000/T$  for the TSC spectra of TlInSeS crystals, calculated from the difference of two successive experimental TSC spectra for the selective pairs of temperatures 30-45 K, 45-52 K and 52-57 K (curves from 1 to 3). Solid lines present the theoretical fits according to the initial rise method. Inset: The logarithmic plot of released charge as a function of activation energy. Squares show the experimental data for the peak. Solid line is theoretical fit according to equation 4.12.

Table 4.4: The illumination temperatures of two successive experimental TSC curves ( $T_{0i}-T_{0i+1}$ ); maximum temperature ( $T_{mi}$ ) and area ( $Q_i$ ) of calculated TSC curves ; mean activation energy ( $E_{ti}$ ), capture cross section ( $S_{ti}$ ), attempt-to-escape frequency ( $\nu_i$ ) and concentration ( $N_{ti}$ ) of traps in TlInSeS crystal.

$T_{0i} - T_{0i+1}$ (K)	$T_{mi}$ (K)	$Q_i$ ( $\mu$ C)	$E_{ti}$ (meV)	$S_{ti}$ ( $\text{cm}^2$ )	$\nu_i$ ( $\text{s}^{-1}$ )	$N_{ti}$ ( $\text{cm}^{-3}$ )
30-45	81.4	94.5	28	$4.7 \times 10^{-25}$	1.4	$1.9 \times 10^{17}$
45-52	93.9	63.8	47	$3.1 \times 10^{-24}$	12.3	$2.3 \times 10^{17}$
52-57	104.2	30.7	67	$1.6 \times 10^{-23}$	78.6	$2.7 \times 10^{17}$

Inset of figure 4.33 presents the plots of  $\ln(Q_i)$  (the amount of the released charge during the

heating process) as a function of the mean activation energies. These dependences are well approximated by the exponent, which suggests the presence of an exponential distribution of the traps. The exponential distribution is consistent with the presence of fluctuations in the crystal potential, caused by structural defects, which give rise to localized states acting as traps for the carriers [101].

The graph  $\ln(Q_i)$  versus mean activation energies based on equation 4.12, the value of  $\alpha = 0.029 \text{ meV}^{-1}$ , corresponding to 79 meV/ decade were found, respectively (inset of figure 4.33).

The obtained values of  $E_{ti}$  and  $T_{mi}$  were used to calculate the attempt-to-escape frequencies  $\nu_i$  from the equation 4.13. The capture cross section of the traps was determined using the following equation 4.14. The effective mass  $m_e^* = 0.14 m_o$  [103] was utilized to calculate  $N_c$  and  $\vartheta_{th}$ . Using the latter values, the capture cross section of the traps in TlInSeS crystals were estimated (table 4.4). It will be noted that the obtained magnitudes of attempt-to-escape frequency and capture cross section of the traps for all studied crystals are low, which suggests a strong repulsive barrier to capture the carriers [104].

The concentration of the traps was estimated using the relations 4.15 and 4.16. The theoretical fit (solid line) using equation 4.17 to the experimental data for TlInSeS crystals is shown in figure 4.34. From the decay of photocurrent, carrier lifetime was obtained as  $\tau = 26.8 \text{ ms}$ . The corresponding photoconductivity gain was found to be  $G = 2080$  from the equation 4.16 utilizing  $V_2 = 100 \text{ V}$  and  $\mu = 28 \text{ cm}^2 \text{ V}^{-1} \text{ sec}^{-1}$  [103]. The trap concentrations ( $N_{ti}$ ) were calculated using the equation 4.15 as  $1.9 \times 10^{17}$ ,  $2.3 \times 10^{17}$  and  $2.7 \times 10^{17} \text{ cm}^{-3}$ .

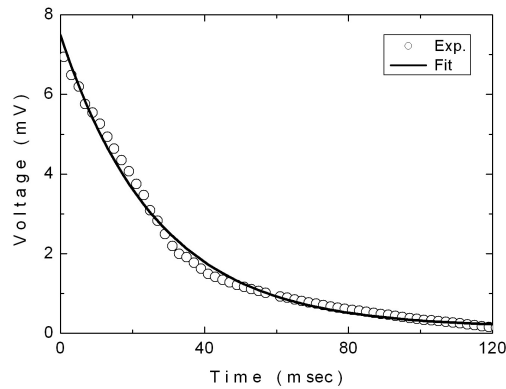


Figure 4.34: The photoconductivity decay curve for the TlInSeS crystals.

## 4.4 Structural, Optical and Electrical Transport Properties of $\text{Tl}_2\text{In}_2\text{SSe}_3$ Layered Crystals

### 4.4.1 Results of X-ray Experiments and Energy Dispersive Spectral Analysis

For  $\text{Tl}_2\text{In}_2\text{SSe}_3$  crystals, the resulting ingot were red in color and the freshly cleaved surfaces were mirror-like. The structure of  $\text{Tl}_2\text{In}_2\text{SSe}_3$  crystal were analyzed by XRD. The Miller indices ( $hkl$ ), the observed and calculated interplanar spacings ( $d$ ) and the relative intensities ( $I/I_0$ ) of the diffraction lines for  $\text{Tl}_2\text{In}_2\text{SSe}_3$  crystal were found. These structural parameters are listed in table 4.5. Figure 4.35 presents the X-ray diffractogram of  $\text{Tl}_2\text{In}_2\text{SSe}_3$  crystal. "DICVOL 04", a least-squares computer program, was used to calculate the lattice parameters of the monoclinic unit cell,  $a = 0.56367$ ,  $b = 0.79060$ ,  $c = 0.70674$  nm, and  $\beta = 92.56^\circ$  [108].

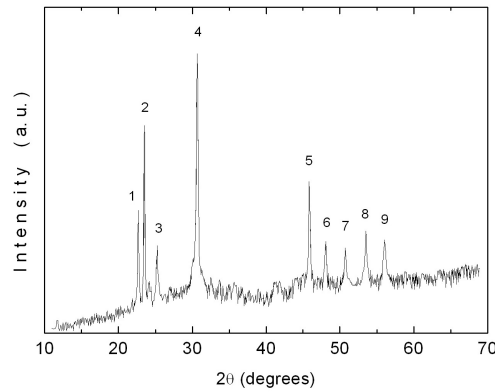


Figure 4.35: X-ray diffraction pattern of  $\text{Tl}_2\text{In}_2\text{SSe}_3$  powder sample.

Table 4.5: X-ray powder diffraction data for  $\text{Tl}_2\text{In}_2\text{SSe}_3$  crystals.

No.	$hkl$	$d_{obs}(\text{nm})$	$d_{calc}(\text{nm})$	$I/I_0$
1	1 1 -1	0.3917	0.3917	42.2
2	1 1 1	0.3786	0.3789	74.5
3	2 0 0	0.3534	0.3534	26.8
4	1 2 1	0.2917	0.2916	100.0
5	0 4 0	0.1978	0.1978	43.4
6	2 2 2	0.1894	0.1893	19.7
7	3 1 -2	0.1800	0.1799	15.6
8	2 3 -2	0.1712	0.1712	20.9
9	2 4 1	0.1639	0.1640	16.1

By the help of EDSA, the chemical composition of  $\text{Tl}_2\text{In}_2\text{SSe}_3$  crystals was determined as

25.7 : 25.9 : 36.2 : 12.2, respectively [108]. The spectrum obtained from EDSA is shown in figure 4.36.

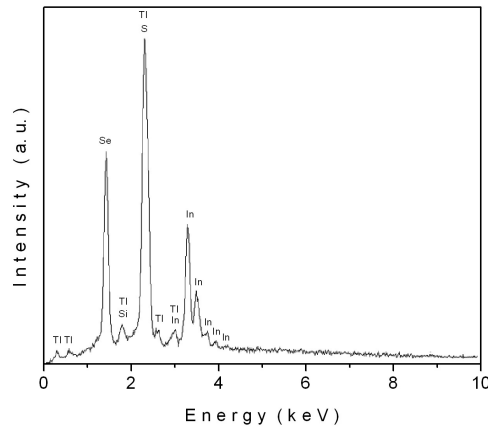


Figure 4.36: Energy dispersive spectroscopic analysis of  $\text{Tl}_2\text{In}_2\text{SSe}_3$  crystal.

#### 4.4.2 Results of Transmission and Reflection Experiments

The transmittance ( $T$ ) and reflectivity ( $R$ ) spectra for  $\text{Tl}_2\text{In}_2\text{SSe}_3$  single crystals were obtained in the wavelength ( $\lambda$ ) range 500-1100 nm (figure 4.37). The absorption coefficient  $\alpha$  and refractive index  $n$  were obtained from the equations 4.1 and 4.2.

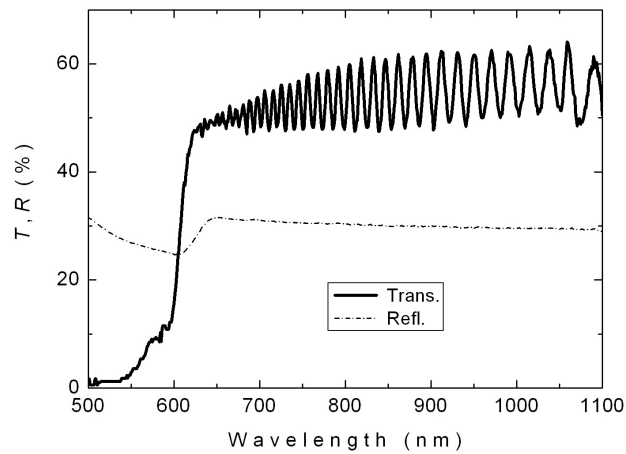


Figure 4.37: The spectral dependence of transmittance and reflectivity for a  $\text{Tl}_2\text{In}_2\text{SSe}_3$  crystal at room temperature.

In the reflection measurements, the samples having thickness such that  $\alpha d \gg 1$  were used whereas in the transmission measurements, the sample thickness was reduced by using transparent tape and determined from transmission interference fringes at wavelength slightly longer than the intrinsic absorption edge, i.e. in a region with relatively high transmission (figure 4.37). Using the the long wavelength value of the refractive index  $n = 3.34$  in the equation 2.21, the thickness of the sample was calculated. Mostly, the sample thickness was of the order of  $10 \mu\text{m}$  [109].

The  $\alpha$  can be represented by the equation 4.3. Figure 4.38 shows the variation of  $\alpha$  from 50 to  $4420 \text{ cm}^{-1}$  with increasing photon energy from 1.80-2.50 eV. From the analysis of the experimental data it was shown that, the absorption coefficient was proportional to  $(h\nu - E_g)^p$  with  $p = 2$  and  $1/2$  for ranges 2.00-2.11 eV and 2.20-2.45 eV, respectively. Insets 1 and 2 of figure 4.38 display the dependencies of  $(\alpha h\nu)^{1/2}$  and  $(\alpha h\nu)^2$  on photon energy  $h\nu$ , respectively. The circles show the experimental data. They were fitted to a linear equation (the solid lines) to find the energy band gaps. The linear dependencies for the relations  $(\alpha h\nu)^{1/2}$  and  $(\alpha h\nu)^2$  versus  $h\nu$  suggests the realization of indirect and direct allowed transitions, respectively. The extrapolations of straight lines, indirect band gap energy  $E_{gi} = 1.96 \pm 0.02 \text{ eV}$  and direct band gaps energy  $E_{gd} = 2.16 \pm 0.02 \text{ eV}$  were calculated, respectively [109]. Indirect and direct inter-band edge transitions can exist for thallium containing layered crystals because of specific features of the prevailing  $p$ -anionic upper valence band and  $s$ -Tl states [90].

Transmission spectra for the  $\text{Tl}_2\text{In}_2\text{SSe}_3$  crystal measured in the temperature range 10-300 K are presented in figure 4.39. The low-temperature measurements were done using thick samples, about  $300 \mu\text{m}$ , as the thin layered samples were very fragile and broke into pieces at low temperatures [109].

As seen from the inset to figure 4.39, the indirect energy gap decreases with increasing temperature, i.e. it shifts from 2.08 to 1.96 eV as the temperature increases from 10 to 300 K. The temperature dependence of the energy band gap can be represented by the relation 4.4. The experimental data for the dependence of  $E_{gi}$  on temperature (10-300 K) were fitted using equation 4.4 as shown in the inset of figure 4.39 (solid line corresponds to the theoretical fit). From the analysis,  $E_{gi}(0) = 2.09 \text{ eV}$ ,  $\gamma = -5.6 \times 10^{-4} \text{ eV K}^{-1}$ , and  $\beta = 130 \text{ K}$  were found [109]. The Debye temperature,  $\beta$ , were estimated using Lindemann's melting rule [91] from the analysis of X-ray results. Melting temperature  $T_m = 1043 \text{ K}$  was used for this calculation

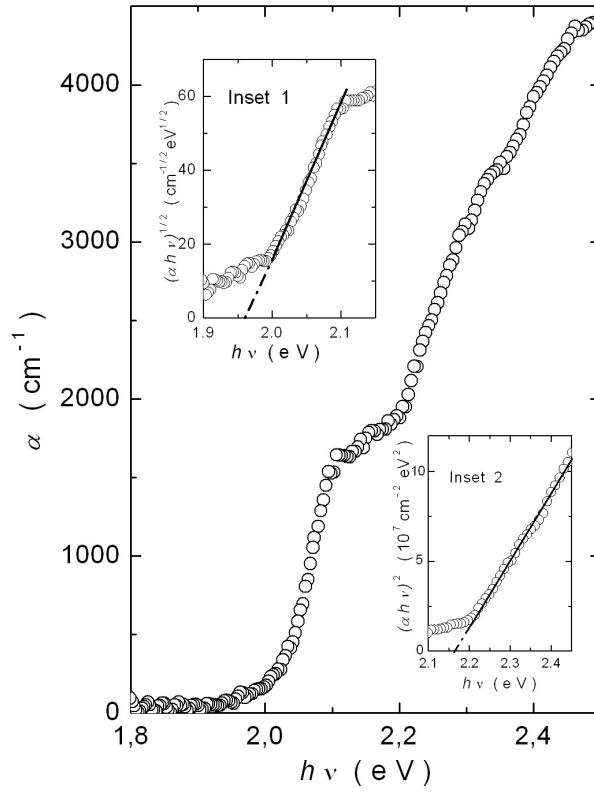


Figure 4.38: The variation of absorption coefficient as a function of photon energy for  $\text{Tl}_2\text{In}_2\text{SSe}_3$  crystal at  $T = 300$  K. Circles represent the experimental data that were fitted to a linear equation (the solid lines) to find the band gaps. Insets 1 and 2 represent the dependencies of  $(\alpha h\nu)^{1/2}$  and  $(\alpha h\nu)^2$  on photon energy, respectively.

and  $\beta = 127$  K was found.

The obtained refractive index  $n$  as a function of wavelength is shown in figure 4.40. The refractive index in the energy region of  $h\nu < E_g$  gradually decreases from 3.56 to 3.34 with increasing wavelength in the region 652-1100 nm. To analyze the data, the single-effective-oscillator model proposed by Wemple and DiDomenico [42, 43] was used. This model could be applied to the ternary  $\text{TlGaSe}_2$  and  $\text{TlGaS}_2$  layered crystals successfully, [92, 93]. There is a relation between the refractive index and photon energy ( see the equation 4.5). Plotting the dependence of  $(n^2 - 1)^{-1}$  on  $(h\nu)^2$  allows the determination of the oscillator parameters by fitting a linear function to the lower energy data range (1.09-1.93 eV). The fitting of the above reported function is presented in inset of figure 4.40. The zero frequency refractive index  $n_0$

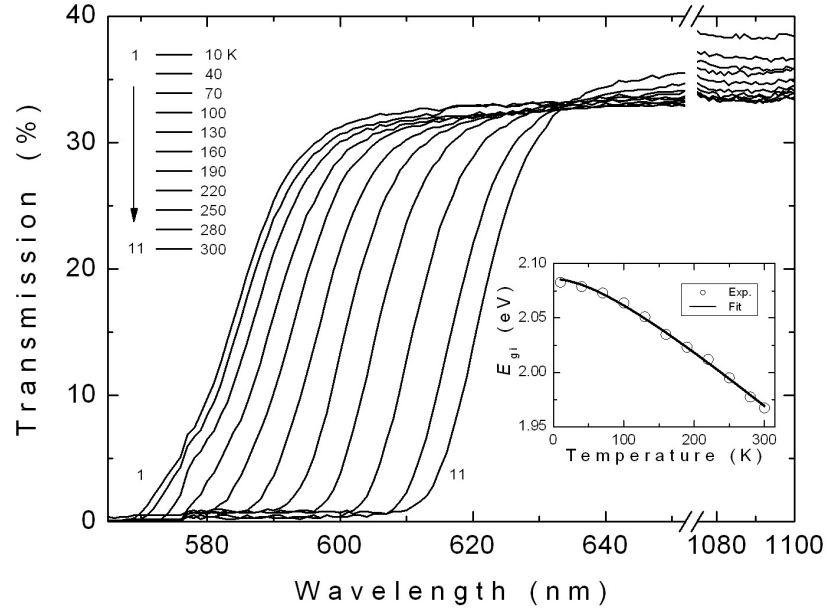


Figure 4.39: The spectral dependence of transmittance for  $\text{Tl}_2\text{In}_2\text{SSe}_3$  crystal in the temperature range of 10-300 K. Inset: The indirect band gap energy as a function of temperature. The solid line represents the fit using equation 4.4.

was estimated from equation 4.5.

The values of the parameters  $E_{so}$  and  $E_d$ , calculated from the slope and the intersection with y-axis of the straight line in inset of figure 4.40, were found to be 4.67 eV and 45.35 eV, respectively. Moreover, the values of zero-frequency dielectric constant  $\epsilon_0 = n_0^2 = 10.71$  and refractive index  $n_0 = 3.27$  were evaluated by means of equation 4.5. The oscillator energy  $E_{so}$  is an "average" energy gap and can be found from the relationship  $E_{so} \approx 2.0 E_{gd}$  where  $E_{gd}$  is the lowest direct band gap [44, 47]. The ratio  $E_{so}/E_{gd}$  was found to be 2.16 [109].

The oscillator strength  $S_{so}$  for  $\text{Tl}_2\text{In}_2\text{SSe}_3$  crystal can be obtained by the help of the refractive index  $n$  analysis using the equations 4.6 and 4.7. The values of  $S_{so}$  and  $\lambda_{so}$ , calculated from the plots of  $(n^2 - 1)^{-1}$  versus  $\lambda^{-2}$ , were found to be  $1.38 \times 10^{14} \text{ m}^{-2}$  ( $212.19 \text{ eV}^2$ ) and  $2.66 \times 10^{-7} \text{ m}$  respectively [109]. The obtained oscillator strength values are in the same order with those obtained for ZnS, ZnSe,  $\text{Ag}_2\text{S}$ ,  $\text{GeSe}_2$  and  $\text{TlGaS}_2$  crystals [43, 46, 93, 94].



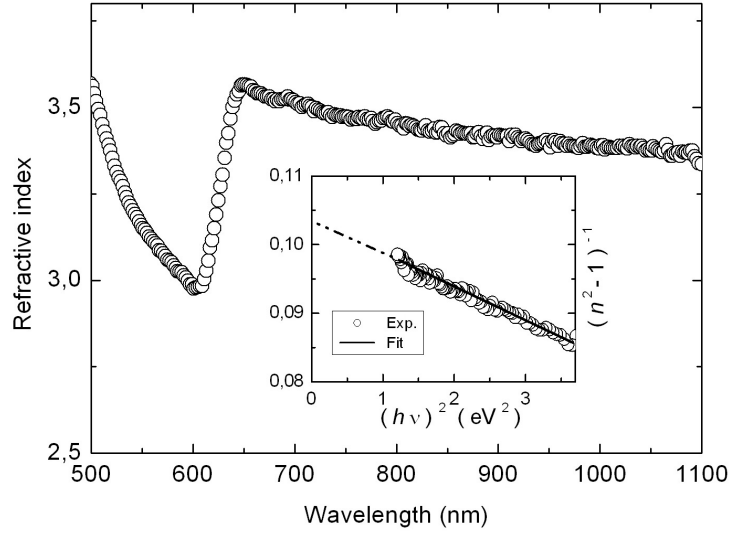


Figure 4.40: The dependence of refractive index on the wavelength for  $\text{Tl}_2\text{In}_2\text{SSe}_3$  crystal. Inset: Plot of  $(n^2 - 1)^{-1}$  versus  $(h\nu)^2$ . The solid line represents the fit using equation 4.5.

#### 4.4.3 Results of Photoluminescence Experiments

Crystals used for PL measurements had dimensions of  $6 \times 3 \times 1 \text{ mm}^3$ . In PL experiments, the sample were illuminated in a direction close to the layer. The temperature was decreased from 300 K to 25 K and it was controlled within an accuracy of  $\pm 0.5 \text{ K}$ . The PL spectra of the sample was analyzed in the wavelength region of 570-700 nm. To adjust the exciting laser intensity from  $2.7$  to  $111.4 \text{ mW cm}^{-2}$ , sets of neutral density filters were used. PL spectra have been corrected for the spectral response of the optical apparatus [108].

Figure 4.41 presents the PL spectra of  $\text{Tl}_2\text{In}_2\text{SSe}_3$  crystals in 25-63 K temperature range at constant laser excitation intensity  $L = 111.4 \text{ mW cm}^{-2}$ . The observed emission band has asymmetric Gaussian line shape and centered at 633 nm (1.96 eV) at  $T = 25 \text{ K}$ . As seen from figure 4.41, emission band changes its peak position, FWHM and intensity as a function of the sample temperature: the peak position shows several degrees of red shift with increasing temperature; the FWHM increases and the peak intensity decreases as temperature is increased. The FWHM rised from 0.11 to 0.14 eV with increasing temperature in the range of 25-63 K [108].

There is a shift in the peak energies towards the lower energies with increasing temperature

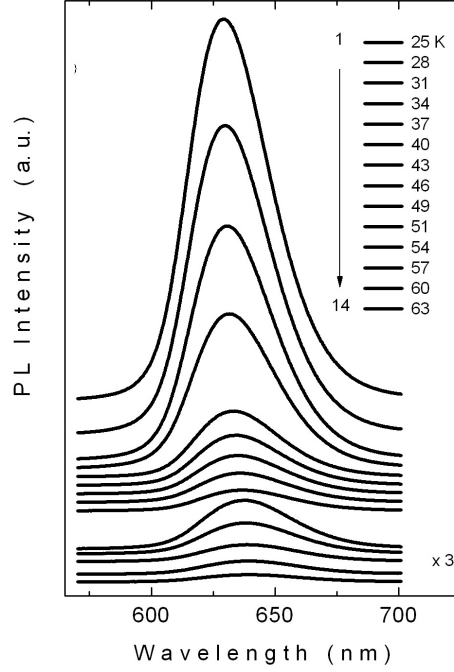


Figure 4.41: Temperature dependence of PL spectra from  $\text{Tl}_2\text{In}_2\text{SSe}_3$  crystal at excitation laser intensity  $L = 111.4 \text{ mW cm}^{-2}$ . Note that for curves 10-14, intensities have been multiplied by a factor of three.

(see the inset of figure 4.42. It is known from the work [49] that when the temperature increases, the donor-acceptor pair transition energy decreases. The experimental data for the temperature dependence of PL bands intensities were fitted by the expression 4.8

Figure 4.42 shows the temperature dependence of the emission band maximum intensity as a function of the reciprocal temperature in the 25-63 K range. The best fit using equation 4.8, demonstrated by the solid curve in figure 4.42, has been achieved with parameters  $I_0 = 242.0$ ,  $E_t = 0.03 \text{ eV}$ ,  $\alpha = 10400$ . Since  $\text{Tl}_2\text{In}_2\text{SSe}_3$  crystal is a n-type semiconductor, as determined by the hot probe technique, it is believed that this level is shallow donor level located at 0.03 eV below the bottom of the conduction band [108]. These shallow levels can be point defects. They were created because of deviations in stoichiometry or uncontrolled impurities. The latter may be attributed to the presence of Si impurities introduced into  $\text{Tl}_2\text{In}_2\text{SSe}_3$  during the crystal growth process in ungraphatized ampoules [95].

The laser excitation intensity dependence of PL spectra is also important to obtain information about the recombination mechanism. The PL spectra at different 19 laser intensities were

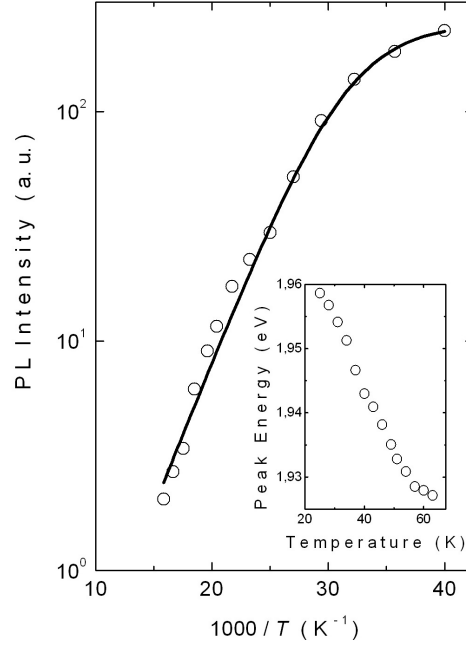


Figure 4.42: Temperature dependences of PL bands intensities for  $\text{Tl}_2\text{In}_2\text{Se}_3\text{S}$  crystal. Circles are the experimental data. Solid curves show the theoretical fits using equation 4.8. The inset: temperature dependences of emission band peak energies

shown in figure 4.43 at  $T = 25$  K. From analysis of the spectra, we obtained the information about the peak energy position and intensity for emission band at different laser excitation intensities. Our analysis reveals that the peak energy position changes with laser excitation intensity (blue shift) [108]. Referring to work [95], it means that there are inhomogeneously distributed donor-acceptor pairs. As obtained from the data analysis, B-band maximum shifts higher energies ( $\Delta E_p = 16$  meV) with increasing excitation laser intensities from 2.7 to 111.4  $\text{mW cm}^{-2}$  (i.e., 10 meV per decade of exciting radiation intensity. The observed blue shift is typical of ternary and quaternary compounds such as  $\text{CdGeAs}_2$  (10-15 meV per decade of intensity of exciting radiation)[96],  $\text{HgInGaS}_4$  (20 meV per decade of intensity of exciting radiation) [97],  $\text{Tl}_2\text{InGaS}_4$  (20 meV per decade of intensity of exciting radiation)[98],  $\text{CuIn}_{1-x}\text{Ga}_x\text{Se}_2$  (15 meV per decade of intensity of exciting radiation) [99].

The dependence of the emission band peak energy ( $E_p$ ) at  $T = 25$  K as a function of excitation laser intensity ( $L$ ) is given in figure 4.44. The experimental data in figure 4.44 were then fitted the expression 4.9. By using a nonlinear least square fit to the experimental data,  $E_\infty$  and  $E_B$  were found as 1.91 eV and 2.04 eV, respectively. These energy values are in good agreement

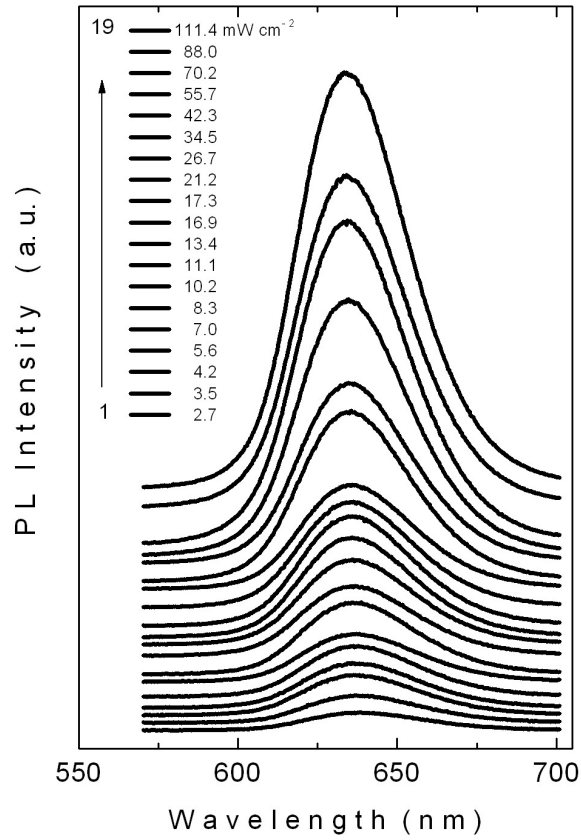


Figure 4.43: PL spectra of  $\text{Tl}_2\text{In}_2\text{SSe}_3$  crystal as a function of excitation laser intensity at  $T = 25$  K.

with the band gap energy ( $E_{gi} = 2.08$  eV) and the observed values of the peak energy position (i.e.,  $E_\infty < 1.94$  eV  $< E_p < 1.96$  eV  $< E_B < E_{gi}$ ) at  $T = 25$  K [108].

In PL spectra of  $\text{Tl}_2\text{In}_2\text{SSe}_3$  crystal, the increase in the peak intensities of the emission band with increase in the laser excitation intensity was also observed. The logarithmic plot of PL intensities versus laser excitation intensities are given in the inset of figure 4.44. Experimental data were fitted by a simple power law that is equation 4.10. Using the equation 4.10, the value of  $\gamma = 0.97$  were found. It is well known from the work [54, 55], laser photon energy must be greater than the band gap energy. If the  $\gamma$  values are between 1 and 2, free- and bound-exciton emission occurs. If the  $\gamma$  values are smaller or equal to 1 free-to-bound and donor-acceptor pair recombination occurs.

As a result of PL spectra analysis with respect to temperature and excitation laser intensity,

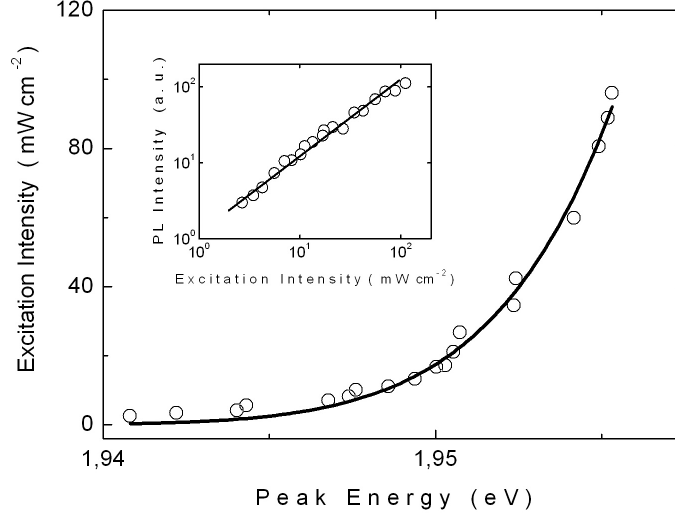


Figure 4.44: Excitation laser intensity versus emission peak energy for  $\text{Tl}_2\text{In}_2\text{SSe}_3$  crystal for B-band at  $T = 22$  K. The solid curve represents the theoretical fit using equation 4.9. Inset: Dependence of PL intensities at the emission maximums versus excitation laser intensity for A- and B-bands at  $T = 22$  K. The solid lines show the theoretical fits using equation 4.10.

there is a possible scheme for the states located in the forbidden energy gap. In the proposed scheme, shallow donor level,  $d$ , is located at 0.03 eV below the bottom of the conduction band. The sum of the donor ( $E_d$ ) and acceptor ( $E_a$ ) levels can be written as [49]:

$$E_d + E_a = E_{gi} - E_{\infty} = 2.08 \text{ eV} - 1.91 \text{ eV} = 0.17 \text{ eV}. \quad (4.19)$$

Considering that the donor level,  $d$ , is located at 0.03 eV below the bottom of the conduction band, this result suggests that the acceptor level,  $a$ , involved in the emission band is located at 0.14 eV above the top of the valence band. Taking into account the above considerations, the observed emission band in the PL spectra has been attributed to the radiative transitions from the donor level,  $d$ , to the acceptor level,  $a$ .

#### 4.4.4 Results of Thermally Stimulated Current Experiments

The TSC measurements were carried out in the temperature range of 10-175 K using a closed cycle helium cryostat. Temperature controller was utilized to provide constant heating rates in the range of 0.4-1.0 K s<sup>-1</sup>. At low temperatures, carriers were excited by a light emitting diode, generating light at a maximum peak of 2.6 eV. Generally, the trap filling was performed by illumination under a bias voltage  $V_1 = 1$  V for about 1300 s at the initial temperature  $T_0 =$

10 K. However for the revealing of traps distribution they were filled at different illumination temperatures ( $T_{0i} = 10, 20, 30, 40, 50$  and  $60$  K). Then the excitation was turned off. The bias voltage  $V_2$  was applied to the sample and the temperature was increased at a constant rate, after an expectation time  $300$  s. The bias voltage  $V_2 = 100$  V could be applied to the sample since the dark current contribution was low in  $\text{Ti}_2\text{In}_2\text{SSe}_3$ . The figure 4.45 shows the illumination and heating parameters of the optimum TSC conditions for  $\text{Ti}_2\text{In}_2\text{SSe}_3$  crystal [110].

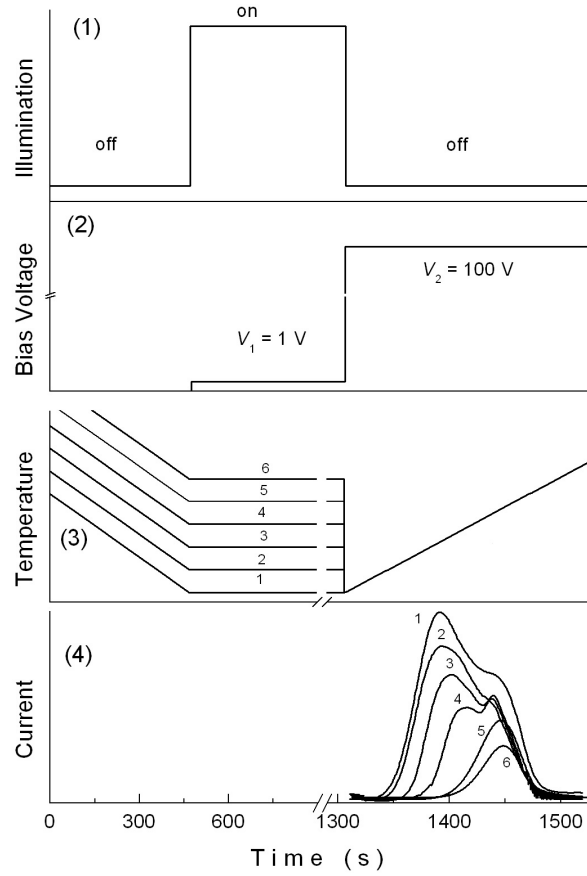


Figure 4.45: Principles of the TSC experiment for  $\text{Ti}_2\text{In}_2\text{Se}_3\text{S}$  crystals; (1) time period of applied illumination; (2) variation of bias voltage; (3) temperature variation with time for four different light illumination temperatures; (4) TSC spectra for four different light illumination temperatures: 10 (1), 20 (2), 30 (3), 40 (4), 50 (5) and 60 K (6).

Figure 4.46 shows the TSC spectra of  $\text{Ti}_2\text{In}_2\text{Se}_3\text{S}$  for two biasing polarities at a constant heating rate  $\beta = 0.8 \text{ K s}^{-1}$  in the temperature range of 10-160 K. Since, the polarity of the illuminated surface is negative, the intensity of the peak is highest. The peak appearing in the TSC spectra of  $\text{Ti}_2\text{In}_2\text{Se}_3\text{S}$  crystal can be considered as electron traps [110].

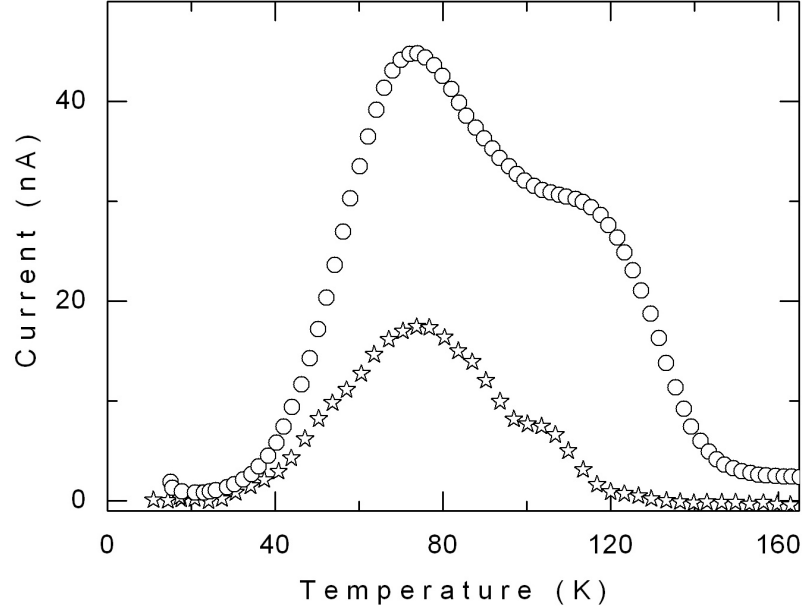


Figure 4.46: Typical experimental TSC curve of  $\text{Tl}_2\text{In}_2\text{SSe}_3$  crystals under bias voltage. Circles and stars show the experimental data obtained when the polarity of illuminated surface was negative and positive, respectively.

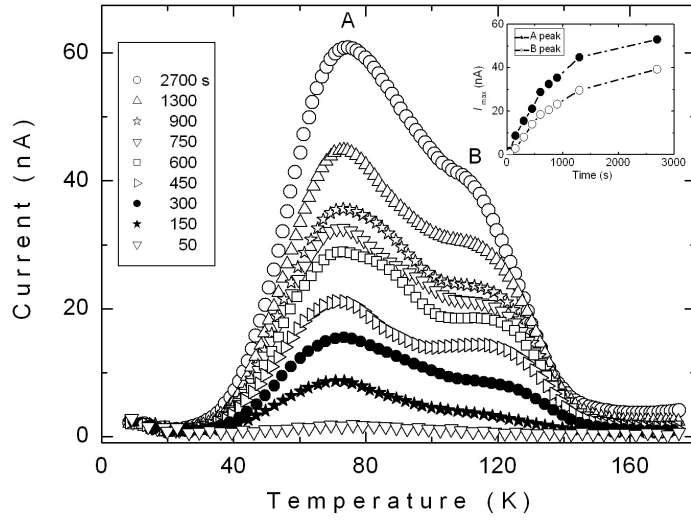


Figure 4.47: TSC spectra of the  $\text{Tl}_2\text{In}_2\text{SSe}_3$  crystals for various illumination times at a constant heating rate of  $\beta = 0.8 \text{ K s}^{-1}$ . Inset: Maximum thermally stimulated currents of A and B peaks as a function of illumination time. The dash-dotted line is only guide for the eye.

Figure 4.47 shows the TSC spectra of  $\text{Tl}_2\text{In}_2\text{SSe}_3$  crystal registered for different illumination time (50-2700 s) at a constant heating rate of  $\beta = 0.8 \text{ K s}^{-1}$ . The plot of the maximum values

of TSC ( $I_{max}$ ) versus illumination time is presented in the inset of figure 4.47. To vary the initial density of filled traps, the illumination time altered and it was observed that there was no change for both the shapes and the peaks positions of A and B peaks in TSC curves. It suggests that the traps may be considered under monomolecular condition. Since the increasing the illumination time from 1300 to 2700 s did not lead to the change for the shapes and the positions of A and B peaks in TSC curves, to decrease the duration of experiment as well as to economize helium gas we carried out the TSC measurements using the illumination time 1300 s [110].

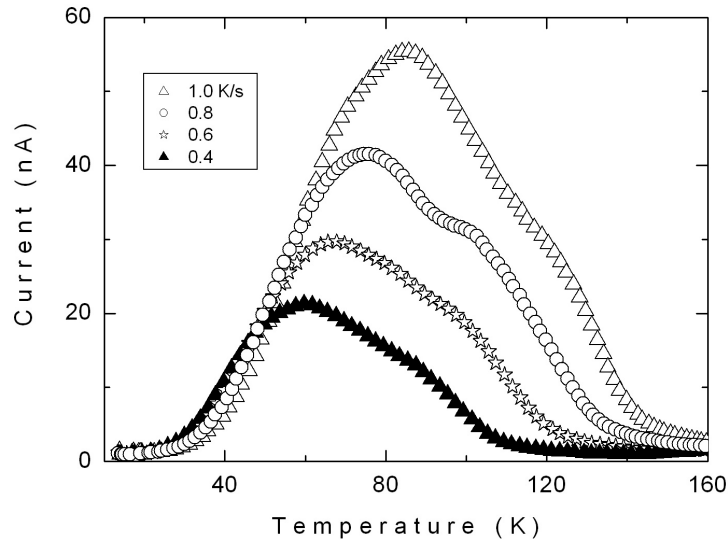


Figure 4.48: The experimental TSC spectra of  $\text{Tl}_2\text{In}_2\text{Se}_3\text{S}$  crystals at different heating rates.

Figure 4.48 presents TSC spectra of the  $\text{Tl}_2\text{In}_2\text{SSe}_3$  crystals measured at four heating rates of  $\beta = 0.4\text{--}1.0 \text{ K s}^{-1}$  with step  $0.2 \text{ K s}^{-1}$  in the temperature range of 10–175 K. As expected, thermally stimulated current gradually increases and maximum current values of A and B peaks shift to higher temperatures with increasing the heating rates [110].

To reveal the traps distribution in  $\text{Tl}_2\text{In}_2\text{SSe}_3$  crystals, the sample was excited by light for 1300 s at different illumination temperatures ( $T_{0i}$ ) ranging from 10 to 60 K. Then the light source was switched off and the sample was cooled down to 10 K. Thereafter, the sample was heated at a constant rate  $\beta = 0.8 \text{ K s}^{-1}$  to excite the trapped electrons to the conduction band. The experimental TSC spectra of  $\text{Tl}_2\text{In}_2\text{SSe}_3$  crystal at different illumination temperatures ( $T_{0i} = 10, 20, 30, 40, 50$ , and 60 K) are shown in figure 4.49 [110]. The intensity of the



TSC spectra decreased and the maximum values of A and B peaks shifted towards higher temperatures with increasing illumination temperatures. This fact supports the validity of a quasi-continuous traps distribution [85], [101], [97], [102].

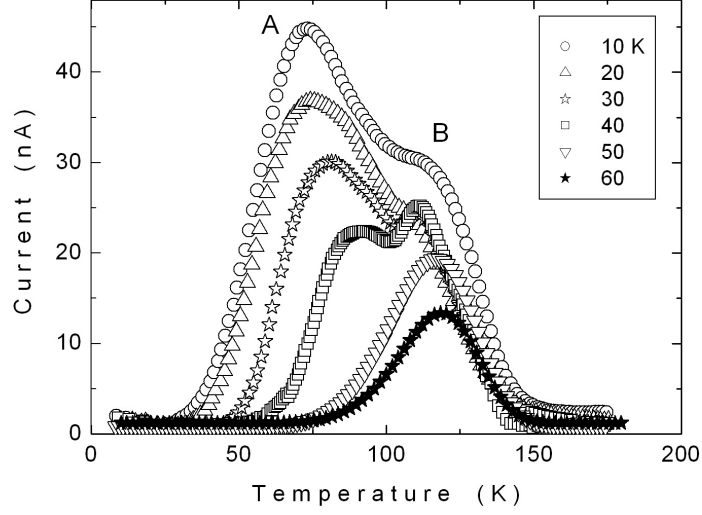


Figure 4.49: The TSC spectra of  $\text{Tl}_2\text{In}_2\text{SSe}_3$  crystals at different illumination temperatures  $T_0$ .

The area enclosed under the curve obtained with illumination at temperature  $T_{0i}$  is proportional to the total number of carriers released from the traps during the heating process. In order to obtain the energetic traps distribution in the studied crystals, the overlapped peaks in the experimental TSC spectra (figure 4.50) were decomposed into separate peaks. The example of the decomposition of TSC curves into two peaks (A and B) for  $T_{0i} = 40$  K was demonstrated in figure 4.50. The total charge released from the traps related to peak A was calculated from the area difference of two successive experimental TSC spectra for the pairs of illumination temperatures  $T_{0i}$  and  $T_{0i+1}$ : 10 and 20 K, 20 and 30 K, 30 and 40 K. The same procedure has been followed for peak B using the pairs of illumination temperatures  $T_{0i}$  and  $T_{0i+1}$ : 30 and 40 K, 40 and 50 K, 50 and 60 K. The maximum temperatures ( $T_{mi}$ ) and areas ( $Q_i$ ) of peaks A and B, evaluated from the subtracted two successive TSC curves related to different pairs of illumination temperatures, are listed in the table 4.6. Since the difference in the current value during heating is due to the trap levels above a certain energy level, the mean activation energy of those traps can be found with the help of the initial rise method. A semi-logarithmic plots of the currents versus  $1/T$  gives the straight lines with the slopes of

$(-E_{ti}/k)$  for A and B peaks as shown in figure 4.51. The mean activation energies of traps calculated for the curves 1, 2 and 3 (A peak) and 4, 5 and 6 (B peak) are presented table 4.6 [110].

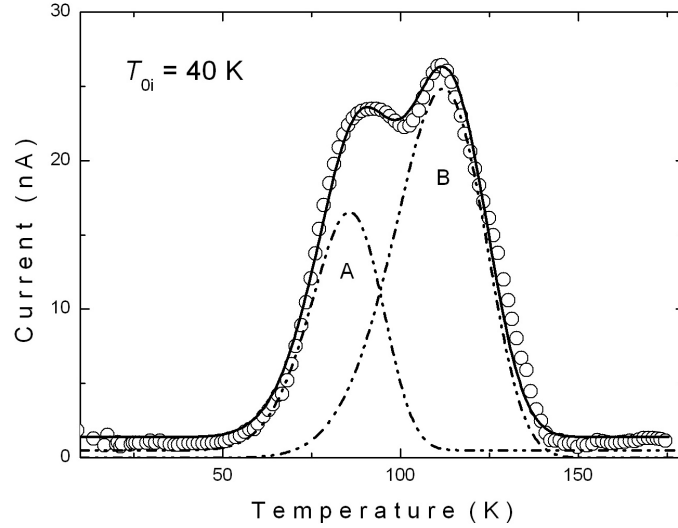


Figure 4.50: Experimental TSC spectrum of  $\text{Tl}_2\text{In}_2\text{SSe}_3$  crystals obtained at illumination temperature  $T_{0i} = 40$  K with a heating rate  $\beta = 0.8$  K  $\text{s}^{-1}$ . Open circles are experimental data. Dash-dotted curves represent the decomposed peaks A and B. Solid curve shows total fit to experimental data.

Inset of figure 4.51 presents the plots of  $\ln Q_i$  (the amount of the released charge during the heating process) as a function of the mean activation energies for peaks A and B. These dependencies are well approximated by the exponent, which suggests the presence of an exponential distribution of the traps. The exponential distribution is consistent with the presence of fluctuations in the crystal potential, caused by structural defects, which give rise to localized states acting as traps for the carriers [101].

The graph  $\ln(Q_i)$  versus mean activation energies of A and B peaks, based on equation 4.12, the value of  $\alpha = 0.076$  meV $^{-1}$ , corresponding to 30 meV/ decade and the value of  $\alpha = 0.039$  meV $^{-1}$ , corresponding to 59 meV/ decade were found, respectively (inset of figure 4.51) [110].

The obtained values of  $E_{ti}$  and  $T_{mi}$  were used to calculate the attempt-to-escape frequencies  $\nu_i$  from the equation 4.13. The capture cross section of the traps was determined using the following equation 4.14. The effective mass  $m_e^* = 0.14 m_o$  [103] was utilized to calculate  $N_c$

Table 4.6: The illumination temperatures of two successive experimental TSC curves ( $T_{0i}$ - $T_{0i+1}$ ); maximum temperature ( $T_{mi}$ ) and area ( $Q_i$ ) of calculated TSC curves ; mean activation energy ( $E_{ti}$ ), capture cross section ( $S_{ti}$ ), attempt-to-escape frequency ( $\nu_i$ ) and concentration ( $N_{ti}$ ) of traps in  $\text{Ti}_2\text{In}_2\text{SSe}_3$  crystal.

$T_{0i} - T_{0i+1}$ (K)	$T_{mi}$ (K)	$Q_i$ ( $\mu$ C)	$E_{ti}$ (meV)	$S_{ti}$ ( $\text{cm}^2$ )	$\nu_i$ ( $\text{s}^{-1}$ )	$N_{ti}$ ( $\text{cm}^{-3}$ )
Peak A						
10-20	54.3	591	11	$1.5 \times 10^{-25}$	0.2	$4.7 \times 10^9$
20-30	60.4	328	20	$9.4 \times 10^{-25}$	1.6	$2.6 \times 10^9$
30-40	71.0	112	33	$4.3 \times 10^{-24}$	9.8	$0.9 \times 10^9$
Peak B						
30-40	92.4	445	35	$5.4 \times 10^{-25}$	2.1	$3.6 \times 10^9$
40-50	107.4	200	57	$3.1 \times 10^{-24}$	16.3	$1.6 \times 10^9$
50-60	112.6	150	62	$3.6 \times 10^{-24}$	20.7	$1.2 \times 10^9$

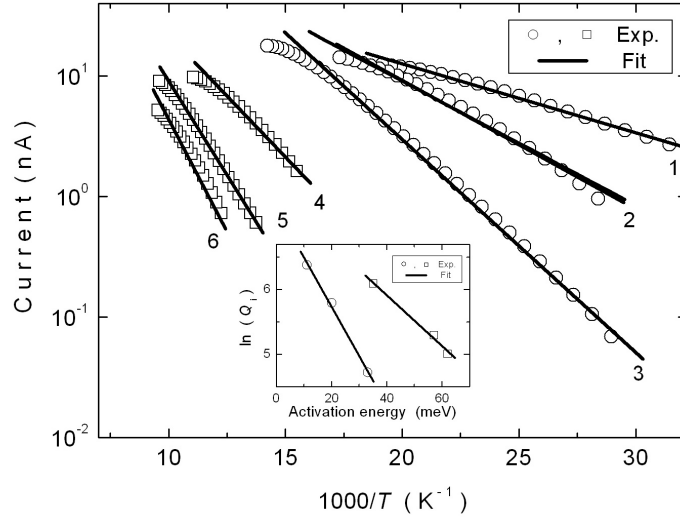


Figure 4.51: Thermally stimulated currents versus  $1000/T$  for the TSC spectra of  $\text{Ti}_2\text{In}_2\text{SSe}_3$  crystals, calculated from the difference of two successive experimental TSC spectra for the selective pairs of temperatures 10-20 K, 20-30 K, 30-40 K for peak A (curves from 1 to 3) and 30-40 K, 40-50 K, 50-60 K for peak B (curves from 4 to 6). Circles and squares show the experimental data for peaks A and B, respectively. Solid lines present the theoretical fits according to the initial rise method. Inset: The logarithmic plots of released charge as a function of activation energy. Circles and squares show the experimental data for peaks A and B, respectively. Solid lines are theoretical fit according to equation 4.12.

and  $\vartheta_{th}$ . Using the latter values, the capture cross section of the traps in  $\text{Ti}_2\text{In}_2\text{SSe}_3$  crystals were estimated (table 4.6). It will be noted that the obtained magnitudes of attempt-to-escape frequency and capture cross section of the traps for all studied crystals are low, which suggests

a strong repulsive barrier to capture the carriers [104].

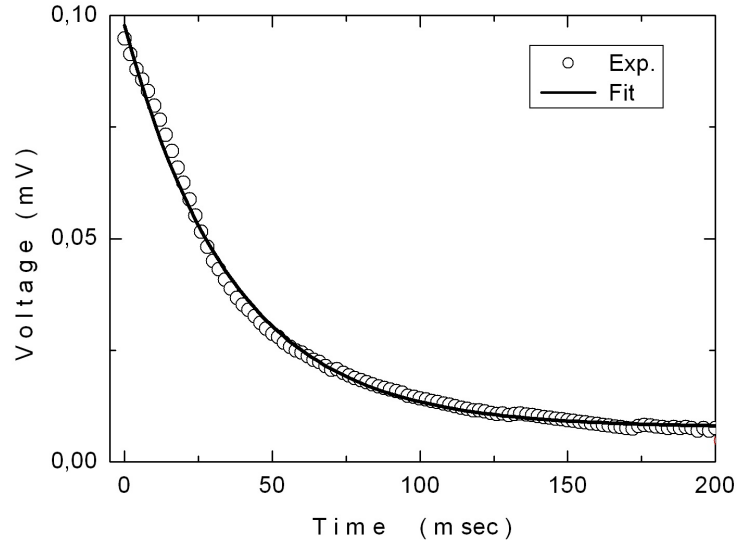


Figure 4.52: The photoconductivity decay curve for the  $\text{Tl}_2\text{In}_2\text{SSe}_3$  crystals.

The concentration of the traps was estimated using the relations 4.15 and 4.16. The theoretical fit (solid line) using equation 4.17 to the experimental data for  $\text{Tl}_2\text{In}_2\text{SSe}_3$  crystals is shown in figure 4.52. From the decay of photocurrent, carrier lifetime was obtained as  $\tau = 36.2$  ms. The corresponding photoconductivity gain was found to be  $G = 4200$  from the equation 4.16 utilizing  $V_2 = 100$  V and  $\mu = 28 \text{ cm}^2 \text{ V}^{-1} \text{ sec}^{-1}$  [103]. The trap concentrations ( $N_{ti}$ ) were calculated using the equation 4.15 as  $4.7 \times 10^9$ ,  $2.6 \times 10^9$  and  $0.9 \times 10^9$  (peak A) and  $3.6 \times 10^9$ ,  $1.6 \times 10^9$  and  $1.2 \times 10^9 \text{ cm}^{-3}$  (peak B) [110].

## CHAPTER 5

### CONCLUSION

The influence of defects on the performance of optoelectronic devices is important. For this reason, in order to obtain the detailed information about defect levels in  $\text{Tl}_2\text{In}_2\text{S}_3\text{Se}$ ,  $\text{TlInSeS}$  and  $\text{Tl}_2\text{In}_2\text{SSe}_3$  crystals, PL and TSC measurements were carried out. Moreover, to reveal the structural and optical properties of crystals, XRD, EDSA, transmission and reflection experiments were performed. These experiments made it possible to characterize the studied crystals.

Lattice parameters and atomic composition of  $\text{Tl}_2\text{In}_2\text{S}_3\text{Se}$ ,  $\text{TlInSeS}$  and  $\text{Tl}_2\text{In}_2\text{SSe}_3$  crystals were determined from XRD and EDSA experiments, respectively. After the analysis of XRD experiment results, it was obtained that all these crystals belong to monoclinic crystal system.

Optical properties of  $\text{Tl}_2\text{In}_2\text{S}_3\text{Se}$ ,  $\text{TlInSeS}$  and  $\text{Tl}_2\text{In}_2\text{SSe}_3$  crystals were investigated by means of transmission, reflection and PL measurements. For  $\text{Tl}_2\text{In}_2\text{S}_3\text{Se}$  crystals, the analysis of the room temperature absorption data revealed the coexistence of indirect and direct transitions with energy band gaps of 2.16 and 2.42 eV, respectively. The refractive index dispersion data were analyzed using the Wemple-DiDomenico single-effective-oscillator model. As a result, the oscillator energy, dispersion energy, oscillator strength, oscillator wavelength and zero-frequency refractive index were found. Temperature-dependent transmission measurements allow to find the rate of change of the indirect band gap with temperature, absolute zero value of the band gap energy and Debye temperature as  $-6.1 \times 10^{-4} \text{ eV K}^{-1}$ , 2.28 eV and 135 K, respectively. The Debye temperature was also estimated by using Lindemann's melting rule and found to be 142 K.

The optical indirect transitions with a band gap energy of 2.05 eV and direct transitions with a band gap energy of 2.21 eV were determined from the analysis of absorption data at room tem-

perature for  $\text{TlInSeS}$  crystals. The refractive index dispersion parameters - oscillator energy, dispersion energy, oscillator strength, oscillator wavelength and zero-frequency refractive index were found. The rate of change of the indirect band gap with temperature ( $-4.7 \times 10^{-4} \text{ eV K}^{-1}$ ), absolute zero value of the band gap energy (2.15 eV) and Debye temperature (130 K) were found as a result of analysis of the temperature-dependent transmission measurements. The Debye temperature 141 K was also obtained using Lindemann's melting rule.

The analysis of the absorption data revealed the presence of both optical indirect and direct transitions for  $\text{Tl}_2\text{In}_2\text{SSe}_3$  crystals with energy band gaps of 1.96 eV and 2.16 eV, respectively. The refractive index dispersion parameters - oscillator energy, dispersion energy, oscillator strength, oscillator wavelength and zero-frequency refractive index were determined. As a result of temperature-dependent transmission measurements, the rate of change of the indirect band gap with temperature, absolute zero value of the band gap energy and Debye temperature were found to be  $-5.6 \times 10^{-4} \text{ eV K}^{-1}$ , 2.09 eV and 130 K, respectively. The Debye temperature was also obtained from the Lindemann's melting rule as 127 K.

From the analysis of the transmission and reflection measurements, it was established that changing the chemical composition parameter  $x$  in the formula  $\text{TlInS}_x\text{Se}_{2-x}$  from 1.5 to 0.5 causes decrease in indirect and direct band gaps energies and increase in the magnitudes of zero-frequency refractive indexes. In other words, when S atoms are replaced by Se atoms, there is a decrease in the values of indirect and direct band gaps energies and an increase in the magnitudes of zero-frequency refractive index. As a result of temperature-dependent transmission measurements, Debye temperatures were calculated. The obtained values were compared with those found from Lindemann's melting rule, using X-ray results, and it was achieved that they were all in agreement with each other.

PL measurements were carried out to obtain the detailed information about defect levels of  $\text{Tl}_2\text{In}_2\text{S}_3\text{Se}$  and  $\text{Tl}_2\text{In}_2\text{SSe}_3$  crystals. For  $\text{Tl}_2\text{In}_2\text{S}_3\text{Se}$  crystals two emission bands centered at 564 nm (A- band) and 642 nm (B- band) were observed at  $T = 22 \text{ K}$ . The behavior of both bands were investigated as a function of excitation laser intensity ( $16\text{-}516 \text{ mW cm}^{-2}$ ) and temperature (22-58 K) in the wavelength range of 535-725 nm. The variation of the spectra with laser excitation intensity and temperature suggest that the transitions between donor and acceptor levels can be responsible for the observed emission bands. Also, the intensity of emission band increases sublinearly with respect to the excitation laser intensity

and confirms that the observed emission bands in  $\text{Ti}_2\text{In}_2\text{S}_3\text{Se}$  are due to the donor-acceptor pair recombination. Radiative transitions from shallow donor levels located at 0.02 and 0.01 eV below the bottom of the conduction band to acceptor levels located at 0.05 and 0.44 eV above the top of the valence band are suggested to be responsible for the observed A- and B-bands in the PL spectra, respectively.

PL experiments were carried out in the temperature range of 25-63 K and laser excitation range of 2.7-111.4  $\text{mW cm}^{-2}$  in the wavelength region of 570-700 nm for  $\text{Ti}_2\text{In}_2\text{SSe}_3$  crystals. A broad PL band centered at 633 nm was observed at  $T = 25$  K. Radiative transitions from shallow donor level located at 0.03 eV below the bottom of the conduction band to acceptor levels located at 0.14 eV above the top of the valence band are suggested to be responsible for the observed band in the PL spectra. From the analysis of temperature-dependent PL spectra, peak positions shows several degrees of red shift with increasing temperature. From the analysis of peak energy position and intensity for emission band at different laser excitation intensities it was established that the behavior of the band is in agreement with the idea of inhomogeneously distributed donor-acceptor pairs for which increasing laser excitation intensity leads to blue shift of the band by exciting more pairs that are closely spaced. The emission band maximum slightly shifts towards higher energies with increasing laser intensities from 2.7 to 111.4  $\text{mW cm}^{-2}$ .

As a consequence of PL experiments, the donor levels were obtained as 0.02 eV (A- band), 0.01 eV (B- band) for  $\text{Ti}_2\text{In}_2\text{S}_3\text{Se}$  and 0.03 eV for  $\text{Ti}_2\text{In}_2\text{SSe}_3$  crystals. The donor states are thought to originate from uncontrolled impurities or point defects created during crystal growth since the studied crystals were not initially doped. Comparing the obtained activation energies with that of  $\text{TiInSeS}$  crystals (0.023 eV) [91], it is possible to observe that these energies were increased with increasing of Se atoms content.

TSC measurements were carried out to obtain information about electrical transport properties of  $\text{Ti}_2\text{In}_2\text{S}_3\text{Se}$ ,  $\text{TiInSeS}$  and  $\text{Ti}_2\text{In}_2\text{SSe}_3$  crystals. For  $\text{Ti}_2\text{In}_2\text{S}_3\text{Se}$  crystals, TSC were studied in the temperature range of 10-170 K. In order to obtain the energetic traps distribution in the crystals the peak was calculated from the area difference of two successive experimental TSC spectra for the pairs of illumination temperatures  $T_{0i}$  and  $T_{0i+1}$ : 20 and 30 K, 30 and 37 K, 37 and 40 K and mean activation energies of traps calculated for curves were found 30, 39 and 55 meV, respectively. The value of 25 meV/decade was obtained for exponential traps

distribution. It was concluded that slow retrapping (monomolecular condition) occurs for the traps in  $\text{Tl}_2\text{In}_2\text{S}_3\text{Se}$  crystals. Attempt-to-escape frequency, concentration and capture cross section of the traps were determined. From the PC experiment, carrier lifetime was obtained as  $\tau = 13.6$  ms.

TSC measurements were carried out on  $\text{TlInSeS}$  layered single crystals in the temperature range of 10-180 K. The electronic traps distributions have been analyzed by the different light illumination temperature technique ( $T_{0i} = 30, 45, 52$  and  $57$  K). Mean activation energies of traps evaluated for curves obtained from the area difference of two successive experimental TSC spectra for the pairs of illumination temperatures 30 and 45 K, 45 and 52 K, 52 and 57 K were found 28, 47 and 67 meV, respectively. The variation of one order of magnitude in the trap density for every 79 meV was estimated. It was revealed that slow retrapping (monomolecular condition) occurs for the traps in  $\text{TlInSeS}$  crystals. Attempt-to-escape frequency, concentration and capture cross section of the traps were determined. The mean activation energy  $E_t$  was obtained as 25 meV from the analysis of TSC experiments using the isothermal decay method. As a result of PC measurements, carrier lifetime was obtained as  $\tau = 26.8$  ms.

$\text{Tl}_2\text{In}_2\text{SSe}_3$  layered single crystals have been studied in the temperature range of 10-175 K using the TSC technique. The TSC spectra demonstrated the presence of overlapped peaks, which were decomposed into two separate peaks (A and B). The analysis of experimental TSC curves registered at different light illumination temperatures (10, 20, 30, 40, 50 and 60 K) revealed the exponential distribution of the traps in the studied crystals. Mean activation energies of traps calculated for curves calculated from the area difference of two successive experimental TSC spectra for the pairs of illumination temperatures 10 and 20 K, 20 and 30 K, 30 and 40 K for peak A and 30 and 40 K, 40 and 50 K, 50 and 60 K for peak B were found 11, 20, 33 meV and 35, 57, 62 meV, respectively. The variations of one order of magnitude in the traps' density for every 30 meV (A peak) and 59 meV (B peak) were estimated. It was reestablished that slow retrapping occurs for the traps in  $\text{Tl}_2\text{In}_2\text{SSe}_3$  crystals. In addition, attempt-to-escape frequency, concentration and capture cross section of the traps were determined for peaks A and B. From the analysis of PC measurements, carrier lifetime was obtained as  $\tau = 36.2$  ms.

Summarizing the above mentioned results of TSC measurements, it was revealed that the



$\text{Tl}_2\text{In}_2\text{SSe}_3$ ,  $\text{Tl}_2\text{In}_2\text{S}_3\text{Se}$  and  $\text{TlInSSe}$  crystals exhibit an exponential distribution of traps. It was observed that when Se atoms are replaced by S atoms there was an increase in the carrier life times. Moreover, slow retrapping was realized for  $\text{Tl}_2\text{In}_2\text{SSe}_3$ ,  $\text{Tl}_2\text{In}_2\text{S}_3\text{Se}$  and  $\text{TlInSSe}$  crystals.

## REFERENCES

- [1] J. Singh, Optical Properties of Condensed Matter and Applications, Wiley John and Sons (2006).
- [2] A. M. Panich, J. Phys.: Condens. Matter 20, 293202 (2008).
- [3] K. R. Allakhverdiev, T. G. Mamedov, B. G. Akinoglu and S. Ellialtioglu, Turkish J. Phys. 18, 1 (1994).
- [4] Y. Shim, W. Okada, K. Wakita and N. Mamedov, J. Appl. Phys. 102, 083537 (2007).
- [5] Y. Rud, V. Rud, S. Iida, M. Morohashi-Yamazaki, H. Uchiki and N. Mamedov, Inst. Phys. Conf. Series 152, 967 (1998).
- [6] M. P. Halias, A. N. Anagnostopoulos, K. Kambas and J. Spyridelis, Phys. B 160, 154 (1989).
- [7] M. K. Rabinal, S. S. K. Titus, S. Asokan, E. S. R. Gopal, M. D. Godzhaev and N. T. Mamedov, Phys. Stat. Sol. (b) 178, 403 (1993).
- [8] K. R. Allakhverdiev, T. G. Mamedov, E. Y. Salaev and I. K. Efendieva, Phys. Stat. Sol. (b) 113, K43 (1982).
- [9] K. R. Allakhverdiev, Solid State Commun. 111, 253 (1999).
- [10] K. A. Yee and A. Albright, J. Am. Chem. Soc. 113, 6474 (1991).
- [11] H. Hahn and B. Wellmann, Naturwissenschaften 54, 42 (1967).
- [12] D. Muller, F. E. Poltmann and H. Hahn, Z. Naturf. B 29, 117 (1974).
- [13] K. J. Range, G. Engert, W. Muller and A. Weiss, Z. Naturf. B 29, 181 (1974).
- [14] N. Kalkan, D. Papadopoulos, A. N. Anagnostopoulos and J. Spyridelis, Mat. Res. Bull. 28, 693 (1993).
- [15] M. P. Halias, A. N. Anagnostopoulos, K. Kambas and J. Spyridelis, Mat. Res. Bull. 27, 25 (1992).
- [16] A. F. Qasrawi and N. M. Gasanly, Cryst. Res. Technol. 39, 439 (2004).
- [17] J. A. Kalominos and A. N. Anagnostopoulos, Phys. Rev. B 50, 7488 (1994).
- [18] K. R. Allakhverdiev, T. G. Mamadov, R. A. Suleymanov and N. Z. Gasanov, J. Phys.: Condens. Matter 5, 1291 (2003).
- [19] T. D. Ibragimov and I. I. Aslanov, Solid State Commun. 123, 329 (2002).
- [20] N. Kalkan, M. P. Halias and A. N. Anagnostopoulos, Mat. Res. Bull. 27, 1329 (1992).

- [21] G. D. Guseinov, E. Mooser, E. M. Kerimova, R. S. Gamidov, I. V. Alekseev and M. Z. Ismailov, *Phys. Stat. Sol.* 34, 33 (1969).
- [22] M. Ya. Bakirov, N. M. Zeinalov, S. G. Abdulayeva, V. A. Gajiyev and E. M. Gojayev, *Solid State Commun.* 44, 205 (1982).
- [23] G. A. Gamal, *Semicond. Sci. Technol.* 13, 185 (1998).
- [24] A. Aydinli, N. M. Gasanly, I. Yilmaz and A. Serpenguzel, *Semicond. Sci. Technol.* 14, 599 (1999).
- [25] S. Ozdemir, R. A. Suleymanov, E. Civan and T. Firat, *Solid State Commun.* 98, 385 (1996).
- [26] N. S. Yuksek, N. M. Gasanly, H. Ozkan and O. Karci, *Acta Phys. Polonica A* 106, 95 (2004).
- [27] M. Isik, K. Goksen, N. M. Gasanly and H. Ozkan, *J. Korean Phys. Soc.* 52, 2 (2008).
- [28] M. Isik, N. M. Gasanly and H. Ozkan, *Acta Phys. Polonica A* 115, 3 (2009).
- [29] A. A. Ketelaar, W. H. t'Hart, M. Moerel and D. Porter, *Z. Kristallogr.* 101, 396 (1939).
- [30] D. Muller and H. Hahn. *Z. Anorg. Allg. Chem.* 438, 258 (1978).
- [31] C. Kittel, *Introduction to Solid State Physics*, John Wiley and Sons (2005).
- [32] S. W. S. McKeever, *Thermoluminescence of Solids*, Cambridge University Press (1985).
- [33] <http://nedwww.ipac.caltech.edu/level5/Sept03/Li/Li4.html> (2010).
- [34] R. J. D. Tilley, *Defects in Solids*, John Wiley and Sons (2008).
- [35] W. L. Bragg, *Proc. Royal Soc. London, Series A* 17, 43 (1913).
- [36] B. D. Cullity, *Elements of X-ray Diffraction*, Addison-Werley Publishing Company (1978).
- [37] H. P. Klug and L. E. Alexander, *X-ray Diffraction Procedures*, John Wiley and Sons (1974).
- [38] [www.tf.uni-kiel.de](http://www.tf.uni-kiel.de) (2010).
- [39] S. M. Sze, *Physics of Semiconductor Devices*, John Wiley and Sons, New York (1981).
- [40] T. S. Moss, G. J. Burrell and B. Ellis, *Semiconductor Opto-Electronics*, John Wiley and Sons, New York (1973).
- [41] J. I. Pankove, *Optical Processes in Semiconductors*, Prentice Hall, New Jersey (1971).
- [42] S. H. Wemple and M. DiDomenico, *Phys. Rev. B* 3, 1338 (1971).
- [43] S. H. Wemple and M. DiDomenico, *Phys. Rev. Lett.* 23, 1156 (1969).
- [44] K. Tanaka, *Thin Solid Films* 66, 271 (1980).
- [45] F. Yakuphanoglu, A. Cukurovali and I. Yilmaz, *Physica B* 351, 53 (2004); *Physica B* 353, 210 (2004).

- [46] E. Marguez, P. Nagels, J. M. Gonzalez-Leal, A. M. Bernal-Oliva, E. Sleetx, and R. Callaerts, *Vacuum* 52, 55 (1999).
- [47] E. Marquez, A. M. Bernal-Oliva, J. M. Gonzalez-Leal, R. Prieto-Alcon, A. Ledesma, R. Jimenez-Garay and I. Martil, *Mater. Chem. Phys.* 60, 231 (1999).
- [48] A. K. Walton and T. S. Moss, *Proc. Phys. Soc.* 81, 509 (1963).
- [49] P. Y. Yu and M. Cardona, *Fundamentals of Semiconductors*, Springer, Berlin (1995).
- [50] T. Taguchi, J. Shirafuji and Y. Inuishi, *Phys. Stat. Sol. (b)* 68, 727 (1975).
- [51] D. E. Cooper, J. Bejaj and P. R. Newmann, *J. Cryst. Growth* 86, 544 (1988).
- [52] Z. C. Feng, A. Mascarenhas and W. J. Choyke, *J. Lumin.* 35, 329 (1986).
- [53] Q. Kim and D. W. Langer, *Phys. Stat. Sol. (b)*, 122, 263 (1984).
- [54] A. Bauknecht, S. Siebentritt, J. Albert and M. Ch. Lux-Steiner, *J. Appl. Phys.* 89, 4391 (2001).
- [55] T. Schmidt, K. Lischka and W. Zulehner, *Phys. Rev. B* 45, 8989 (1992).
- [56] E. Zacks and A. Halperin, *Phys. Rev. B* 6, 3072 (1972).
- [57] D. G. Thomas, J. J. Hopfield and W. M. Augustiniak, *Phys. Rev. A* 140, 202 (1965).
- [58] P. J. Dean and Lyle Patrick, *Phys. Rev. B* 2, 1888 (1970).
- [59] M. Lax, *J. Phys. Chem. Solids* 8, 66 (1959).
- [60] C. C. Klick and J. H. Schulman, *Solid State Physics*, Academic, New York (1957).
- [61] P. Lautenschlager, P. B. Allen and M. Cardona, *Phys. Rev. B* 31, 2163 (1985).
- [62] Y. P. Varshni, *Physica* 34, 149 (1967).
- [63] C. J. Hwang, *Phys. Rev.* 180, 827 (1969).
- [64] R. Chen, S.W.S. McKeever, *Theory of Thermoluminescence and Related Phenomena*, Word Scientific, Singapore (1997).
- [65] G. Kitis, R. Chen and V. Pagonis, *Phys. Stat. Sol. (a)* 205, 1181 (2008).
- [66] E. Borch, M. Bruzzi, S. Pirollo and S. Sciortino, *J. Phys. D: Appl. Phys.* 31, L93 (1998).
- [67] V. M. Skorikov, V.I. Chmyrev, V.V. Zuev and E.V. Larina, *Inorg. Mater.* 38, 751 (2002).
- [68] Z. Q. Fang, B. Claflin and D.C. Look, *J. Appl. Phys.* 103, 073714 (2008).
- [69] J. M. Wrobel, A. Gubanski, E. Placzek-Popko, J. Rezmer and P. Becla, *J. Appl. Phys.* 103, 063720 (2008).
- [70] J. Schafferhans, A. Baumann, C. Deibel and V. Dyakonov, *Appl. Phys. Lett.* 93, 093303 (2008).
- [71] R. Schmechel and H. Seggern, *Phys. Stat. Sol. (a)* 201, 1215 (2004).

- [72] J. T. Randall and M. H. F. Wilkins, Proc. Roy. Soc. A 184, 366 (1945).
- [73] J. T. Randall and M. H. F. Wilkins, Proc. Roy. Soc. A 184, 390 (1945).
- [74] G. F. J. Garlick and A. F. Gibson, Proc. Phys. Soc. 60, 574 (1948).
- [75] B. S. Acharya and M. L. Mukherje, Phys. Stat. Sol (a), 53, 373 (1979).
- [76] D. F. Mariani, G. Gonzales, J. Vignolo, M. Jimenez de Castro and I. Ibama, Phys. Stat. Sol. (a) 112, K53 (1989).
- [77] E. I. Adirovitch, Phys. Rev. 17, 705 (1956).
- [78] R. Chen and Y. Kirsh, Analysis of Thermally Stimulated Processes, Pergamon Press, Oxford (1981).
- [79] A. Halperin and A. A. Braner, Phys. Rev. 117, 408 (1960).
- [80] G. A. Dussel and R. H. Bube, Phys. Rev. 155, 764 (1967).
- [81] I. J. Saunders, J. Phys. C: Solid. St. Phys. 2, 2181 (1969).
- [82] D. De Muer, Physica 48, 1 (1970).
- [83] P. Kelly and P. Bräunlich, Phys. Rev. B 1, 1587 (1970).
- [84] A. Serpi and P. Serpi Macciotta, J. Luminescence 6, 361 (1972).
- [85] A. Serpi, J. Phys. D: Appl. 9 , 1881 (1976).
- [86] C. Manfredotti, R. Murri, Q. Quirini and L. Vasanelli, Phys. Stat. Sol. (a) 38, 685 (1976).
- [87] R. Bube, Photoelectronic Properties of Semiconductors, Cambridge University Press, Cambridge (1992).
- [88] T. Pisarkiewicz, Opto-Electron. Rev. 12, 33 (2004).
- [89] N. M. Gasanly, I. Guler and K. Goksen, Cryst. Res. Technol. 42, 6 621 (2007).
- [90] M. I. Kolinko, I. V. Kityk and A. S. Krochuk, J. Phys. Chem. Sol. 53, 1315 (1992).
- [91] N. M. Gasanly, A. Aydinli and N. S. Yuksek, J. Phys.: Condens. Matter 14, 13685 (2002).
- [92] M. M. El-Nahass, M. M. Sallam, S. A. Rahman and E. M. Ibrahim, Solid State Sci. 8, 488 (2006).
- [93] A. F. Qasrawi and N. M. Gasanly, Phys. Stat. Sol. (a) 202, 2501 (2005).
- [94] M. M. El-Nahass, A. M. M. Farag, E. M. Ibrahim and S. A. Rahman, Vacuum 72, 453 (2004).
- [95] I. Guler, K. Goksen and N. M. Gasanly, Acta Physica Polonica A, 110, 6 823 (2006).
- [96] L. Bai, P. G. Schunemann, T. M. Polak and N. C. Giles, Opt. Mater. 26, 501 (2004).
- [97] A. Anedda, M. B. Casu, A. Serpi, I. I. Burlakov, I. M. Tiginyanu and V.V. Ursaki, J. Phys. Chem. Sol. 58, 325 (1997).

- [98] N. M. Gasanly, A. Serpenguzel, O. Gurlu, A. Aydinli and I. Yilmaz, Solid State Commun. 108, 525 (1998).
- [99] R. Bacewicz, A. Dzierzega and R. Trykozko, Jpn. J. Appl. Phys. 32, Suppl. 3, 194 (1993).
- [100] I. Guler and N. M. Gasanly, Physica B. 404, 2034 (2009).
- [101] A. Bosacchi, B. Bosacchi, S. Franchia and L. Hernandez, Solid State Commun. 13 1805 (1973).
- [102] P. C. Ricci, A. Anedda, R. Corpino, I. M. Tiginyanu and V. V. Ursaki, J. Phys. Chem. Sol. 64 1941 (2003).
- [103] A. F. Qasrawi and N.M. Gasanly, Cryst. Res. Technol. 41, 174 (2006).
- [104] D. C. Look, Z. Q. Fang, W. Kim, O. Aktas, A. Botchkarev, A. Salvador and H. Morkoc, Appl. Phys. Lett. 63, 3775 (1996).
- [105] C. Manfredotti, R. Murri, Q. Quirini and L. Vasanelli, Phys. Stat. Sol. (a) 38, 685 (1976).
- [106] N. M. Gasanly and I. Guler, Int J Mod Phys B. 22, 22 3931 (2008).
- [107] I. Guler and N. M. Gasanly, Journal of Alloys and Compounds, 485, 41 (2009).
- [108] I. Guler, K. Goksen, N. M. Gasanly and R. Turan, Physica B, 395, 116 (2007).
- [109] İ. Guler and N. M. Gasanly, Philosophical Magazine, 90, 13, 1799 (2010).
- [110] I. Guler and N. M. Gasanly, Solid State Communications, 150 176 (2010).

## CURRICULUM VITAE

Surname, Name: Güler, İpek

Date of birth and place : 25.08.1980 , Ankara

Nationality : Turkish

E-mail: ikocer@metu.edu.tr

### EDUCATION:

2008 Researcher in Physics Department, Bari University, Italy

2003 - present Ph. D in Physics Department, METU

2002 - 2003 M. Sc in Physics Education, Ankara University

2001 Trainee, Ankara Nuclear Research and Education Center, Ankara.

1998 - 2002 B. Sc in Physics, Ankara University

### EMPLOYMENT:

2003- present Research Asistant in Physics depatment at METU

### PUBLICATIONS:

1. **I. Güler**, K. Goksen and N. M. Gasanly ” Excitation and Temperature Tuned Photoluminescence in  $\text{Ti}_2\text{In}_2\text{S}_3\text{Se}$  Layered Crystals ” Acta Physica Polonica A, Vol. 110, 823-831 2006
2. **I. Güler**, N. M. Gasanly ” Optical Properties of  $\text{TiGaSeS}$  Layered Single Crystals ” Journal of Korean Physical Society, Vol. 51, No.6, 2031-2035 2007
3. **I. Güler**, K. Goksen, N. M. Gasanly and R. Turan. ”Low-Temperature Visible Photoluminescence and Optical Absorption in  $\text{Ti}_2\text{In}_2\text{Se}_3\text{S}$  Semiconductor ” Physica B, Vol. 395,

116-120 2007

4. N. M. Gasanly, **I. Guler**, and K. Goksen. " Specific features of the optical spectra in  $\text{Ti}_2\text{In}_2\text{S}_3\text{Se}$  layered single crystals " Crystal Research Technology, Vol. 42, 621-625 2007
5. N. M. Gasanly, **I. Guler** " Temperature-Tuned Band Gap Energy and Oscillator Parameters of  $\text{TiInSSe}$  Layered Single Crystals " International Journal of Modern Physics B, Vol. 22, No.223, 931-939 2008
6. **I. Guler**, N. M. Gasanly " Determination of trapping center parameters in  $\text{Ti}_2\text{In}_2\text{S}_3\text{Se}$  layered single crystals by thermally stimulated current measurements " Physica B, Vol. 404, 2034-2038 2009
7. **I. Guler**, N. M. Gasanly " Trapping Center Parameters in  $\text{TiInSSe}$  Layered Single Crystals By Thermally Stimulated Currents Measurements" Journal of Alloys and Compounds, Vol. 485, 41-45 2009
8. **I. Guler**, N. M. Gasanly " Trapping Centers and Their Distribution in  $\text{Ti}_2\text{In}_2\text{Se}_3\text{S}$  Layered Single Crystals" Solid State Communications Vol. 150, 176-180 2010
9. **I. Guler**, N. M. Gasanly " Optical Properties of  $\text{Ti}_2\text{In}_2\text{Se}_3\text{S}$  Layered Single Crystals " Philosophical Magazine, Vol. 90, 13, 1799-1806 2010

#### INTERNATIONAL CONFERENCES

10. **I. Guler**, N. M. Gasanly " Dispersive optical constants of  $\text{TiInSSe}$  crystals " Condensed Matter Physics Conference of Balkan Countries, Muğla University, Muğla, Turkey, 26-28 May 2008
11. **I. Guler**, N. M. Gasanly " Temperature- and Excitation- Dependent Photoluminescence in Quaternary  $\text{Ti}_2\text{In}_2\text{S}_3\text{Se}$  Layered Crystals " 2nd International Meeting on Materials for Electronic Applications, Hammamet, Tunisia, 8-10 May 2009
12. **I. Guler**, N. M. Hasanli " Trapping Centers and Their Distribution in  $\text{Ti}_2\text{In}_2\text{Se}_3\text{S}$  Layered Single Crystals " 7th BPU General Conference, Alexandroupolis, Greece, 9-13 Sept 2009
13. **I. Guler**, N. M. Hasanli "Optical Properties of in  $\text{Ti}_2\text{In}_2\text{Se}_3\text{S}$  Layered Single Crystals " 26. International Physics Congress, Bodrum, Turkey, 24-27 Sept 2009



14. T. Yıldırım, H. Nasser, İ. Küçük, **I. Güler**, M. Işık, H. Özkan and N. Hasanli ” Determination of Trapping Center Parameters And Their Distribution In  $\text{Tl}_2\text{Ga}_2\text{S}_3\text{Se}$  Layered Crystals by Thermally Stimulated Current Measurements ” 26. International Physics Congress, Bodrum, Turkey, 24-27 Sept 2009

15. **I. Güler**, N. Hasanli and H. Ozkan ” Trapping Centers and Their Distribution in  $\text{TlInSeS}$  Single Crystals ” 11th Europhysical Conference on Defects in Insulation Materials (EU-RODIM 2010), University of Pecs, Hungary, 12-16 July 2010

#### NATIONAL CONFERENCES

16. **I. Güler**, N. M. Gasanly ” Donor-acceptor pair recombination in  $\text{Tl}_2\text{In}_2\text{Se}_3\text{S}$  layered crystals ” 13. Yoğun Madde Fiziği Ankara Toplantısı, ODTÜ, Ankara, Türkiye, 13 Kasım 2006

17. **I. Güler**, N. M. Hasanli ” Katmanlı  $\text{Tl}_2\text{In}_2\text{S}_3\text{Se}$  Kristallerinde Uyarılma ve Sıcaklık Bağımlı Fotoışırma ” 15. Yoğun Madde Fiziği Ankara Toplantısı, Bilkent Üniversitesi, Ankara, Türkiye, 7 Kasım 2008

18. **I. Güler**, N. M. Hasanli, H. Özkan ” Katmanlı Yarıiletken  $\text{Tl}_2\text{In}_2\text{S}_3\text{Se}$  Kristallerinde Tuzakların Dağılımı ” MYOMAT 2009: I. Ulusal Metal, Yarıiletken ve Oksit Materyallerin Üretiminde Kullanılan Sistemler ve Analiz Teknikleri Kongresi, ESOGÜ, Eskişehir 15-16 Haziran 2009

19. İlker Küçük, Tacettin Yıldırım, Mehmet Kabaer, Hisham A. Nasser, Mehmet Işık, Nizami Hasanli, Hüsnü Özkan, Kadir Ertürk, **İpek Güler** ” Katmanlı Yapıya Sahip Yarıiletken Kristallerde Tuzak Dağılımının Modellenmesi ” MYOMAT 2009: I. Ulusal Metal, Yarıiletken ve Oksit Materyallerin üretiminde Kullanılan Sistemler ve Analiz Teknikleri Kongresi, ESOGÜ, Eskişehir, 15-16 Haziran 2009

20. **I. Güler**, N. M. Hasanli ”  $\text{Tl}_2\text{In}_2\text{S}_3\text{Se}$  Katmanlı Yarı İletkenlerin Optik Spektrumlarının Belirgin Özellikleri ” 16. Yoğun Madde Fiziği Ankara Toplantısı, Gazi Üniversitesi, Ankara, Türkiye, 6 Kasım 2009